Fall 2022

Chemical and Thermal Influence on Intermediate Magma Storage Conditions: Volcán Ollagüe, Chile-Bolivia, Central Andes

Drew Allen Laviada-Garmon
Missouri State University, garmon467@gmail.com

CHEMICAL AND THERMAL INFLUENCE ON INTERMEDIATE MAGMA STORAGE CONDITIONS: VOLCÁN OLLAGÜE, CHILE-BOLIVIA, CENTRAL ANDES

A Master's Thesis

Presented to

The Graduate College of

Missouri State University

In Partial Fulfillment

Of the Requirements for the Degree

Master of Science, Geography and Geology

By

Drew Allen Laviada-Garmon

December 2022

CHEMICAL AND THERMAL INFLUENCE ON INTERMEDIATE MAGMA STORAGE CONDITIONS: VOLCÁN OLLAGÜE, CHILE-BOLIVIA, CENTRAL ANDES

Geography, Geology, and Planning

Missouri State University, December 2022

Master of Science

Drew Allen Laviada-Garmon

ABSTRACT

Continental arc volcanoes are the single best portrayal of the evolution of recycled earth material stemming from subduction, one of the most important and foundational phenomena in global tectonics. Understanding the genesis of intermediate-composition magmas produced at arc volcanoes is a difficult process making them a focal point for investigation. Geochemical investigation of zircon and plagioclase mineral phases erupted from continental arcs can provide insight into magma process, generation, storage conditions, timescales and differentiation of sub-volcanic plumbing systems prior to eruption events. The Central Volcanic Zone is a prime example of continental arc volcanism through subduction, and is host to one of the largest magma reservoirs in the world, the Altiplano-Puna Magma Body (APMB). Specifically, Volcán Ollagüe, a continental arc volcano located on some of the thickest continental crust in the world (60-75km) and producing intermediate composition magmas is a prime candidate to investigate the magma source and storage conditions of intermediate-composition lavas and their interactions with the APMB. Using $^{40}Ar/^{39}Ar$ eruption ages, U-Pb zircon crystallization ages, and zircon trace element contents I assess the storage conditions, zircon crystal residence times, and magma accumulation of the erupted magmas at Ollagüe. Additionally, plagioclase textural and geochemical analysis are used to suggest a model of evolution of the sub-volcanic plumbing system, and magma storage conditions at Ollagüe. These data reveal rejuvenation conditions and the complexities of the plumbing system of Ollagüe. Ultimately these data confirm that compositional hybridization is being controlled through periodic high-to-low volume injections from an external source. With Ollagüe located on the edge of the APMB, it is very likely that the complexities and geochemical constraints of Ollagüe's magma plumbing system are linked to the APMB.

KEYWORDS: Central Andean Volcanic Zone, Ollagüe, geochronology, geochemistry, composite volcanism, Altiplano-Puna Magma Body

CHEMICAL AND THERMAL INFLUENCE ON INTERMEDIATE MAGMA STORAGE CONDITIONS: VOLCÁN OLLAGÜE, CHILE-BOLIVIA, CENTRAL ANDES

By

Drew Allen Laviada-Garmon

Master's Thesis
Submitted to the Graduate College
Of Missouri State University
In Partial Fulfillment of the Requirements
For the Degree of Master of Science, Geography and Geology

December 2022

Approved:

Gary Michelfelder, Ph.D., Thesis Committee Chair

Melida Gutierrez, Ph.D., Committee Member

Douglas Gouzie, Ph.D., Committee Member

Julie Masterson, Ph.D., Dean of the Graduate College

ACKNOWLEDGEMENTS

I would like to thank the faculty and staff of the Department of Geography, Geology, and Planning for the support and contributions of my journey at Missouri State University. A special thank you to Dr. Gary Michelfelder for the establishment of this project and for his considerable guidance and encouragement throughout my two years and the completion of this project. I would also like to thank Dr. Douglas Gouzie and Dr. Melida Gutierrez for their insight and support pertaining to this project. Further, I would like to thank Kenny Horkley, from the University of Iowa, Dr. Matt Heizler, from New Mexico Tech, Dr. Barry Shaulis, from the University of Arkansas, and Dr. Christie Jilly-Rehak, from Stanford University. This project was funded through the National Science Foundation, NASA-Missouri Space Grant Consortium, and the Missouri State University Graduate College.

Not only would I like to thank those who have directly influenced this project, I would like to thank everyone who has pushed and supported me through this journey. To my father and mother, Troy and Renae, thank you for your love and support and most importantly, all you have sacrificed in wake of allowing me to chase my dreams. To my sister, Kenzie, thank you for your constant check-ins and long talks, it means more than you know. To the rest of my family and friends, thank you for accompanying me through this journey with nothing but words of love and support. A very warm thank you to Oliver and Willow my furry companions keeping me company during long days of writing and studying. Lastly, a special thank you to my Fiancé Angela, you were with me through every stressful day, keeping me saine and giving me sound advice. You have supported me from the very day I met you and I could not have done this without you.

TABLE OF CONTENTS

LIST OF TABLES

LIST OF FIGURES

Manuscript 1

Manuscript 2

OVERVIEW

Continental arc volcanoes are the single best portrayal of the evolution of recycled earth material stemming from subduction, one of the most important and foundational phenomena in global tectonics (Feeley et al., 1993; Michelfelder et al., 2013; Conway et al., 2020). Constraining intermediate-composition magmas produced at arc volcanoes is a difficult process making them a focal point for investigation. Magma mixing is a process that has relevance, as the hybridization of felsic and mafic materials has been suggested to act as an eruption event trigger (Kent et al., 2010; Conway et al., 2020). However, the passage of subduction zone magmas through a thick continental crust can create a melting-assimilation-storage-homogenization (MASH) zone, which can substantially differentiate and melt the crustal rocks and diversifies the igneous characteristics (Michelfelder et al., 2013; Delph et al., 2017). Geochemical investigation of mineral phases erupted from continental arcs can provide insight into magma processes, generation, storage conditions, timescales, and differentiation of sub-volcanic plumbing systems prior to eruption events (Renjith, 2014; Kern et al., 2016; Conway et al., 2020). This thesis consists of two manuscripts that primarily focus on Volcán Ollagüe, a continental arc composite volcano located on some of the thickest (65-70km) continental crust in the world (Gregory-Wodzicki, 2000) and which displays intermediate-composition lavas.

Research questions directing this work and regarding the intermediate composition of Ollagüe are: 1) What is the architecture of the magma plumbing system beneath Ollagüe, and how long does magma reside; and 2) What evidence is there for the involvement of regional crustal magma reservoirs controlling the magma compositions at Ollagüe? To assess these questions, this thesis uses rocks from each stage of Ollagüe's eruptive history to investigate the process controlling primary magma generation and storage conditions and their effect on the

chemical nature of Ollagüe. Although this thesis will not be able to provide a complete detailed answer for each of these questions, it will contribute to the wide-ranging efforts to understand intermediate magma genesis.

Volcán Ollagüe provides an ideal location for this study as it is constructed on thick continental crust and is 25km behind the arc front of the Andean Central Volcanic Zone (CVZ). Further, the CVZ is home to one of the largest imaged magma reservoirs on Earth, the Altiplano-Puna Magma Body (APMB; Chmielowski and Zandt, 1999; Zandt et al., 2003; Ward et al., 2014; Perkins et al. 2016). The presence of the APMB and thick continental crust make Ollagüe an ideal candidate to investigate the magma source and storage conditions of intermediate-composition lavas and their interactions with the APMB. The subsequent chapters of this thesis highlight two manuscripts discussing textural, geochemical, and geochronological analyses of individual mineral phases from the andesitic to dacitic lavas erupted at Ollagüe.

In the first manuscript, titled "Rapid Rejuvenation and Magma Storage Conditions Revealed by Zircon Geochronology and Geochemistry at Volcán Ollagüe, Chile-Bolivia, Central Andes," I present new $^{40}Ar/^{39}Ar$ eruption ages, U-Pb zircon crystallization ages, and zircon trace element data to assess the storage conditions, zircon crystal residence times, magma accumulation, and the effect of the regional APMB on the erupted magmas at Ollagüe. Two groups of zircons exist within the analyzed lavas, aiding in determining pre-eruptive storage conditions. Eruption ages were compared to U-Pb zircon crystallization ages to understand zircon residence within the melt. Trace element contents and ratios show how magma was stored and remobilized in the system. This study shows that magma is stored in a crustal hot zone and rejuvenated rapidly. Trace element ratios in the zircon suggest inheritance from a more mafic source.

The second manuscript, entitled “Geochemical Investigation of Intermediate Lavas: Using Plagioclase to Decipher the Magma Plumbing System of Volcán Ollagüe, Chile-Bolivia, Central Andes,” introduces a textural and geochemical analysis of plagioclase phenocrysts from Ollagüe. I use these data to suggest a model of magma evolution of the sub-volcanic plumbing system, the magma storage conditions at Ollagüe and determine its relation to the APMB. Four groups of plagioclases based on textures were present in the lavas analyzed. Plagioclase texture analysis helps to understand the processes occurring during crystallization and storage. Major and trace element geochemistry of plagioclase show chemical differentiation within the distinct groups, allowing insight into the construction of the magma plumbing system. Plagioclase phenocrysts in this study show complex storage conditions and evidence of a hybridizing chamber, likely sourced from the APMB.

MANUSCRIPT 1: RAPID REJUVENATION AND MAGMA STORAGE CONDITIONS REVEALED BY ZIRCON GEOCHRONOMETRY AND GEOCHEMISTRY AT VOLCÁN OLLAGÜE, CENTRAL ANDES, CHILE-BOLIVIA

Abstract

The thermal history and thermal evolution of magma storage are imperative to understanding crustal magma chamber behavior. Measuring crystallization age and temperature in zircon are powerful tools in the process. The Central Volcanic Zone is host to one of the largest magma reservoirs in the world, the Altiplano-Puna Magma Body (APMB); the APMB's effects on composite volcanism's evolutionary history are unclear. Here, I couple U-Pb zircon crystallization ages, Ti-in-zircon temperatures, and zircon trace-element contents from Ollagüe lavas to reveal the connection of rejuvenation and magma storage conditions to a regional magma body. The crystallization ages of zircon analyzed from Ollagüe span a ~ 1.2 Ma interval from 0.3 Ma to 1.5 Ma with temperatures between 670 and 770˚C. Coupling these temperatures with Hf contents and Eu/Eu* values suggest rejuvenation of zircon. Trace element ratios of zircon were analyzed to show trends of multiple influences, including zircon crystallization and cooling, amphibole fractionation, and titanite/apatite fractionation. Further, a population of zircons from Ollagüe has cores with trace element signatures suggesting a garnet signature, a mafic signature chemically distinct from the others. These data suggest that the Altiplano Puna Magma Body influences magma composition during Ollagüe's evolutionary history.

Introduction

Time scales of magma accumulation, storage, and cooling can seldomly be observed within a human lifespan or throughout written history (Schmitt et al. 2011). Beyond written history, geochronology is a necessary tool in reconstructing past eruptive events and determining the rates at which magma systems evolve prior to eruption events. Among these tools are $^{40}Ar/^{39}Ar$ radiometric dating and U-Th-Pb zircon geochronology (Schmitt et al., 2011). Ages determined from the $^{40}Ar/^{39}Ar$ method are the most common data interpreted as eruption ages for volcanic systems that are older than a few thousand years (Kern et al., 2016). Uranium-Th-Pb zircon geochronology yields crystallization ages, which can be compared with eruption ages exhibiting a representation of the duration of zircon crystallization in the system (Kern et al., 2016). The variation in age between eruption ages and zircon crystallization ages represents the

duration of zircon crystallization. Further, these ages give insight into whether zircon growth is continuous before eruption (Kern et al., 2016). This allows the U-Th-Pb zircon crystallization ages to be used as a tool to understand the pre-eruptive magmatic history leading up to an eruption event.

The Central Andes is home to the longest continental-margin volcanic arc on earth, where the Nazca plate subducts at approximately 30° beneath the South American Plate, referred to as the Andean Central Volcanic Zone (CVZ; Tilling, 2009). Previous studies of Quaternary volcanic rocks in the CVZ have demonstrated an eastward increase in the contents of K_2O and other incompatible trace elements (Feeley, 1993; Michelfelder et al., 2013). Godoy et al. (2017) reviewed previously collected Nd and Sr isotope data in the region and suggested the eastward trend of trace elements could be related to the presence of the large regional Altiplano-Puna Magma Body (APMB). Even with previous research on composite volcanism in the CVZ showing these chemical trends, detailed analysis of individual centers and specific chains in the region remains limited (Feeley, 1993; Michelfelder et al., 2013; Godoy et al., 2017). This study focuses on Volcán Ollagüe, an isolated composite volcano 25km behind the arc front of the CVZ. Previous studies suggest that Ollagüe's magma began heterogenous and became more homogenized over time (Feeley et al. 1993; Feeley and Davidson 1994). However, the magmatic source of Ollagüe is not clearly defined. I hypothesize that the volcano's initial wide range of compositions that become more homogenous over time could be the result of influence from the APMB. To test this hypothesis, I present new $^{40}Ar/^{39}Ar$ eruption ages, U-Pb zircon crystallization ages, and zircon trace element data to assess the storage conditions, magmatic accumulation, and the effect, if any, of the APMB on magma composition. Together, these data allow subsequent

modeling to provide insight into the pre-eruptive conditions of Ollagüe's magmas and to ascertain if the APMB is the source of magmas feeding Ollagüe.

Geologic Background

Geologic Setting. The Andean orogeny's tectonic style varies along and across strike (Gregory-Wodzicki, 2000; Michelfelder et al., 2013; Scott et al., 2018). Along strike, the Andes are split into two tectonic styles. Between latitudes 2-15° S and 33°30' S, the Nazca plate subducts beneath the South American plate at 5° to 10° (Kay et al., 1991; Gregory-Wodzicki, 2000, Scott et al., 2018). The lack of volcanic activity has identified these regions of low-angle subduction (flat-slab zones) from the Miocene to the Holocene (Gregory-Wodzicki, 2000). Using earthquake hypocenter and focal mechanism data, Cahill and Isacks (1992) show that the Nazca Plate subducts at around 33° beneath the area of active volcanism in the Central Andes (Feeley and Hacker, 1995; Gregory-Wodzicki, 2000). This area of steep subduction directly corresponds to young volcanic activity and has been labeled the Central Volcanic Zone (CVZ; Gregory-Wodzicki, 2000). Across strike, the CVZ shows an eastward migration of magmatism and deformation through time (Gregory-Wodzicki, 2000). This modern region is divided into three smaller regions via north- to north-west striking geological provinces. They are as follows from west to east: The Western Cordillera, the Altiplano, and the Eastern Cordillera (Jorden et al., 1983; Michelfelder et al., 2013).

The Central Volcanic Zone. The Central Volcanic Zone (CVZ) encases a substantial volume of volcanic material with 20 identified caldera complexes, erupting silicic ignimbrites, and an estimated 50 active or recently active composite volcanoes erupting andesites to dacites in the last 10 Ma (Michelfelder et al., 2013). Magmatic activity in the CVZ is associated with the addition of crustal volume, delamination of the lithosphere, and thermal weakening of the

continental crust (Isacks, 1988). Subduction zone volcanism has been active in the Central Andes since the Jurassic, beginning at the present coastal area (Salisbury et al., 2010; Gregory-Wodzicki, 2000). From the early Cretaceous to the early Eocene, the arc began to migrate eastward and was located at the western foothills of the present-day Western Cordillera (Gregory-Wodzicki, 2000). Between 35-25 Ma, the CVZ experienced a period of volcanic hiatus related to flat-slab subduction. After the approximately 10 Ma hiatus, volcanism began to spread to the Altiplano Plateau, forming the Altiplano-Puna Volcanic Complex, which is related to the delamination of the lithosphere (Salisbury et al., 2010; Gregory-Wodzicki, 2000).

Composite volcanoes in the CVZ arc front are differentiated by their degrees of glacial erosion as Pleistocene volcanoes and the younger, unglaciated volcanic centers of Holocene age (Avila-Salinas, 1991). An estimated 3,000 km^3 of intermediate composition lavas have erupted from the composite volcanoes of the Western Cordillera (Baker and Francis, 1978; Michelfelder et al., 2013). These lavas extend nearly 200 km to the east onto the Altiplano Plateau, where observed volumes drastically decrease (Michelfelder et al., 2013).

Volcan Ollagüe. East-southeast of the CVZ arc front, straddling the Chilean-Bolivian Border, is Volcán Ollagüe (Fig. 1), an isolated composite volcano with evidence of a multistage eruptive history (Feeley et al., 1993; Feeley and Hacker, 1995; Klemetti and Grunder, 2008; and Vezzoli et al. 2008). Lavas at Volcán Ollagüe have displayed a large range of compositions with the occurrence of basaltic andesite inclusions within intermediate composition lavas. This suggests that the shallow chambers are periodically replenished by a more basaltic parental magma source (Feeley and Davidson, 1994). Approximately 80-90 km^3 of lavas erupted, initially defining four separate eruptive series: Vinta Loma, the Chaska Orkho, the post-collapse series, and the La Celosa (Feeley et al., 1993).

Vezzoli et al. (2008) revised Ollagüe's eruptive history with the addition of new eruption ages as the Vinta Loma (1200 ka to 910 ka), the Santa Rosa (870 ka to 641 ka), the El Azufre (507 ka to 292 ka) which includes the La Celosa parasitic dome and the inclusion bearing Chaska Orkho stages, and the Santa Cecilia (220 ka to 130 ka). The Vinta Loma series represents the dominant stage of cone growth at Volcán Ollagüe, cropping out in the northern and eastern sectors of the volcano (Fig. 1; Vezzoli et al., 2008). The Vinta Loma consists of two pyroxene andesite and dacite lavas. These lavas erupted from the central vent of the volcano's older cone showing outward dips and radial distribution (Vezzoli et al., 2008). The Santa Rosa series comprises a sequence of summit lava flows, pyroclastic deposits from the northern summit cinder cone, and several lateral lava flows. This series concludes with a debris avalanche (Vezzoli et al., 2008). The lavas from Santa Rosa range from amphibole-biotite dacites to andesites and basaltic andesites. The El Azufre series is mainly comprised of andesitic lavas and consists of a sequence of fresh lava beds around 200m thick, with a sub-horizontal attitude, at the base of the series and interpreted as the products of a summit lava lake (Vezzoli et al., 2008). The upper summit lava flow is two-pyroxene andesite that reaches the southern flank. The south summit cinder cone makes up the south peak of Ollagüe and is composed of stratified, pumice-rich pyroclastic deposits (Vezzoli et al., 2008). The Santa Cecilia series is defined by a debris avalanche event that resulted from sector collapse of the west flank of Ollagüe (Vezzoli et al., 2008). Volcanic rocks are compositionally defined by a range of andesite lava domes and by voluminous andesite lateral lava flows found on the southwest flank of the edifice (Vezzoli et al., 2008). The lateral lava flows were extruded from vents located downslope of the lava dome range, forming a complex lava field (Vezzoli et al., 2008). The lava domes align in an NW-SE direction, with at least four of the domes being younger, moving south-east (Vezzoli et al.,

2008). Additionally, Vezzoli et al. (2008) $^{40}Ar/^{39}Ar$ ages were combined with the tectonic history, suggesting that NW-trending regional tectonics are responsible for geometric and compositional variations in the shallow magma feeding system. However, the storage conditions and a model for the plumbing and magma source of Ollagüe are still not clearly defined.

Analytical Methods

$^{40}Ar/^{39}Ar$ Geochronology. Rocks from the eruptive stages of Ollagüe were selected for $^{40}Ar/^{39}Ar$ geochronology based on the presence of zircon, six samples resulting in being sent for analysis at the New Mexico Geochronology Research Laboratory at the New Mexico Tech University. Mineral phases targeted for analysis included biotite and hornblende when available, and plagioclase for all samples. Rocks selected were crushed, milled, and sieved to obtain appropriate grain size for analysis (between 250-425 μm). Mineral separation was carried out by a Frantz Isodynamic Magnetic Separator and approximately 50-100 mg of each mineral phase was handpicked under binocular microscope. Mineral separates were then etched, packaged, and transported to the mineral separation lab at the New Mexico Tech University. Mineral separates were then given an ultrasonic water or hydrofluoric acid bath, based on the clarity of the separate, before going through a final handpick before irradiation. Information on the irradiation and ^{39}Ar production can be found in McDougall and Harrison (1999).

SHRMP-RG. Volcanic rocks from the eruptive stages of Ollagüe were selected for U-Pb and U-Th isotope ratios and trace-element analyses based on the availability of zircon. Zircon was separated from five samples representing the volcanic stratigraphy of Ollagüe. I utilized mechanical separation via crushing, milling, and sieving. A < 200 μm fraction for each sample was then funneled through a Frantz Isodynamic Magnetic Separator followed by a heavy liquid separation using lithium sodium tungstate. Finally, individual loose zircons were handpicked

from the heavy liquid separate. Approximately 6-22 zircon grains per sample (87 total) were mounted in epoxy at Stanford University. Zircons were hand selected, mounted on double-sided tape on a glass slide, and cast in a 25mm diameter by 5mm thick epoxy disc. Mount was ground and polished to a 1-micron finish. Grains were imaged with a reflected light microscope, and with cathodoluminescence (CL) and backscattered electron imaging (BSE) on a JEOL JSM-IT500HP scanning electron microscope (SEM). The mount was cleaned with a 10% EDTA (ethylenediaminetetraacetic acid) wash, then with a 1M HCl solution, thoroughly rinsed with DI water, and dried in a vacuum oven set to 55℃. The sample was finally coated with ~10-20nm of gold.

Isotope ratios (^{238}U-^{206}Pb, ^{235}U-^{207}Pb, and ^{238}U-^{232}Th) and trace element compositions were obtained via sensitive high-resolution ion microprobe with reverse geometry (SHRIMP-RG) at the Stanford -U.S. Geological Survey Microscope Analytical Center (SUMAC). The 126 spot analyses were performed on 67 individual zircon grains separated from five different samples. Cathodoluminescent images of mounted grains were used to select targets with dark areas within the CL images, as they are inferred to be uranium enriched, to improve the SHRIMP-RG analyses and counting statistics of ^{206}Pb. Cores that appeared to be altered or complex were avoided. Both core and rim concentrations within each zircon were analyzed when available.

Spots were analyzed with an O_2- primary beam, an accelerating voltage of 10kV was used to sputter secondary ions from the sample surface. Analytical current was set to 5nA for a spot size of ~25 microns. Spots were presputtered for 2 minutes to remove gold coating and surface contamination. For each spot, the primary and secondary beams were auto-tuned to maximize transmission. The run table included 26 masses for U-Pb geochronology and trace

element analysis: ^{46}SiO, ^{48}Ti, ^{49}Ti, ^{56}Fe, ^{89}Y, ^{139}La, ^{140}Ce, ^{146}Nd, ^{147}Sm, ^{153}Eu, ^{155}Gd, ^{179}DyO, ^{182}ErO, ^{188}YbO, $^{196}Zr_2O$, ^{196}HfO, ^{204}Pb, Background, ^{206}Pb, ^{207}Pb, ^{232}Th, ^{238}U, ^{248}ThO, ^{254}UO, $^{270}UO_2$, each mass was collected by magnet peak-jumping on an electron multiplier detector. Count times on ^{206}Pb and ^{207}Pb were set to 60s for higher precision of the young grains. Count times on all other masses ranged from 2-15s per mass to optimize counting statistics for each isotope. Data were collected over 5 scans, for a total of ~40min per spot. Mass resolution was set to ~9000 to resolve isobaric interferences.

Trace elements were standardized to MAD559 zircon standard (Coble et al., 2018), and U-Pb ages were standardized to TEMORA-2 (416.8 Ma; Black et al., 2003). Data were reduced using the MS Excel add-in programs Squid2.51 and Isoplot 3.76 from Ken Ludvig (2001;2003). Measures $^{206}Pb/^{238}U$ was corrected for common Pb using ^{207}Pb, based on a model Pb composition from Stacey and Kramers (1975), and the U-Pb ages were corrected for ^{230}Th concentration. Spot data was discarded if Iron was detected greater than 50ppm, due to the probability of hitting a mineral inclusion.

Results

Cathodoluminescence Imaging. Zircon grains from all samples ranged from 90 to 250 μm in length, generally euhedral and prismatic, with some containing mineral and/or melt inclusions. Imaged zircons revealed U content oscillatory zoning patterns ranging from ~5 to 20 μm. Overall, zircon crystals from Ollagüe are relatively dim, with thin brighter zones throughout crystals from the five samples. Zircon crystals contained interior resorption zones and truncated zoning, often seen as rounded or curved zone boundaries in the five samples. Melt/mineral inclusions were observed in some of the zircons on the edges of interior resorption. Splotchy zoning areas were observed in zircon containing resorption from all five samples. Resorption and

splotchy zoning of some cores were observed and generally was found with some resorption of mantles as well. Some zircon grains have what look to be bright overgrowths. Zircon CL images are displayed in Figure 2. Using these textures, I can group the zircons from Ollagüe into two distinct groups. Group one contains zircon with interior mantle resorption, truncated zones, and associated melt/mineral inclusions. Group two, which may have interior mantle resorption, also displays resorption in the core with the occasional melt inclusion.

^{40}Ar/^{39}Ar Geochronology. Results of ^{40}Ar/^{39}Ar geochronology analyses are illustrated in Figure 3 and Table 1. ^{40}Ar/^{39}Ar radiometric ages were obtained from available biotite and hornblende. Biotite produced ^{40}Ar/^{39}Ar plateau ages for OLA-9006 (0.79 ± 0.07 Ma), OLA-9007 (0.80 ± 0.04 Ma), and OLA-9041 (0.82 ± 0.03 Ma; Table 1; Fig. 3). Hornblende produced ^{40}Ar/^{39}Ar plateau ages for OLA-9006 (1.28 ± 0.12 Ma), OLA-9007 (1.29 ± 0.12), and OLA-9041 (1.01 ± 0.13; Table 1). OLA-9034 and OLA-9046 did not contain biotite or amphibole and as a result the plagioclase phase was picked for analyses. Plagioclase did not produce usable ^{40}Ar/^{39}Ar plateau ages. Due to the more defined plateaus of the biotite analyses I chose to use the biotite (as opposed to the hornblende) ages.

U-Pb Zircon Geochronology. The results of U-Pb geochronology are illustrated in Figures 4 and 5 and presented in Table 2. All ^{206}Pb/^{238}U ages collected span a ~ 1.2 Ma interval from 0.3 Ma to 1.5 Ma, with a mean 1σ error (Fig. 4). The weighted mean zircon crystallization age of OLA-9006 is 0.769 ± 0.038 Ma (MSWD 1.8), the weighted mean age of the cores is 0.757 ± 0.049 Ma (MSWD 2.0), and the rims is 0.784 ± 0.050 Ma (MSWD 1.7). The weighted mean crystallization age of OLA-9007 is 0.749 ± 0.038 Ma (MSWD 1.6), the weighted mean crystallization of cores is 0.782 ± 0.049 Ma (MSWD 1.5), and the weighted mean crystallization of the rims is 0.730 ± 0.037 (MSWD 1.5). The weighted mean crystallization age of OLA-9034

is 0.63 ± 0.11 Ma (MSWD 2.5), weighted mean crystallization of cores is 0.70 ± 0.1 (MSWD 1.3), and weighted mean crystallization of rims is 0.59 ± 0.18 Ma (MSWD 3.6). The weighted mean crystallization age of OLA-9041 is 0.821 ± 0.03 (MSWD 2.6), weighted mean of cores is 0.82 ± 0.056 Ma (MSWD 2.7), and the weighted mean of rims is 0.824 ± 0.07 Ma (MSWD 2.5). Weighted mean crystallization age of OLA-9046 is 0.81 ± 0.1 Ma (MSWD 2.2), the weighted mean of core crystallization is 0.765 ± 0.067 Ma (MSWD 1.5), and the weighted mean of rims is 0.97 ± 0.12 Ma (MSWD 1.15; Table 2). Probability density function (PDF) curves of U-Pb zircon crystallization ages from the eruptive stages of Ollagüe show dominant peaks from 0.6 to 0.8 Ma. These peaks illustrate strongly overlapping ages with no clear age gaps, showing the highest densities of ages from each sample. All five samples demonstrate a singular dominant density peak (Fig. 5). OLA-9046 also shows a possible sub-population of ages which we interpret to be due to small sample size (Fig 5). Generally, significant age differentiation between core and rim analyses are minimal through all five samples, with most zircon analytically within error. However, some core and rim analyses are separated by hundreds of thousands of years. Core PDFs show dominant peaks with the same range (0.6-0.8) however, the five samples show small shoulders on each of the curves. The cores creating the shoulders are related to grains with resorbed cores and melt inclusions and are likely of xenocrystic/antecrystic nature.

Zircon Trace Element Geochemistry. Results of trace element analyses are illustrated in Figure 6, 7, and 8, Table 3, and Appendix A. Concentrations of Dy range from 20 – 400 (ppm) with 78% of analyses between 20 – 100 (ppm) and 22% greater than 100 (ppm). Concentrations of Dy show a decreasing trend as values of Yb/Dy increase (Fig. 6). Uranium concentrations of zircons analyzed range from 65 – 1,000 ppm with 87% of analyses between 65 and 450ppm and only 6% above 600ppm. Thorium concentrations range from 40–1,450 ppm with 89% of

analyses between 40–400 ppm and only 6% above 600 ppm (Fig. 6). Hafnium content in zircons analyzed from Ollagüe range from 5,600–13,400 ppm with 63% of analyses above 10,000 ppm and 37% under 10,000 ppm. Both U and Th concentrations remain relatively uniform with Hf less than 12,000 ppm. Thorium/uranium ratios range from 0.22 – 2.02 with the most extreme enrichment of Th relative to U corresponding to cores with higher Hf content (greater than 10,000 ppm; Fig. 6). Values of Eu/Eu* range from 0.1 to 0.8 with 85% of analyses between 0.4 and 0.6, 11% between 0.1 and 0.4, and 3% between 0.6 and 0.8 (Fig. 6). Values of Eu/Eu* between 0.6 and 0.8 shows an increasing trend with decreasing Hf. Ytterbium/gadolinium ratios range from 0.6 to 22 with cores generally having lower values between 0.6 and 16, and rims exhibiting higher values between 9 and 22. Further, Yb/Gd values show a decreasing trend with decreasing Hf (Fig. 6). Compared to the Chao dacites and the Purico and Pasas Grandes ignimbrite systems, concentrations of Th (ppm), U (ppm), and Hf (ppm) show some overlap with Ollagüe with most concentrations being higher. Values of Eu/Eu* tend to be greater in Ollagüe than in the ignimbrite systems. Ignimbrite Yb/Gd values show some overlap with Ollagüe, but generally have higher values (Fig. 6).

Trace element ratios and concentrations versus age exhibits similarity across the five samples (Fig. 7). Between 0.5 and 1 Ma there is a dense population of Eu/Eu*, Th/U, and Y contents. However, Yb/Gd ratios show a separation between core and rim concentrations with rims showing higher ratios than cores. It should also be noted that Hf concentrations show a population of cores and rims exhibiting an increase in Hf content over time (Fig. 7).

Chondrite-normalized REE patterns of typical natural zircon have highly enriched heavy-REEs with respect to light-REEs and will have positive Ce and negative Eu anomalies (Sun and McDonough, 1989; Fig. 8). These common characteristics are dominant in the zircons that

represent the eruptive stages of Ollagüe. However, even as the five samples follow the general natural trend cores from the five samples typically have higher concentrations of the lighter REEs than the rims of the zircons (Fig. 8).

Ti-in-Zircon Thermometry. Zircon saturation temperature is the biggest constraint on zircon crystallization within a melt. Zircon crystallization will only occur in a melt once it has cooled below the zircon saturation temperature (Kern et al., 2016). Once these conditions are met typical zircon (~100μm) can crystallize over 1,000-10,000 years, and can be resorbed if introduced to a hotter zircon unsaturated melt over similar timescales (Kern et al., 2016). Further, if the zircon saturation conditions are met again, the surviving zircon acts as a base for additional zircon growth (Kern et al., 2016). This advocates zircon recording magmatic events, such as mixing with hotter melts raising the zircon above saturation temperatures, attributed to resorption surfaces and or crystal residency in sub-solidus conditions (Kern et al., 2016).

Titanium-in-Zircon temperatures were calculated using the revised equation from Ferry and Watson (2007) utilizing αTiO_2 and αSiO_2, shown as:

$$T(K) = \frac{-4{,}800 \pm 86}{logTi(ppm) + \log\alpha SiO_2 - \log\alpha TiO_2 - (5.711 \pm 0.072)}$$

The most accurate use of the above equation requires knowledge of αTiO_2 and αSiO_2 at the time of zircon crystallization. With careful consideration of the system-specific melt compositions and mineral assemblages, the effects of melt evolution during crystallization processes or mixing events on these activities over time allow a useful application of the thermometer, even when specific activities cannot be definitively identified (Claiborne et al., 2010). For these specific calculations, I used αSiO_2 as a constant of 1 and 0.75 and carried out the calculations for αTiO_2 ranging from 0.1 to 1 to get a range of temperatures that closely resemble the average zircon

saturation temperature of 735˚C. After running the calculations, I decided the best fit of temperatures yielded from an αSiO_2 of 1 and an αTiO_2 of 0.7.

Calculated temperatures from the Ti-in-Zircon thermometer range from 633˚C to 1193˚C (Fig. 9). Titanium-in-zircon temperatures of cores and rims across all samples show a distinct population of zircon of an approximate 100˚C range between 670 and 770˚C (Fig 7). Rims of zircons from all five samples line up on the zircon saturation temperature. Cores show a dense population of cooler temperatures than the zircon saturation temperatures and a small population of higher temperatures. When comparing temperatures to Th/U, Yb/Gd, and Yb/Dy ratios, zircon cores exhibit lower ratios with lower temperatures, and zircon rims exhibit higher ratios with relatively higher temperatures (within 50˚C). Thorium/uranium ratios show a linear correlation as temperatures decrease the Th/U ratios also decrease for both cores and rims. However, Yb/Gd and Yb/Dy ratios show a negative linear correlation in the cores, but the rims show relatively consistent concentrations and temperatures. Further, Eu/Eu* values plotted to temperature show a split between cores and rims (Fig. 10).

Discussion

Assessment of Petrogenetic Process via Textures. Zircon crystallization is a function of temperature as they will not begin to crystallize until reaching the zircon saturation temperature (Kern et al., 2016; Kent and Cooper, 2017). As a melt is heated and cooled, textures of the crystals themselves can show evidence of these processes. The zircons from Ollagüe show complex zoning patterns, which indicates that zircon likely grew in a high complexity melt with fluctuations of conditions. This is supported by the interior and core resorption surfaces within the zircon grains. Further, this can suggest that zircon saturated magmas were likely repeatedly rejuvenated or mixed with a hotter, zirconium undersaturated melt (Claiborne et al., 2010). The

presence of xenocryst cores in zircon from all five samples implies that their melt is being introduced into Ollagüe's system from elsewhere, where the melt has time to crystallize and possibly store before being relocated.

Zircon Crystallization and Eruption Ages. Utilizing U-Th-Pb geochronology of zircon can yield a perception of the state of crystallization within a given magma chamber. Determination of whether zircon was continuously crystallized, or crystallized at different times, suggests multiple periods where zircon saturation temperatures were reached (Samperton et al., 2015; Kern et al., 2016). The $^{40}Ar/^{39}Ar$ method yields the data most interpreted as eruption ages for volcanic systems older than a few thousand years (Kern et al., 2016). Integrating zircon crystallization ages with eruption ages can give insight into the residence times of crystallized zircons in a melt before an eruption event (Kern et al., 2016).

Aside from a small population of zircon cores showing older crystallization ages and outside of error from the weighted mean crystallization ages, zircon crystallization ages in the five samples appear to be relatively continuous. The weighted mean ages of the five samples are interpreted as the most common crystallization of autocrysts in the system prior to eruption. Populations of the older zircon cores, outside of error in the individual samples, are attributed to inheritance due to the complex textures seen in the CL images and the shoulders in the PDF curves (Samperton et al., 2015; Kern et al., 2016). The eruption ages of OLA-9006, OLA-9007, and OLA-9041, are all within error of the mean zircon crystallization ages. The near overlapping of an eruption age with the mean crystallization age is attributed to the melt experiencing geologically short (0.005 to 0.05 Ma) residence times after reaching the zircon's closure temperature. With the presence of inherited zircon, I suggest the introduction of a foreign melt rejuvenating the host melt just prior to an eruption event.

Pre-eruption Geochemical Evolution. Mafic ratios of Th/U are typically between 0.8 and 1.2, while zircon from felsic systems has distinctly lower ratios ranging from 0.55 to 0.8 (Kirkland et al., 2015). However, as the two end members are relatively defined, intermediate compositions are harder to distinguish (Kirkland et al., 2015). A small population of cores from Ollagüe exhibit the higher Th/U ratios you would expect to see from more mafic systems, while the largest population of zircons falls between the two end-member ranges. Inheritance of the mafic signature zircon from a more chemically distinct primitive melt shows evidence of a hybridizing chamber feeding Ollagüe. I attribute the lower values of Th/U exhibiting decreasing values with decreasing temperature at Ollagüe to a fractionating melt (Kirkland et al., 2015; McKay et al., 2018). Further, even though trends of Th/U ratios fluctuate with temperatures, there does not appear to be a correlation between Th/U ratios to age.

Low Th/U ratios (<1) with higher Yb/Gd ratios (12-40) and Hf (>9,500ppm) and lower Eu/Eu* anomalies (0.25-0.4) are indicative of a crystal mixture strongly promoting plagioclase and zircon crystallization (Klemetti and Clynne, 2014; Rentz et al., 2018; Burgess et al., 2021). Zircons analyzed from Ollagüe do not uniformly plot into the crystal mush conditions but instead suggest multiple storage and rejuvenation conditions. Modeling the rejuvenation conditions yields two separate populations of zircons (Fig. 11). First, a population of zircon plots within a range of <10,000 ppm Hf and >0.40 Eu/Eu* values which have been attributed to rejuvenation with higher Ti-in-Zircon temperatures (Klemetti and Clynne, 2014; Rentz et al., 2018). Within this population, zircon rims display higher temperatures, Th/U values, and Yb/Gd values than the cores. Second, a population of zircons shows characteristics of warm storage conditions (Fig. 11; Klemetti and Clynne, 2014). When compared to the eruption and zircon crystallization ages, it can be inferred that these rejuvenation conditions will likely occur at geologically rapid rates (5-

50 ka). These data exhibit evidence that the parent fractionating melt is re-introduced or rejuvenated into a more primitive basaltic melt, happening quickly before an eruption event.

Accessory mineral fractionation within a melt influences zircon composition. It can be a major contribution to the heterogeneity in zircons from a single sample (Grimes et al., 2015), specifically, the behavior of U/Yb to Gd/Yb and Gd/Yb to Ce/Yb ratios (Fig. 12). Zircons from Ollagüe cluster tightly in both comparisons, likely due to multiple influences including zircon crystallization and cooling, amphibole fractionation, and titanite/apatite fractionation. A subplot of zircons from Ollagüe suggests a garnet signature, unlike zircons from the ignimbrites, which show strong trends of zircon cooling and crystallization and titanite fractionation (Fig. 12). The garnet signature is indicative of zircons originating from a more basaltic melt source. The evidence of influence from accessory mineral fractionation, crystalizing and cooling of zircon, and the mafic garnet signature supports the idea of a homogenizing chamber feeding Ollagüe.

Conclusion

Textural analyses of zircon from Ollagüe showed complex chemical zoning patterns, which indicates that these zircons likely grew in a high complexity melt with fluctuating conditions. Zircon crystallization ages from the five samples display similar dominant density plot peaks with minimal differentiation in ages from cores to rims. Coupling the zircon crystallization ages with the eruption ages suggests a limited amount of crystal residence time after zircon crystallization. Additionally, a geochemical group of zircons plot within a previously defined set of storage and rejuvenation conditions was proposed by Klemetti and Clynne (2014). From the model, there are two separate populations of zircon. One population suggests rejuvenation with high Ti-in-Zircon temperatures. The second population of zircon shows the characteristics of the zircon storage conditions. Coupling the eruption ages, zircon crystallization

ages, and our rejuvenation model, I suggest an outside source influenced the system, supporting a geologically rapid rejuvenation of a warm crystal mixture with a more primitive basaltic melt before an eruption event. Geochronological data shows a population of inherited cores suggesting the introduction of new material into the host melt. The behavior of U/Yb to Gd/Yb and Gd/Yb to Ce/Yb ratios overlap, but a population of cores infers a garnet signature, suggesting inherited cores represent a more primitive basaltic material supporting the hybridization of a magma chamber feeding Ollagüe. Ultimately, I conclude that there are zircons in the system originating from a foreign basaltic melt source which is a primary force behind the rapid magma rejuvenation just before an eruption event. Due to the geographic location of Ollagüe, this is likely the influence of the APMB.

Acknowledgements

This project was funded and supported by the National Science Foundation, the NASA-Missouri Space Grant Consortium, and the Missouri State University Graduate College. The authors would like to thank Christie Jilly-Rehak of the University of Stanford for use and assistance with the SHRIMP-RG analyses and data reduction, and Dr. Matt Heizler of New Mexico Tech University for the use of the $^{40}Ar/^{39}Ar$ laboratory and data reduction.

Literature Cited

Avila-Salinas, W., 1991, Petrologic and tectonic evolution of the Cenozoic volcanism in the Bolivian western Andes. Geologic Society of America Memoir 265, 245-257.

Baker, M.C.W., Francis, P.W., 1978. Upper Cenozoic volcanism in the Central Andes – Ages and volumes. Earth Planet. Sci. Lett. 41, 175-187. https://doi.org/10.1016/0012-821X(78)90008-0.

Black, L.P., Kamo, S.L., Allen C.M., Aleinikoff, J.N., Davis, D.W., Korsch, R.J., Foudoulis, C., 2003. TEMORA 1: a new zircon standard for phanerozoic U-Pb geochronology. Chemical Geology 200, 155-170. https://doi.org/10.1016/S0009-2541(03)00165-7.

Burgess, S.D., Coble, M.A., Vazquez, 2021. Zircon geochronology and geochemistry of Quaternary rhyolite domes of the Coso volcanic field, Inyo County, California. J. Volcanol. Geotherm. Res. 417, 1-14. https://doi.org/10.1016/j.jvolgeores.2021.107276.

Cahill, T., Isacks, B., 1992. Seismicity, and shape of the subducted Nazca Plate: J. Geophys. Res. 97, 17503-17529. https://doi.org/10.1029/92JB00493.

Claiborne, L., Miller, C.F., Wooden, J.L., 2010. Trace element composition of igneous zircon: A thermal and compositional record of the accumulation and evolution of a large silicic batholith, Spirit Mountain, Nevada. Contrib. Minerol. Petrol. 160, 511-531. https://doi.org/10.1007/s00410-010-0491-5.

Coble, M.A., Vazquez, J.A. Barth, A.P., Wooden, J., Burns, D., Kylander-Clark, A., Jackson, S., Vennari, C.E., 2018. Trace Element Characterization of MAD-559 Zircon Reference Material for Ion Microprobe Analysis. Geostand. and Geoanal. Research 42, 481-497. https://doi.org/10.1111/ggr.12238.

Cooper, K.M., Kent, A.J.R., 2014. Rapid remobilization of magmatic crystals kept in cold storage. Nature 506, 480-483. https://doi.org/10.1038/nature12991.

Feeley, T.C., 1993. Crustal Modification during subduction-zone magmatism: evidence from the southern Salar de Uyuni region (20°-22°S), central Andes. Geology 21, 1019-1022. https://doi.org/10.1130/0091-7613(1993)021<1019:CMDSZM>2.3.CO;2.

Feeley, T.C., Davidson, J.P., Armendia, A., 1993. The volcanic and magmatic evolution of Volcán Ollagüe, a high-K, late Quaternary stratovolcano in the Andean Central Volcanic Zone: J. Volcanol. Geotherm. Res. 54, 221-245. https://doi.org/10.1016/0377-0273(93)90065-Y.

Feeley, T.C., Davidson, J.P., 1994. Petrology of Calc-Alkaline Lavas at Volcán Ollagüe and the Origin of Compositional Diversity at Central Andean Stratovolcanoes, J. Petrol. 35, 1295-1340. https://doi.org/10.1093/petrology/35.5.1295.

Feeley, T.C., Hacker, M.D., 1995. Intracrustal Derivation of Na-Rich Andesitic and Dacitic Magmas: An Example from Volcán Ollagüe, Andean Central Volcanic Zone. The Journal of Geology 103, 213-225. https://doi.org/10.1086/629737.

Ferry, J. M., Watson, E. B., 2007. New thermodynamic models and revised calibrations for the Ti-in-zircon and Zr-in-rutile thermometers. Contrib. Mineral. Petrol. 154, 429-437. https://doi.org/10.1007/s00410-007-0201-0.

Godoy, B., Wörner, G., Le Roux, P., de Silva, S., Parada, M., Kojima, S., González-Maurel, M.D., Polanco, E., Martínez, P., 2017. Sr- and Nd-isotope variations along the Pleistocene San Pedro-Linzor volcanic chain, N. Chile: Tracking the influence of the Altiplano-Puna Magma Body. J. Volcanol. Geotherm. Res. 341, 172-186. https://doi.org/10.1016/j.jvolgeores.2017.05.030.

Gregory-Wodzicki, K.M., 2000. Uplift history of the Central and Northern Andes: A review. GSA Bulletin 112, 1091-1105. https://doi.org/10.1130/0016-7606(2000)112<1091:UHOTCA>2.0.CO;2.

Grimes, C. B., Wooden, J. L., Cheadle, M. J., John, B. E., 2015. "Fingerprinting" tectono-magmatic provenance using trace elements in igneous zircon: Contributions to Minerology and Petrology 170:46. https://doi.org/10.1007/s00410-015-1199-3.

Isacks, B.L., 1988. Uplift of the Central Andean Plateau and bending of the Bolivian Orocline. J. Geophys. Res. 93, 3211-3231. https://doi.org/10.1029/JB093iB04p03211.

Jordán, T.E., Isacks, B.L., Allmendinger, R.W., Brewer, J.A., Ramos, V.A., Ando, C.J., 1983. Andean tectonics related to geometry of subducted Nazca plate. GSA Bulletin 94, 341-361. https://doi.org/10.1130/0016-7606(1983)94<341:ATRTGO>2.0.CO;2.

Kay, S.M., Mpodozis, C., Ramos, V.A., Munizaga, F., 1991. Magma source variation for mid-late Tertiary magmatic rocks associated with a shollowing subduction zone and a thickening crust in the central Andes (28 to 33°S). Geological Society of America Memoir 265, 113-137.

Kaiser, J.F., de Silva, S., Schmitt, A.K., Economos, R., Sunagua, M., 2016. Million-year melt-presence in monotonous intermediate magma for a volcanic-plutonic assemblage in the Central Andes: Contrasting histories of crystal-rich and crystal-poor super-sized silicic magmas: Earth Planet. Sci. Lett. 457, 73-86. https://doi.org/10.1016/j.epsl.2016.09.048.

Kent, A.J.R., Cooper, K.M., 2018. How well do zircons record the thermal evolution of magmatic systems? Geology 46, 111-114. https://doi.org/10.1130/G39690.1.

Kern J.M., de Silva, S.L., Schmitt, A.K., Kaiser, J.F., Iriarte, R.A., Economos, R., 2016. Geochronological imaging of an episodically constructed subvolcanic batholith: U-Pb in zircon chronochemistry of the Altiplano-Puna Volcanic Complex of the Central Andes. GSA Geosphere 12, 1054-1077. https://doi.org/10.1130/GES01258.1.

Kirkland, C.L., Smithies, R.H., Taylor, R.J.M., Evans, N., McDonald, B., 2015. Zircon Th/U ratios in magmatic environs. Lithos 212-215, 397-414. https://doi.org/10.1016/j.lithos.2014.11.021.

Klemetti, E.W. and Clynne, M.A., 2014. Localized Rejuvenation of a Crystal Mush Recorded in Zircon Temporal and Compositional Variation at the Lassen Volcanic Center, Norther California, PLoS ONE 9(12). https://doi.org/10.1371/journal.pone.0113157.

Ludwig, K.R., 2001, Squid 1.0--A user's manual: Berkeley, California, Berkeley Geochronology Center, Special Publication No. 2, 21 p.

Ludwig, K. R. (2003). *User's Manual for Isoplot 3.00: A Geochronological Toolkit for Microsoft Excel*.

McDougall, I., Harrison M.T., 1999. Geochronology and Thermochronology by the $^{40}Ar/^{39}Ar$ Method: Oxford University Press 1999.

McKay, M.P., Jackson, W.T., Hessler, A.M., 2018. Tectonic stress regime recorded by zircon Th/U. Gondwana Res. 57, 1-9. https://doi.org/10.1016/j.gr.2018.01.004.

Michelfelder, G.S., Feeley, T.C., Wilder, A.D., Klemetti, E.W., 2013. Modification of the Continental Crust by Subduction Zone Magmatism and Vice-Versa: Across-Strike Geochemical Variations of Silicic Lavas from Individual Eruptive Centers in the Andean Central Volcanic Zone. Geosciences 3, 633-667. https://doi.org/10.3390/geosciences3040633.

Rentz, S.P., Michelfelder, G.S., Coble, M.A., and Salings, E., 2018. U-Pb zircon geochronology of calc-alkaline ash-flow tuff units in the Mongollon-Datil volcanic field, southern New Mexico: Geologic Society of America 538, 409-434.

Salisbury, M.J., Jicha, B.R., de Silva, S.L., Singer, B.S., Jiménez, N.C., Ort, M.H., 2011. $^{40}Ar/^{39}Ar$ chronostratigraphy of Altiplano-Puna volcanic complex ignimbrites reveals the development of a major magmatic province. GSA Bulletin 123, 821-840. https://doi.org/10.1130/B30280.1.

Samperton, K.M., Schoene, B., Cottle, J.M., Keller, B.C., Crowley, J.L., Schmitz, M.D., 2015. Magma emplacement differentiation and cooling in the middle crust: Integrated zircon geochronological-geochemical consraints from the Bergell Intrusion, Central Alps. Chemical Geology 417, 322-340. https://doi.org/10.1016/j.chemgeo.2015.10.024.

Scott, E.M., Allen, M.B., Macpherson, C.G., McCaffrey, K.J.W., Davidson, J.P., Saville, C., Ducea, M.N., 2018. Andean surface uplift constrained by radiogenic isotopes of arc lavas. Nat. Commun. 9, 969. https://doi.org/10.1038/s41467-018-03173-4.

Sun, S., and McDonough, W.F., 1989. Chemical and isotopic systematics of oceanic basalts: implications for mantle composition and processes. Geological Society, London, Special Publications 42, 313-345. https://doi.org/10.1144/GSL.SP.1989.042.01.19.

Thorpe, R.S., Francis, P.W., 1979. Variations in Andean andesite compositions and their petrogenetic significance. Tectonophysics 57, 53-70. https://doi.org/10.1016/0040-1951(79)90101-X.

Tierney, C.R., Schmitt, A.K., Lovera, O.M., de Silva, S.L., 2016. Voluminous plutonism during volcanic quiescence revealed by thermochemical modeling of zircon. Geology 44, 683-686. https://doi.org/10.1130/G37968.1.

Tilling I., R. 2009. Volcanism and associated hazards: the Andean perspective. Advances in Geosciences 22, 125-137. https://doi.org/10.5194/adgeo-22-125-2009.

Vezzoli, L., Tibaldi, A., Renzulli, A., Menna, M., Flude, S., 2008. Faulting-assisted lateral collapses and influence on shallow magma feeding system at Ollagüe volcano (Central Volcanic Zone, Chile-Bolivia Andes): J. Volcanol. Geotherm. Res. 171, 137-159. https://doi.org/10.1016/j.jvolgeores.2007.11.015.

Wörner, G., Hammerschmidt, K., Henjes-Kunst, F., Lezaun, J., Wilke, H., 2000. Geochronology ($^{40}Ar/^{39}Ar$, K-Ar and He-exposure ages) of Cenozoic magmatic rocks from Northern Chile (18-22°S): implications for magmatism and tectonic evolution of the central Andes. Revista geológica de Chile 27, 205-240. http://dx.doi.org/10.4067/S0716-02082000000200004.

Table 1. $^{40}Ar/^{39}Ar$ eruption ages of Biotite and Hornblende from Ollagüe Volcano

Sample	Age (Ma)	Uncertainty (1σ)	MSWD*	Integrated age (Ma)
Biotite				
OLA-9006	0.81	0.007	1.7	0.79 ± 0.07
OLA-9007	0.838	0.018	1.89	0.80 ± 0.04
OLA-9041	0.88	0.04	4.9	0.82 ± 0.03
Hornblende				
OLA-9006	1.1	0.08	12.82	1.28 ± 0.12
OLA-9007	1.32	0.1	8.31	1.25 ± 0.16
OLA-9041	0.84	0.13	0.78	1.01 ± 0.13

* Mean standard weight of the deviants

Table 2. Mean U-Pb ages of zircon cores and rims

Sample	Age (Ma)	Uncertainty (1σ)	MSWD*	n	Eruption Age (Ma)**
OLA-9006	0.769	0.034	1.8	39 of 40	0.79 ± 0.07
OLA-9007	0.749	0.038	1.6	20 of 22	0.80 ± 0.04
OLA-9034	0.63	0.11	2.5	11 of 14	-
OLA-9041	0.821	0.054	2.6	27 of 28	0.82 ± 0.03
OLA-9046	0.81	0.1	2.2	9 of 12	-
Cores					
OLA-9006	0.757	0.049	2	20 of 21	0.79 ± 0.07
OLA-9007	0.782	0.049	1.5	10 of 12	0.80 ± 0.04
OLA-9034	0.7	0.1	1.3	6 of 7	-
OLA-9041	0.82	0.056	2.7	15 of 15	0.82 ± 0.03
OLA-9046	0.765	0.067	1.5	5 of 5	-
Rims					
OLA-9006	0.784	0.05	1.7	18 of 18	0.79 ± 0.07
OLA-9007	0.73	0.037	1.5	10 of 10	0.80 ± 0.04
OLA-9034	0.59	0.18	3.6	5 of 7	-
OLA-9041	0.824	0.07	2.5	12 of 13	0.82 ± 0.03
OLA-9046	0.97	0.12	1.15	4 of 4	-

* Mean standard weight of the deviants
** Biotite integrated eruption age

Table 3. Trace element analysis of select zircon cores (xx.1) and rims (xx.2)

	OLA-9006 1.1	OLA-9006 1.2	OLA-9007 9.1	OLA-9007 9.2	OLA-9034 2.1	OLA-9034 2.2	OLA-9041 15.1	OLA-9041 15.2	OLA-9046 4.1	OLA-9046 4.2
48Ti	5.2	5.4	4.9	6.1	4.0	6.3	5.1	6.5	21.5	6.0
49Ti	5.2	5.6	5.2	6.2	4.0	6.7	5.1	6.6	20.7	6.1
Fe	4.53	4.21	5.99	4.36	5.44	5.05	4.25	7.51	7.27	4.82
Y	627	702	1212	1345	417	571	594	753	1322	628
La	0.008	0.004	0.038	0.006	0.182	0.068	0.004	0.007	0.134	0.006
Ce	13.7	19.3	55.8	52.7	10.5	16.2	13.7	14.3	51.7	21.3
Nd	2.00	1.33	2.94	2.83	1.42	1.66	0.88	1.06	39.80	1.26
Sm	3.61	2.06	4.85	5.24	1.42	1.55	1.86	2.02	38.86	2.10
Eu	1.40	0.88	1.86	1.84	0.56	0.65	0.79	0.78	17.28	0.87
Gd	16.0	11.5	29.3	32.2	6.6	8.4	10.7	12.4	122.1	11.9
Dy	55	55	112	135	34	38	47	43	181	48
Er	77	96	146	178	56	80	71	96	119	84
Yb	152	200	270	314	125	171	173	212	128	173
Hf	10583	10308	10840	11430	8304	9890	11219	11346	10752	11123
Eu/Eu*	0.562	0.548	0.477	0.433	0.556	0.547	0.542	0.477	0.765	0.531
Yb/Gd	9.5	17.4	9.2	9.8	19.1	20.3	16.1	17.2	1.0	14.5

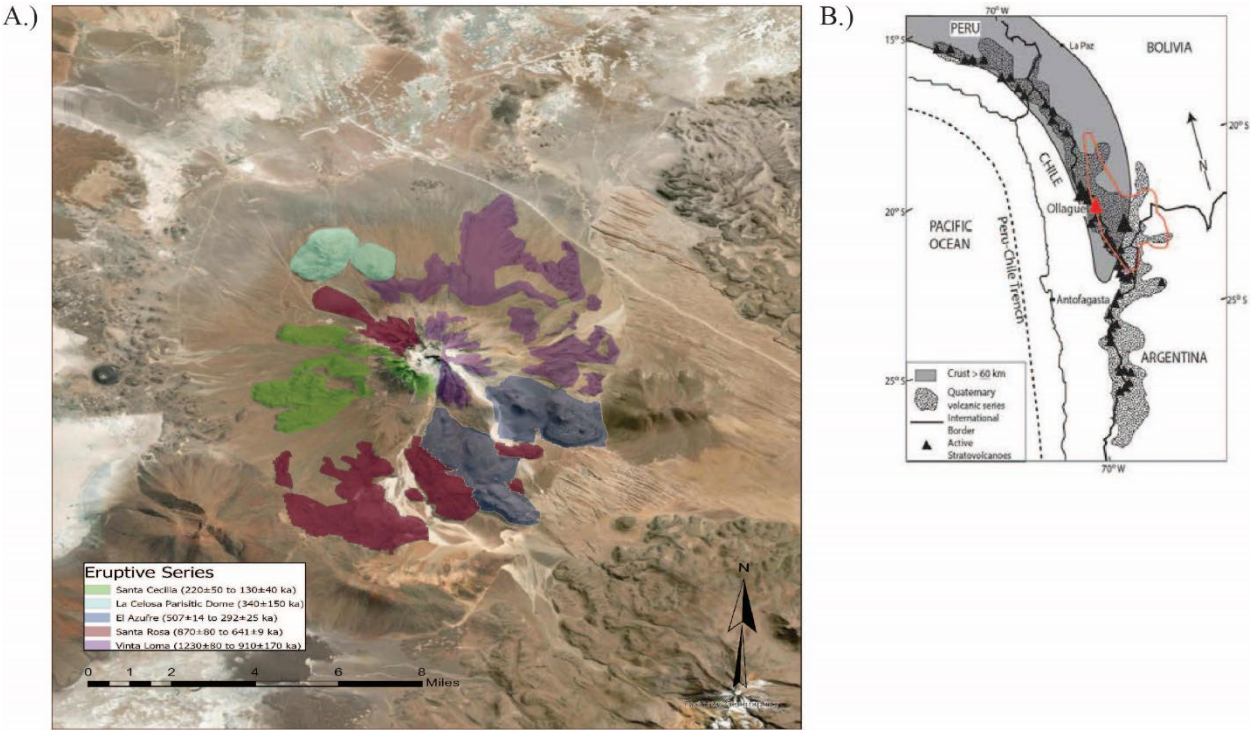

Figure 1: (A) Geologic map of Ollagüe, a composite volcano primarily active from 1,200ka to 130ka in the arc front of the CVZ drafted in ArcGIS modified from Feeley and Davidson (1994) and Vezzoli et al., (2008). Figure 1B: Location map showing multiple volcanic centers within the CVZ including Ollagüe (red) on the Chile-Bolivian Border. The APMB thought to be affecting magma storage conditions of Ollagüe is outlined in orange.

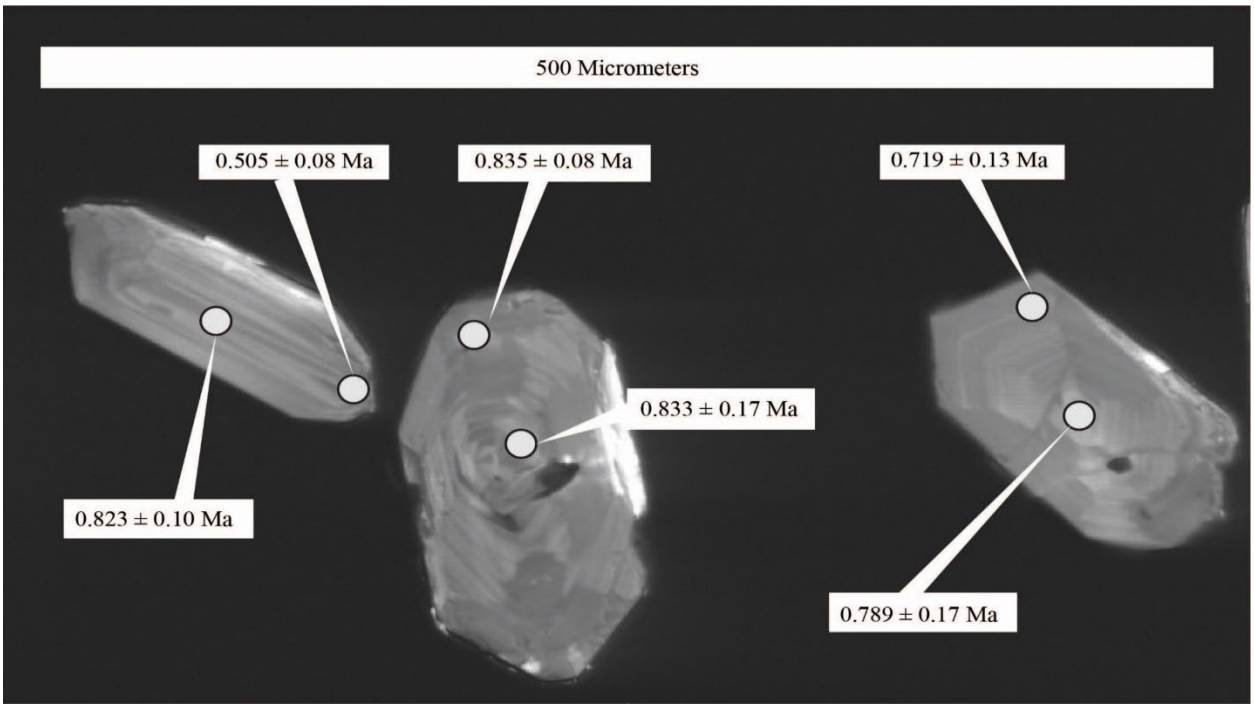

Figure 2: $^{206}Pb/^{238}U$ ages on top of cathodoluminescence images of zircon from sample OLA-9006 taken on a JEOL JSM-IT500HP SEM.

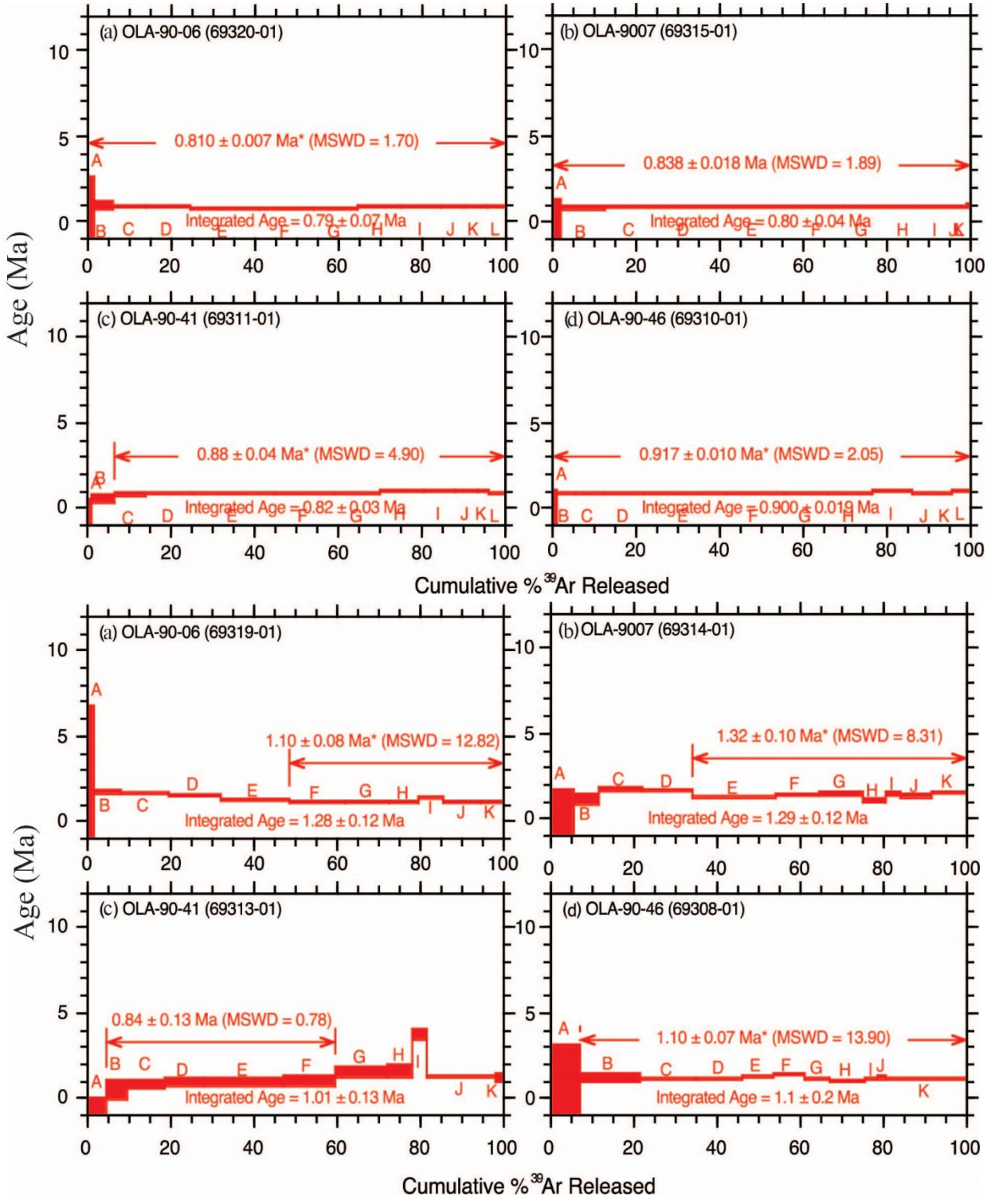

Figure 3: Biotite (top) and hornblende (Bottom) $^{40}Ar/^{39}Ar$ eruption age plateaus.

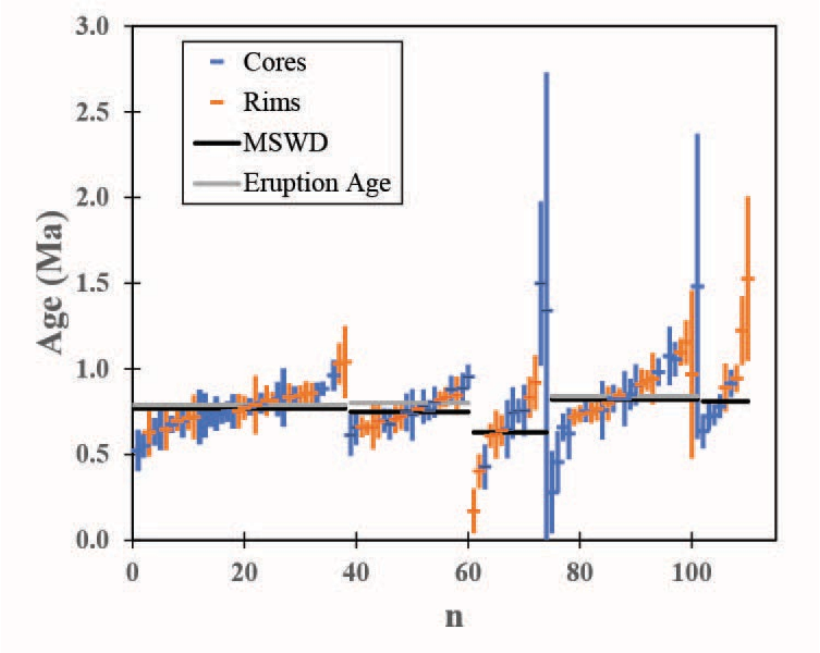

Figure 4: U-Pb age plots and $^{40}Ar/^{39}Ar$ eruption ages in millions of years from available zircons of five representative samples from Ollagüe. From left to right OLA-9006, OLA-9007, OLA-9034, OLA-9041, and OLA-9046.

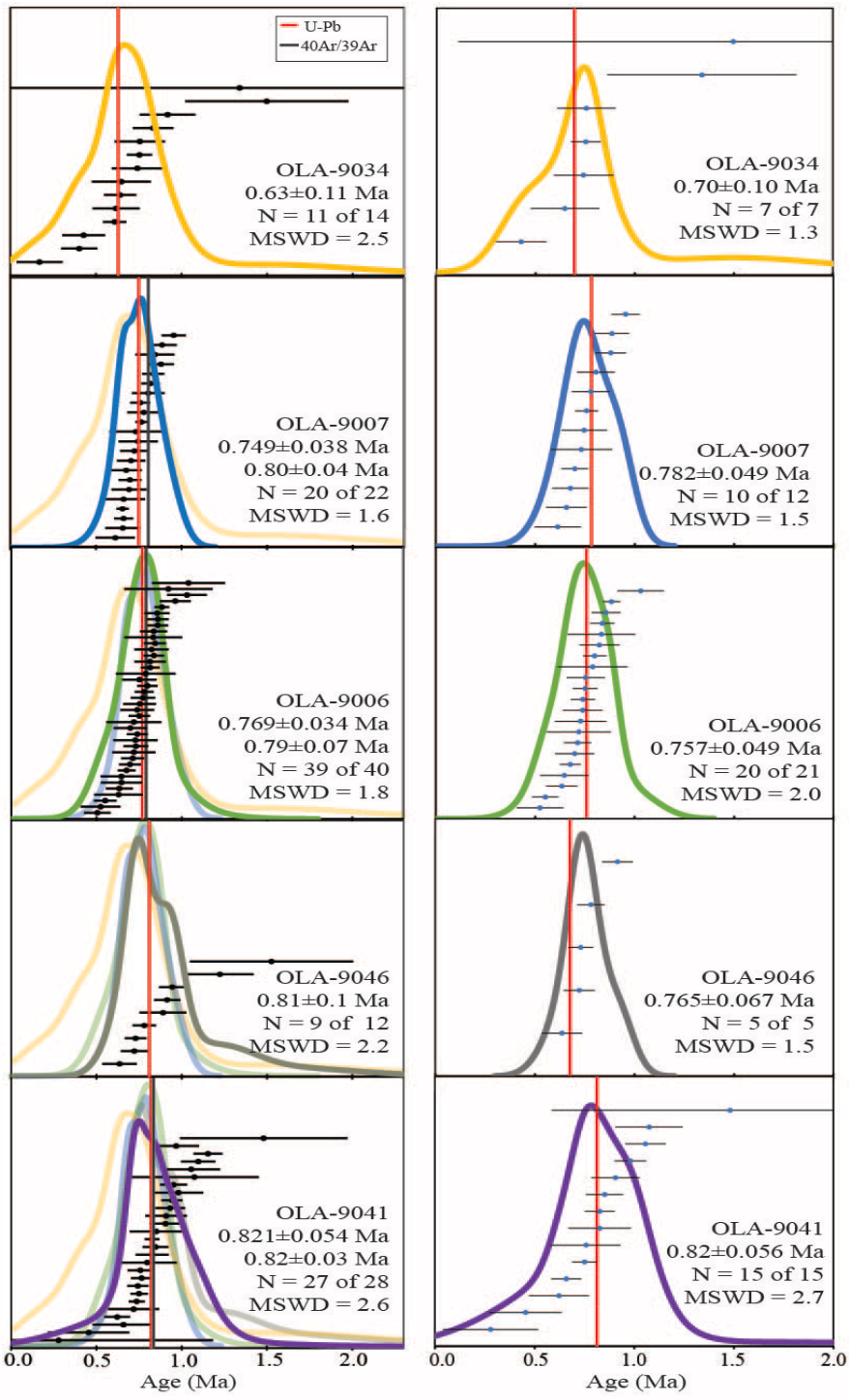

Figure 5: Rank order plots (ROP) and zircon $^{206}Pb/^{238}U$ ages as probability density functions (PDF) curves for available zircon from five samples representing Ollagüe. Samples rank ordered from oldest to youngest bottom to top of cores and rims (left) and cores (right). Ages stated are weighted mean and 1σ for the dominate peaks. $^{40}Ar/^{39}Ar$ ages are presented for OLA-9006, 9007, and 9041. MSWD is mean square of weighted deviates.

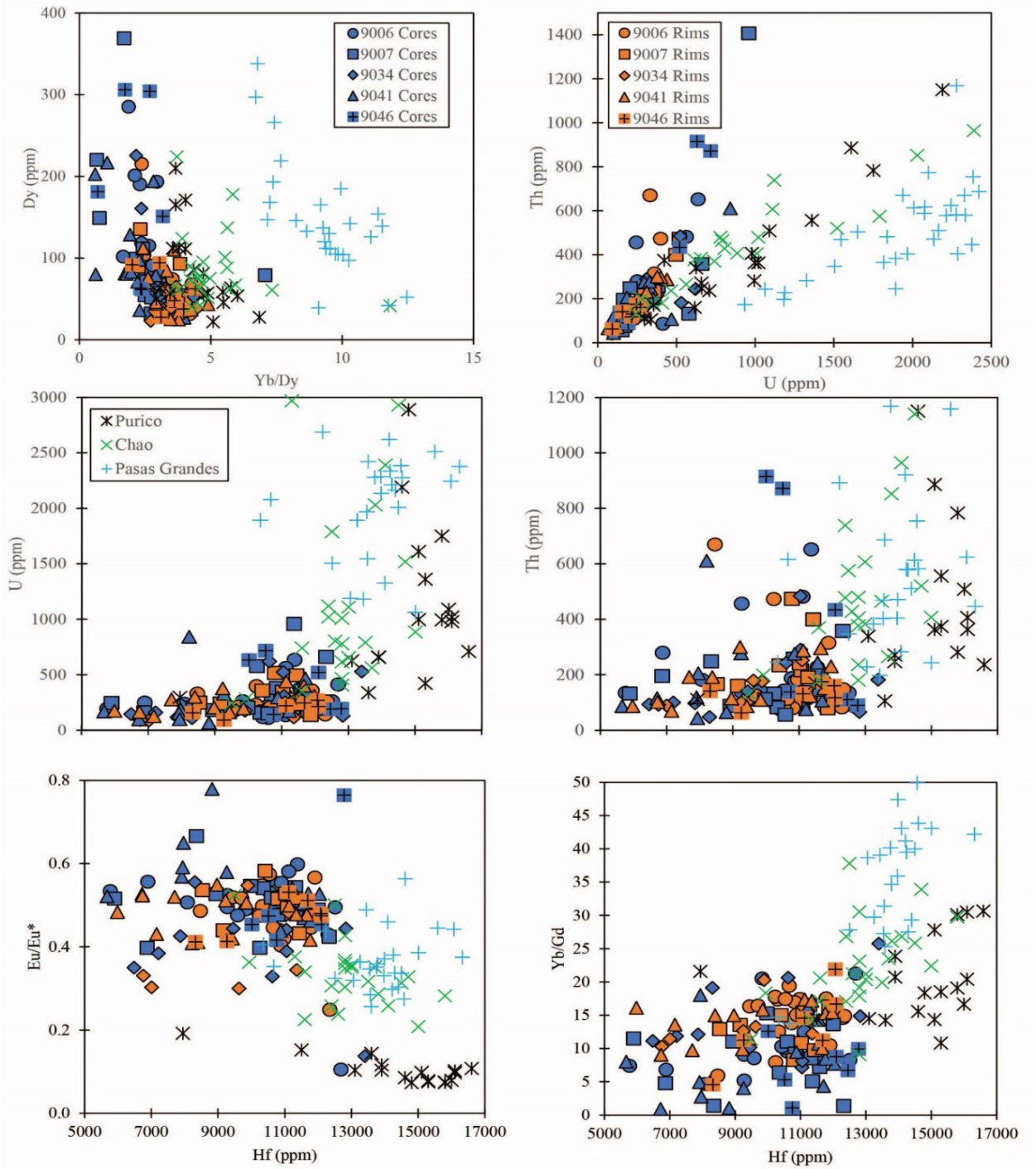

Figure 6: Secondary ionization mass spectrometry-determined trace elements in zircon from the five samples representing Ollagüe compared to trace element data from Purico (Kern et al., 2016), Chao (Tierney et al., 2016), and Passas Grandes (Kaiser et al., 2016). Top left, Dy concentrations versus Yb/Dy values. Top right, Th versus U concentrations. Middle left, U versus Hf concentrations. Middle right, Th versus Hf concentrations. Bottom left, Eu/Eu* values versus Hf concentrations. Bottom right, Yb/Gd values versus Hf concentrations.

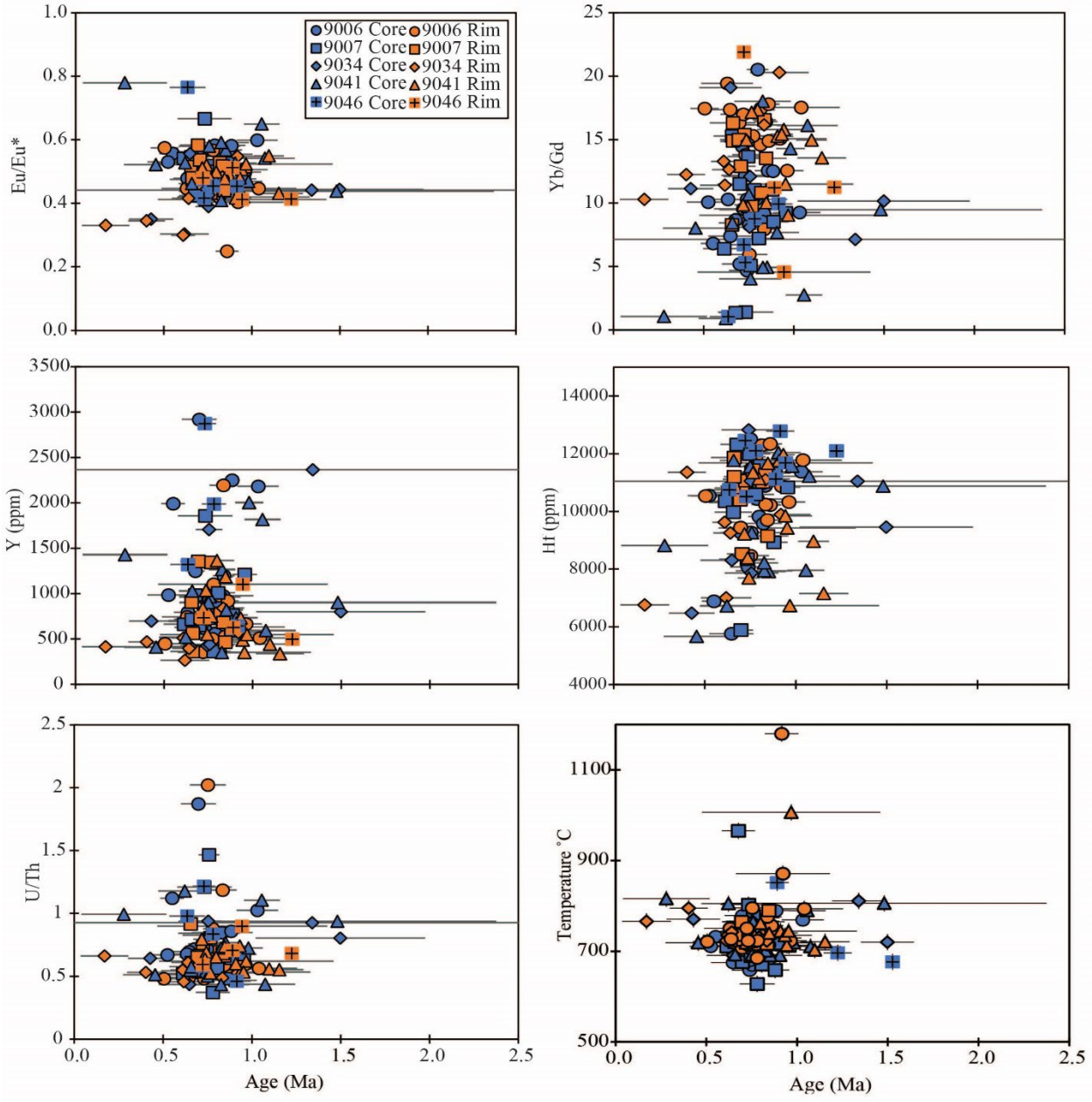

Figure 7: Trace element ratios and concentrations of Eu/Eu*, U/Th, Yb/Gd, Y, and Hf as well as Titanium-in zircon temperatures calculated plotted against age in millions of years with 1σ error.

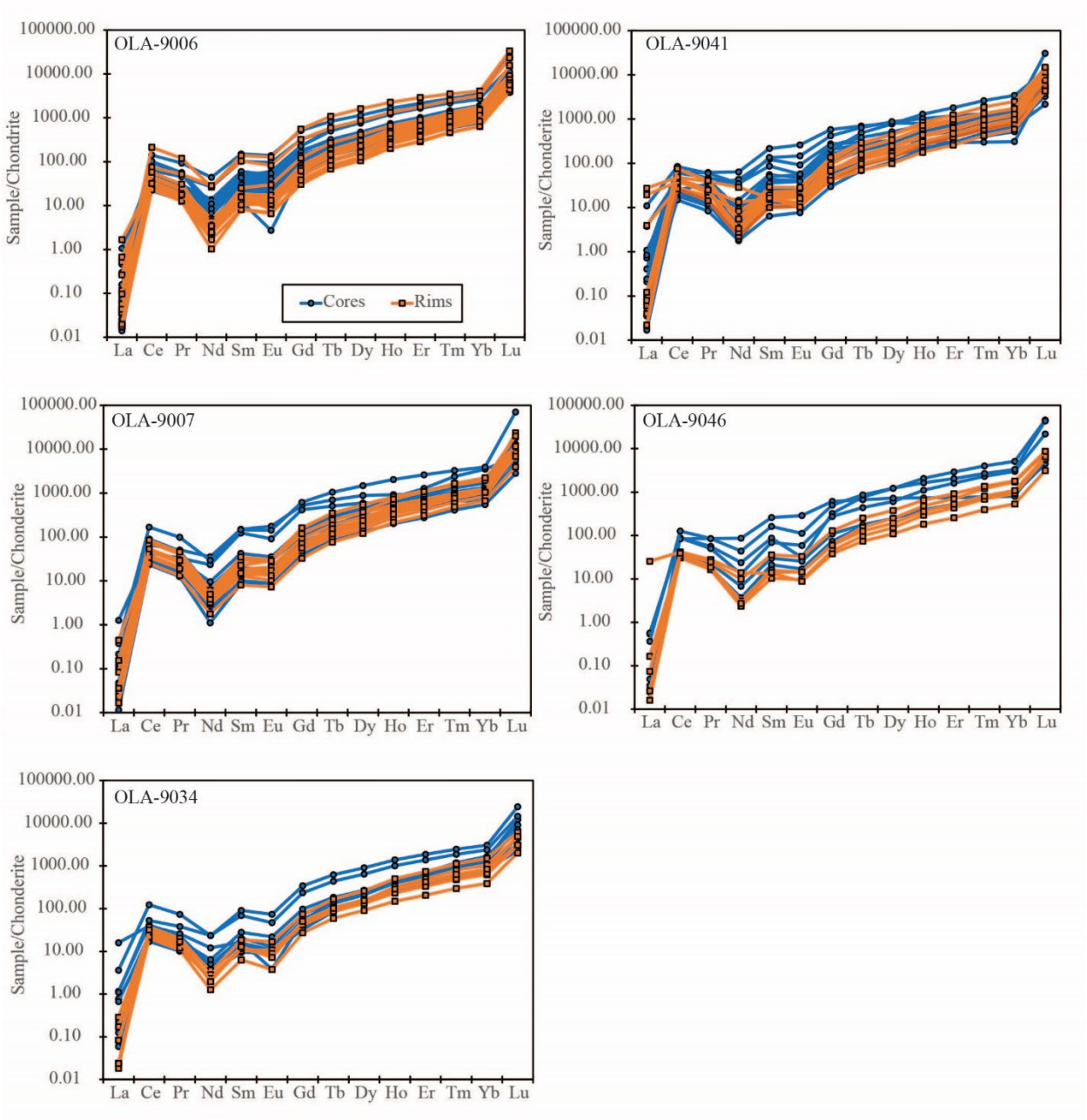

Figure 8: Rare earth element (REE) plots (light to heavy) of Zircon from the volcanic rocks of Ollagüe.

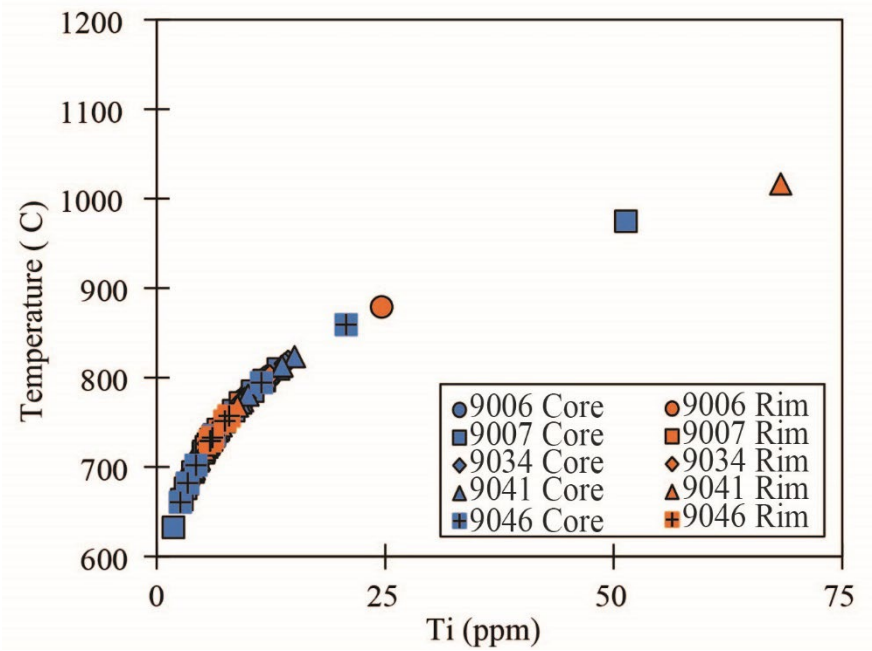

Figure 9: Ti-in-Zircon temperatures plotted against Ti (ppm) content.

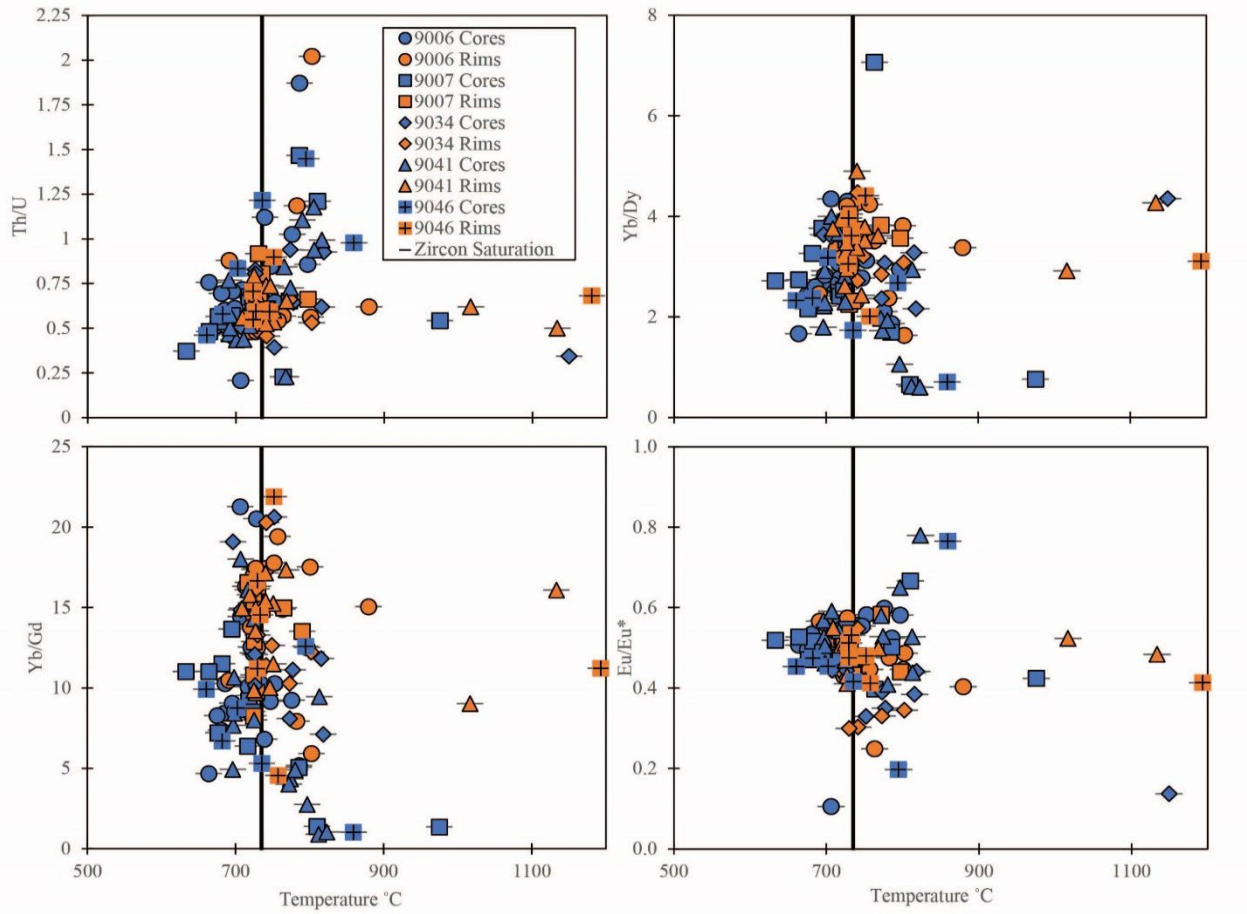

Figure 10: Ratios of Th/U, Yb/Dy, Yb/Gd, and Eu/Eu* plotted against Ti-in zircon temperatures with the zircon saturation temperature represented by the solid black line.

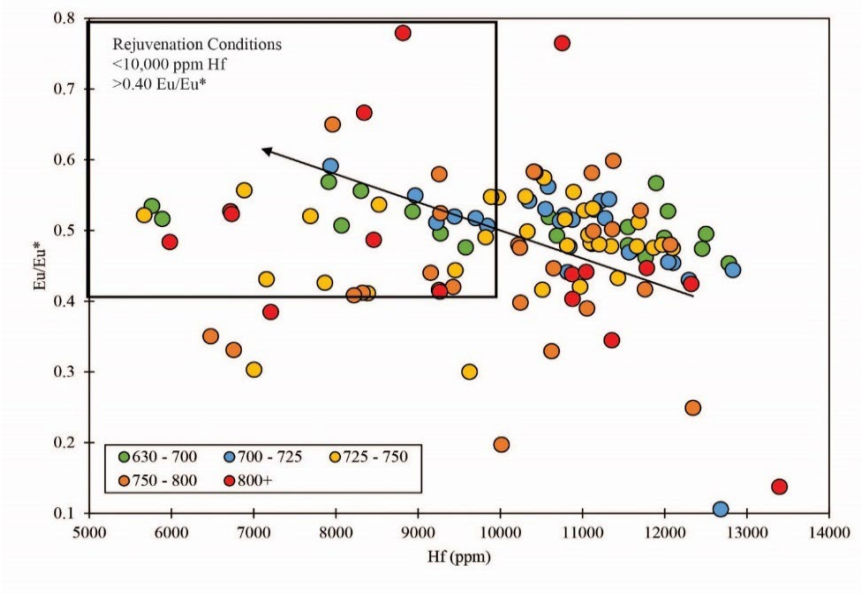

Figure 11: Eu/Eu* versus Hf (ppm) split by Ti-in zircon temperatures. Hotter magmatic conditions suggestive of mush remobilization or rejuvenation is contained by the black box. Eu/Eu* values increase with decreasing Hf content.

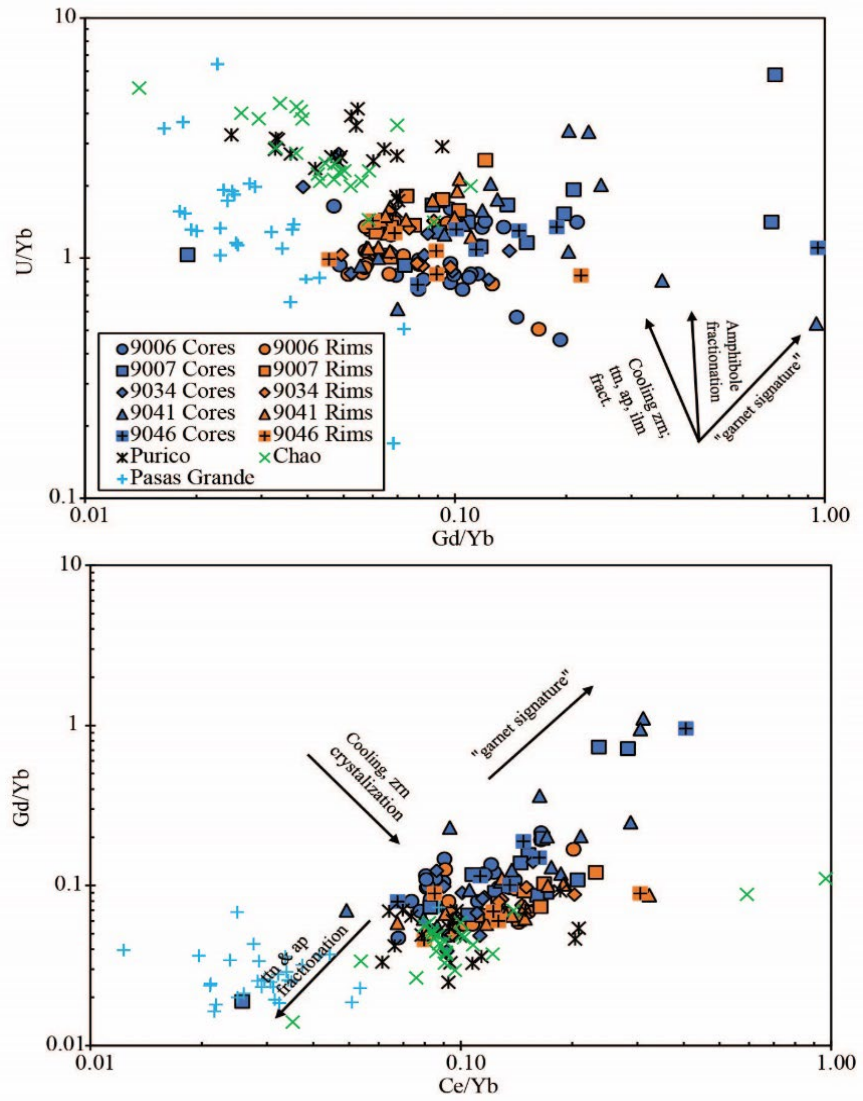

Figure 12: Petrogenetic interpretation diagram for zircon utilizing U/Yb, Gd/Yb, and Ce/Yb characteristics.

MANUSCRIPT 2: GEOCHEMICAL INVESTIGATION OF INTERMEDIATE LAVAS: USING PLAGIOCLASE TO DECIPHER THE MAGMA PLUMBING SYSTEM OF VOLCÁN OLLAGÜE, CHILE-BOLIVIA CENTRAL ANDES

Abstract

Volcanic plumbing systems and their pre-eruptive processes are crucial to understanding the genesis of intermediate-composition lavas. Textural and geochemical analyses of plagioclase feldspar are effective tools in the construction of plumbing architectures. The Central Volcanic Zone of the Central Andes is host to one of the largest magma reservoirs in the world, the Altiplano-Puna Magma Body, and its effects on Volcan Ollagüe's evolutionary history are unclear. Micro-textures reveal four distinct populations of plagioclase. Group 1 shows fine-scaled oscillatory zoning and resorption, Group 2 shows similar resorption in the crystal interior but also shows a prominent lighter patchy resorption to finely sieved rims on the phenocrysts, Group 3 shows coarse spongy sieving to patchy textures around the cores, and Group 4 with no evidence of resorption or spongy textures and exhibit euhedral crystal faces and weak oscillatory zoning. Geochemically, plagioclase cores from Ollagüe show a more mafic endmember in the Vinta Loma flows and a more felsic endmember in the La Celosa parasitic dome. Coupling the textures and geochemical data suggests a complex plumbing system with three separate chambers spanning the volcanic activity and displaying possible influence from the Altiplano-Puna Magma Body.

Introduction

Understanding the genesis, pre-eruptive dynamics, and processes influencing intermediate-composition lavas remains a primary task in modern petrology and volcanology. Magma mixing is a process that is thought to be a primary explanation, as hybridizing of felsic and mafic materials has been attributed to triggering eruption events (Kent et al., 2010; Conway et al., 2020). However, within subduction zones, the ascension of subduction zone magmas through a thick continental crust can create a melting-assimilation-storage-homogenization (MASH) zone that can evolve melt and crustal material to constrain igneous characteristics (Michelfelder et al., 2013; Delph et al., 2017). Plagioclase is one of the most ubiquitous mineral phases used for the documentation of magmatic processes and magmatic plumbing systems due

to the phase's stability over a wide range of physical and chemical conditions and sensitivity to changes in thermal parameters during growth, storage, and transport (Renjith, 2014; Viccaro et al., 2016). The Central Andes is home to the longest continental-margin volcanic arc on earth, where the Nazca plate subducts beneath the South American Plate; this is referred to as the Andean Central Volcanic Zone (Tilling, 2009).

This study focuses on Volcán Ollagüe, a composite volcano along the arc front of the Central Volcanic Zone (CVZ). Further, this zone is home to one of the largest geophysically imaged crustal magma reservoirs (>500,000 km3) in the world, the Altiplano-Puna Magma Body (APMB; Fig.1; Chmielowski and Zandt, 1999; Zandt et al., 2003; Ward et al., 2014; Perkins et al. 2016). The magmatic source and plumbing system of Ollagüe are not clearly defined. An initial wide range of compositions exhibited by the volcano becoming more homogenous over time could be linked to the influence of a regional magma body, the APMB. Here I test the hypothesis that the APMB's influence on Ollagüe becomes greater over time. To test this hypothesis, I present major and trace element mineral chemistry, and textural analyses of plagioclase utilizing electron probe micro analyzer (EPMA) and laser ablation inductively coupled plasma mass spectrometry (LA-ICP MS). I use these data to suggest a model of the evolution of the sub-volcanic plumbing system and magma storage conditions at Ollagüe and determine its relation to the APMB.

Background

The CVZ encases a substantial amount of volcanism with 20 identified caldera complexes, silicic ignimbrites, and an estimated 50 active or recently active composite volcanoes in the last 10 Ma (Michelfelder et al., 2013). East-southeast of the CVZ arc front and straddling the Chilean-Bolivian border is the isolated volcano, Ollagüe (Fig. 1). Published data for Ollagüe

suggests the volcano has a multistage eruptive history (Feeley et al., 1993; Feeley and Hacker, 1995; Klemetti and Grunder, 2008; and Vezzoli et al. 2008). Approximately 80-90 km^3 of basaltic andesite to dacite lavas have erupted from Ollagüe, spanning from 1200 ka to 130 ka, and were defined into four distinct series: the Vinta Loma, Chaska Orkho, post-collapse series, and the La Celosa (Feeley et al., 1993; Vezzoli et al., 2008). Vezzoli et al. (2008) revised Ollagüe's eruptive history with the addition of new eruption ages as the Vinta Loma (1200 ka to 910 ka), the Santa Rosa (870 ka to 641 ka), the El Azufre (507 ka to 292 ka) which includes the La Celosa parasitic dome and the inclusion bearing Chaska Orkho stages, and the Santa Cecilia (220 ka to 130 ka). Vezzoli et al. (2008) are the definitions used for this study.

The Vinta Loma series (Fig. 1) represents the dominant stage of cone growth at Volcán Ollagüe, cropping out in the northern and eastern sectors of the volcano (Vezzoli et al., 2008). The Vinta Loma consists of two-pyroxene andesite and dacite lavas. Most Vinta Loma lavas are porphyritic to seriate, sparsely glomeroporphyritic with 22 to 41% phenocrysts of plagioclase (Feeley et al., 1993). Rare quartz, biotite, and olivine are present in some lavas and, in most cases, are probably xenocrystic (Feeley et al., 1993). Microphenocrysts of plagioclase, pyroxene, and Fe-Ti oxides are abundant in the groundmass of the Vinta Loma lavas, but amphibole is absent in the groundmass (Feely et al., 1993). These lavas have erupted from the central vent of the volcano's older cone showing outward dips and radial distribution (Vezzoli et al., 2008).

The Santa Rosa series comprises a sequence of summit lava flows, pyroclastic deposits from the northern summit cinder cone, and several lateral lava flows; this series concludes with a debris avalanche (Vezzoli et al., 2008). The lavas from Santa Rosa range from amphibole-biotite dacites to andesites and basaltic andesites.

The El Azufre series is mainly comprised of andesitic and dacitic lavas and consists of a sequence of fresh lava beds around 200m thick, with a sub-horizontal attitude, at the base of the series and is interpreted as the products of a summit lava lake (Vezzoli et al., 2008). The upper summit lava flow is two-pyroxene andesite that reaches the southern flank. The south summit cinder cone makes up the south peak of Ollagüe and is composed of stratified, pumiceous pyroclastic deposits (Vezzoli et al., 2008). Petrographically, textures range from porphyritic-seriate to nearly vitrophyric. Plagioclase is the most common phase in the andesites and dacites and is accompanied by lesser amphibole, biotite, pyroxene, and Fe-Ti oxides (Feeley et al., 1993). A few of the more silicic samples contain trace quartz and titanite. Groundmass textures range from hypocrystalline to trachytic, defined by an alignment of stubby plagioclase microlites (Feeley et al., 1993). The La Celosa parasitic dome consists of dacitic lavas that erupted on the lower northwest flank of Ollagüe (Fig. 1; Feeley et al., 1993). Textures of the La Celosa rocks range from porphyritic to vitrophyric. Plagioclase is the most common phenocrystic phase, followed by amphibole, biotite, and Fe-Ti oxides; however, pyroxene is generally absent from La Celosa rocks (Feeley et al., 1993).

The Santa Cecilia series is defined by a debris avalanche event that resulted from sector collapse of the west flank of Ollagüe (Vezzoli et al., 2008). Volcanic rocks are compositionally defined by a range of andesite lava domes and by voluminous andesite lateral lava flows found on the southwest flank of the edifice (Vezzoli et al., 2008). In all lavas, crystal contents range from 30 to 42% plagioclase (Feeley et al., 1993). Plagioclase dominates the mode as both phenocryst and as groundmass phase. In the older lavas on the western flank, pyroxenes are more abundant than hornblende and biotite (Feeley et al., 1993). These flows are overlain by shorter, amphibole- biotite-bearing flows (Feeley et al., 1993). The lateral lava flows were extruded from

vents located downslope of the lava dome range, forming a complex lava field (Vezzoli et al., 2008).

Analytical Methods

Six polished thin sections representing the stratigraphy of Ollagüe were analyzed via petrographic microscope to target plagioclase feldspar zoning profiles. A range of 20-25 phenocrysts per sample were selected for textural and major element analyses at the University of Iowa via electron probe microanalyzer (EPMA) based on the complexities of the zoning profiles. Backscatter Electron (BSE) imaging and chemical analyses was conducted on a JEOL JXA-8230 superprobe equipped with five spectrometers using a voltage of 15 kV, a working distance of 10-12 mm, and variable magnification depending on the desired resolution of the phenocryst. EPMA analysis for major elements (Si, Al, Na, Mg, Ca, K, Ba, Fe and Ti) was conducted in conjunction with the BSE on the plagioclase phenocrysts. Operating conditions during analyses consisted of an accelerating voltage of 15 kV, a beam current of 20 nA, with a focused beam of 1 μm, utilizing UI Block 1 mineral standards labradorite (USNM 115900) for Na, Al, Si, and Ca, and microcline (USNM 143966) for Al, Si, and K. Plagioclase phenocrysts were analyzed utilizing spot analysis on textures observed within the plagioclase. A range of two to ten spots were analyzed per phenocryst.

Trace element contents (Li, Mg, Si, Ca, Sc, Ti, Cr, Fe, Zn, Rb, Sr, Y, Zr, Nb, Cs, Ba, La, Ce, Pr, Nd, Sm, Eu, Gd, Tb, Dy, Ho, Er, Tm, Yb, Lu, Hf, Pb, Th, and U) of ten plagioclase phenocrysts per sample were analyzed via laser ablation inductively coupled plasma mass-spectrometry (LA-ICPMS). LA-ICPMS analyses were performed using a Thermo Scientific iCapQ Quadrupole Mass Spectrometer and ESI NWR 193nm laser ablation system at the University of Arkansas. A detailed description of the techniques used can be found in Kent et al.

(2006) and Loewen and Kent (2012). Laser ablation points were selected from BSE images showing complex micro textures and zoning. Laser ablation conditions for analyses include a frequency of 10 Hz with a spot size of 50 μm. Reference material glass, NIST 610, and NIST 612 (Jochum et al., 2011) were used for the calibration of plagioclase, and as analytical standards for precision monitoring during repeated analysis. The ICPMS nebulizer flow rate was set to 0.84 L/min, auxiliary was set to 0.8 L/min, the helium flow rate was set to 0.8 L/min, and the cool flow was set at 14.002 L/min for the analysis. Data was reduced using Iolite4 software (Paton et al., 2011). Spot analyses were discarded from interpretations if trace element concentrations were indicative of hitting a mineral/melt inclusion within the phenocryst (ex., Fe >8,000ppm).

Results

Two samples in this study are from the Vinta Loma, one sample is from the El Azufre, one sample is from the La Celosa parasitic dome, and one sample from the Santa Cecilia. A sixth sample was analyzed, OLA-9036, from an unknown lava flow of Ollagüe. Plagioclase phenocrysts from the six lava flows analyzed show broad textural similarity. Most phenocrysts show strong chemical oscillatory zoning patterns with a select few being un-zoned or weakly zoned. However, the complexity of the zoning within the phenocrysts is rather distinct. Specifically, there are resorption surfaces in the cores, mantles, and rims, sieving in the rims, and spongy textures observed around cores and on the rims of phenocrysts. Resorption was observed in all six samples. Spongy and sieving textures were only observed within the Vinta Loma and El Azufre series samples. A dominant population of plagioclase phenocrysts (60%) exhibit resorption surfaces, rounded zoning, and fine-scale oscillatory zoning (Fig. 2). Typically, resorption in this group is seen as rounded patchy cores, with rounded irregular mantles with the

occasional truncation of zones. A second, smaller (20%) population of plagioclase phenocrysts exhibit similar resorption in the crystal interior but also show a prominent lighter patchy resorption to finely-sieved rims on the phenocrysts (Fig. 2) A third population of plagioclase crystals (10%) show coarse spongy sieving to patchy textures around the cores of the phenocrysts (Fig. 2) and are only observed in the Vinta Loma series. Finally, a fourth population of plagioclase (10%) are observed with no resorption or Spongy textures and exhibit euhedral crystal faces and weak oscillatory zoning (Fig. 2). Average trace element compositions of the four distinct groups showing more mafic core compositions in Vinta Loma cores and more felsic compositions in La Celosa cores are presented in Table 1.

Plagioclase cores analyzed on the EPMA range from An_{25-74}; Fe: 0.18-0.68 wt.% oxide; Mg: 0.002-0.061 wt.% oxide; Ba: 0.003-0.11 wt.% oxide; Ti: 0.002-0.079 wt.% oxide. Mantles range from An_{24-73}; Fe: 0.19-0.67 wt.% oxide; Mg: 0.001-0.067 wt.% oxide; Ba: 0.002-0.12 wt.% oxide; Ti: 0.002-0.09 wt.% oxide. Rims range from An_{19-60}; Fe: 0.19-0.77 wt.% oxide; Mg: 0.003-0.07 wt.% oxide; Ba: 0.007-0.12 wt.% oxide; and Ti: 0.002-0.85 wt.% oxide (Fig 3). The full list of major element data of plagioclase cores, mantles, and rims can be viewed in Appendix B.

Plagioclase cores analyzed on the LA-ICPMS from Ollagüe range from An_{30-62}; Sr: 1,060-2,300ppm; Ba: 115-1,630ppm; Fe: 1,100-3,980ppm; Mg: 190-1,400ppm; and Eu/Eu* 0.4-35 values. Ratios of La/Nd range from 1-4.72 and ratios of Nd/Dy range from 0.0001-0.15. Mantles of phenocryst analyzed range from An_{24-68}; Sr: 270-2,300ppm; Ba: 270-2,350ppm; Fe: 570-3,700ppm; Mg: 75-1,350ppm; and Eu/Eu* 0.35-58. Mantle ratios of La/Nd range from 0.5-9 and ratios of Nd/Dy range from 0.001-0.23. Rims analyzed range from An_{25-59}; Sr: 600-2,450ppm; Ba: 185-2050ppm; Fe: 825-3350ppm; Mg: 900-1,510ppm; and Eu/Eu* 0.38-18 (Fig

4). Rims ratios of La/Nd range from 0.5-6.26 and ratios of Nd/Dy range from 0.0001-0.2. The full list of trace element data of plagioclase cores, mantles, and rims can be viewed in Appendix C.

Compositions from the Vinta Loma series cores show three populations of Molar Anorthite % (An %). A calcic group (53-63 An %; 1,900-2,400ppm Sr), an intermediate group (45-46 An %; 1,200-1,700ppm Sr), and a sodic group (35-37 An %; 1,050-1,200ppm Sr; Fig. 4). Core compositions from the La Celosa parasitic dome plot in the sodic range as well (30-36 An %). Cores from the remaining series show some overlap with the sodic and calcic groups, but ultimately fill in the intermediate area between the two, leaning closer to the sodic group. Mantles analyzed show similar grouping to the cores, showing a calcic and sodic group with an intermediate ground (Fig. 4). The rim analyses range from 25-59 % Molar An, however, the analyses are densely packed between 35-50% Molar An showing a more intermediate grouping of the rims (Fig. 4).

Iron and magnesium content of the Vinta Loma cores display similar trends to the Molar An % groups, with a high Fe high Mg group (1,730-1,850ppm Fe; 390-425ppm Mg), intermediate group (1,440-1,620ppm Fe; 210-360ppm Mg), and a lower group (1,110-1,300ppm Fe; 190-275ppm Mg; Fig. 4). Cores from the La Celosa Series fall below all other cores in a depleted Fe group (500-725ppm Fe; 40-70ppm Mg). Cores, mantles, and rims from the remaining series fill in the intermediate group. However, a small population of mantles from the El Azufre also fall into the depleted Fe group.

Cores in the Vinta Loma series display two trends of Ba, a high Sr low Ba population (1,900 to 2,400ppm Sr; 270-525ppm Ba) trending linearly, and a lower Sr with higher Ba trend (1,130-2,020ppm Sr; 650-1,630ppm Ba; Fig. 4). Cores from the remaining series plot similarly to

the higher Ba trending cores. Mantles and rims mimic the liner trend of lower Sr higher Ba with some higher variation and very little overlap of the high Sr low Ba trend (Fig. 4).

Chondrite-normalized REE patterns show diversity throughout the four plagioclase groups (Fig. 5). Group one, light-REEs (left side) have a steep curve, steep positive Eu anomalies, and heavy-REEs (right side) showing variation. Group two REE plots show a combination of steep to shallow positive Eu anomalies within individual crystals. Further, the partitioning of the light and heavy-REEs shows more variation within individual crystals than group 1. Similar to group 2, group 3 phenocrysts show combinations of steep and shallow positive Eu anomalies within individual crystals with some variation in light and heavy partitioning. Finally, similar to group 1 plagioclase, group 4 plagioclase show steeper partitioning of light-REEs and relatively similar Eu anomalies (Fig 5).

Core-to-rim spot analyses transects on the LA-ICPMS of plagioclase phenocrysts show oscillatory chemical profiles (Fig. 6). Concentrations of Fe, Mg, Sr and Ba were pinpointed in this study as they are elements sensitive to changes in the magmatic system. When these elements are coupled together, they can be used as a proxy for melt differentiation (Renjith, 2014; Shane, 2015). Iron and Mg typically show similar trends from the cores to rims of phenocrysts. However, there are crystals where an inverse relationship of Fe and Mg is present, this trend is only observed in the group 1 and group 4 plagioclase phenocrysts. Phenocrysts that display an inverse relationship between Fe and Mg content also display an inverse relationship between Sr and Ba contents. The phenocrysts in plagioclase groups 2 and 3 exhibit mimicking Fe and Mg trends while Sr and Ba trends are inversely related (Fig. 6).

Discussion

Micro-textures within plagioclase phenocrysts record key information about magmatic processes and storage conditions beneath Ollagüe (Renjith 2014; Coote et al. 2018). Major and trace element plagioclase geochemistry allows constraining intensive magma storage parameters such as temperatures, pressures, oxygen fugacity, and major element composition and initial H2O contents of parental melts (Claeson and Meurer, 2004). Additionally, trace element compositions of plagioclase allow insight into temperature-dependent processes within a system (Cooper and Kent, 2014). Ultimately, grouping these data helps to understand the processes of the storage conditions of Ollagüe's plumbing system.

Plagioclase from group 1 dominantly displays resorption surfaces with truncated fine scale oscillatory zoning and rounded corners. The absence of sieving/spongy textures within this plagioclase group yields strong evidence that the processes experienced are chemically dominated as opposed to decompression melting or major heating alone (Giacomoni et al., 2014). Group 1 plagioclase is suggested to have experienced heat flux and mixing of more primitive magmas into the melt, resulting in partial or heavy dissolution within the cores and interior zoning of the phenocrysts. The finer-scaled oscillatory zoning seen in many of the phenocrysts is evidence of some convection-driven process (Renjith, 2014). During convection, the zoning patterns are developed through regular variations of temperature, composition, and/or water content (Renjith, 2014). The typical geochemical profile of a group 1 phenocryst (Fig. 6) supports the idea of chemical and temperature oscillation throughout the life of the crystal. Group 1 plagioclase experienced multiple periodic injections of a more primitive melt keeping the plagioclase growth in the intermediate boundaries. This is shown by group 1 ranging from An24-62 with the majority of plagioclase phenocryst from group 1 clustering between An35-50

and Sr contents between 1,000-1,700ppm and Fe contents between 850-1,250ppm. Further, cores with resorbed surfaces and fine-scaled oscillatory zoning of group 1 interiors support a more primitive melt introduced to the system.

Group 2 plagioclase exhibits similar interior crystal resorption to group 1 phenocryst but shows bright patchy resorption to finely sieved rims. Fine-sieving textures in plagioclase indicate partial dissolution through a reaction with a more Ca-rich melt with some partial regrowth in a more chemically primitive melt showing geochemical spikes of Fe, Mg, Sr, and Ba at the rims (Renjith, 2014; Fabbro et al., 2017). The typical geochemical profile of group 2 crystals shows larger chemical changes throughout the crystal. Variations of Fe, Mg, Sr, and Ba contents show low initial concentrations decreasing outside the core, with all four elemental concentrations spiking at the rims (Fig. 6). The typical REE plot of group 2 plagioclase mimics the geochemical profile showing steep light-REE profiles and positive Eu anomalies at the cores and rims of phenocryst. However, the interior mantles contain lower light-REE and middle-REE ratios. The variation in trace element compositions across the phenocryst suggests a period of prolonged crystallization prior to mixing a hotter, more primitive melt into the system, creating sieving textures at the rim. Resorption and sieving likely occurred relatively quickly at shallow depths with H2O dissolved in the introduced melt. Previous studies have shown that the moderate presence of H2O in magma lowers the solidus of plagioclase (Nelson and Montana, 1992; Viccaro et al., 2016). It should be noted that basaltic magmas are typically not water-rich until they ascend to shallow crustal levels (<5 km; Baker and Alletti, 2012; Viccaro et al., 2016). Ultimately, this indicates that within magmas rising toward the surface, the presence of H2O assists plagioclase resorption during decompression, leading to the development of sieving textures (Viccaro et al., 2016). The injected melt likely led to an eruption event on a quick

ascent, pushing the sieving and decompression melting to occur in the conduit just before eruption (Viccaro et al., 2016).

When coarse sieving is confined to a phenocryst core, as seen in group 3, with no growth zoning, it indicates that the core had grown in an equilibrated magmatic environment (Renjith, 2014; Viccaro et al., 2016). The cores then experienced a temperature/pressure gradient likely related to the introduction of H2O volatiles, lowering the solidus of the plagioclase in the melt, allowing for the dissolution of the cores (Nelson and Montana 1992; Viccaro et al., 2016). However, the geochemical profiles show some chemical oscillation from core-to-rim, suggesting an introduction of new material periodically, possibly at low volumes (Renjith, 2014; Viccaro et al., 2016). However, the mantles and rims of the plagioclase do not display micro-textures showing evidence of partial dissolution or partial melting and suggest crystallization at, or near, chemical and thermal equilibrium. The periodic flux of new material could be slow enough to keep phenocryst from partial dissolution or melting. Geochemically and texturally, group 3 is distinct from groups 1 and 2, suggesting that it crystallized in a different setting. The higher contents of Fe and Sr suggest that the source material is more basaltic.

Group 4 crystals are like mantles and rims of Group 3 phenocrysts, suggesting crystallization while in equilibrium within their respective isolated melts (Annen et al., 2006; Renjith, 2014; Coote and Shane, 2016). Evidence of plagioclase micro textures resulting from temperature or chemical changes was not observed, and geochemical profiles of the crystals do not exhibit distinctive oscillatory spikes across crystals. Geochemically, cores from group 4 are chemically similar in that they are high in Fe and Sr, seemingly originating from similar parental materials. The mantles and rims, however, do not show the same chemical oscillation in group 4 as they do in group 3. Mantles and rims of group 4 phenocrysts show decreasing Fe, Mg, Sr, and

Ba from core to rim, which could be attributed to prolonged crystallization with little to no interference after the events of the cores and chemical zoning in group 3 (Renjith, 2014).

Magma Plumbing Model

Geochemically, Ollagüe displays two distinct end members in the Vinta Loma and the La Celosa series, with the remaining series being compositional hybrids of the end members. Comparing the geochemical analyses to those previously reported by Vezzoli et al. (2008), the evolution of Ollagüe's plumbing system becomes clearer. The Vinta Loma series marks the earliest volcanic activity at Ollagüe (1.2 ka to 910 ka; Vezzoli et al., 2008). Plagioclase in this series shows phenocryst in Groups 1, 3, and 4, containing populations of cores with calcic, intermediate, and sodic compositions. The calcic cores are geochemically distinct from all other cores analyzed, which are attributed to core inheritance in an isolated chamber (Fig. 7; Annen et al., 2006; Coote and Shane, 2016). This is further supported by Group 3 and Group 4 plagioclases showing both inherited higher calcic cores and autocrystic plagioclase that seem to have crystallized in equilibrium with a respective melt. The chemistry and textures displayed in Groups 3 and 4 are unique to the Vinta Loma series, suggesting the isolated chamber was mainly active during the early stages of Ollagüe (Fig. 7). The remaining plagioclase cores of the Vinta Loma likely were mobilized to a larger more homogenized chamber, exhibiting intermediate to sodic compositions (Fig. 7) of the remaining series where the dominant Group 1 plagioclase population is located (Giacomoni et al. 2014). The hybridizing composition signatures of Group 1 cores suggest they are autocrystic within Ollagüe's system. These data suggest that the hybridization of plagioclase phenocrysts began within the volcanic constraints of the Vinta Loma (1.2 ka to 910 ka), likely closer to the events of the Santa Rosa series (870 ka to 641 ka; Vezzoli et al., 2008). Textural and geochemical data from the Santa Rosa and El Azufre (507 ka to 292

ka; Vezzoli et al., 2008) suggest the hybridized chamber experienced periodic flux of new magmas that chemically hybridize the melt over time with multiple high-to-low volume magma mixing events.

The parasitic dome events of the La Celosa occur within the El Azufre at approximately 340 ka. Phenocrysts of the El Azufre fall into the dominant population of Group 1, showing characteristics of the hybridizing chamber. However, phenocrysts from the La Celosa dome make up the Group 2 plagioclase and geochemically exhibit the sodic endmember of the system (Fig 6). The sodic endmember of the La Celosa shows the lowest Fe and Mg content of all the series and little to no interior chemical zoning. This suggests magma from the hybridized chamber mobilized to a new chamber within the time constraints of the Santa Rosa (870 ka to 641 ka) or El Azufre (507 ka to 292 ka), working as an extension of the hybridized chamber where it granted extended periods of crystallization (Fig. 7; Vezzoli et al., 2008; Coote and Shane, 2016). This secondary chamber likely had limited outward interference, suggested by autocrystic cores, which eventually received a hotter mixing melt causing the complexity of the group 2 plagioclase rims. Within magmas rising rapidly toward the surface, H2O presence assists plagioclase resorption during decompression, leading to the development of sieving textures (Viccaro et al., 2016). The injection of new melt would likely lead to an eruption event on a quick ascent, pushing the sieving and decompression melting to occur in the conduit just before eruption (Fig. 6; Viccaro et al. 2016). The Santa Cecilia (220 ka to 130 ka; Vezzoli et al., 2008) phenocrysts sit in the dominant Group 1; this suggests that even though magma was supplying a separate chamber feeding the parasitic dome, the hybridization of the primary magma chamber continued throughout the volcanic activity of Ollagüe (Fig. 7).

Conclusions

Plagioclase textures and compositional changes are imperative to understanding how magma systems are stored, evolved, and mobilized. Using this strong combination at Ollagüe, I construct a magma plumbing system model to help understand the storage conditions within the system. Group 1 plagioclase showing interior resorption with chemically oscillatory zoning likely experienced heat flux and mixing of more primitive magmas into the melt, resulting in partial or heavy dissolution within the cores and interior zoning of the phenocrysts. The finer-scaled oscillatory zoning seen in many of the phenocrysts is evidence of some convection-driven process caused by the periodic flux of magmatic volume. Group 2 plagioclase phenocrysts show prolonged crystallization with a rapid introduction to a more primitive melt right before eruption, seen as a geochemical spike and fine sieving textures at the rims. Group 3 plagioclase phenocrysts display adiabatic decompression melting in the interiors and cores, likely during mobilization into a new melt. Group 4 plagioclase phenocrysts show no evidence of resorption or decompression melting, likely crystalizing in equilibrium with their respective melts. Ultimately, the textures and trace element trends observed in plagioclase phenocrysts indicate that the volcanic plumbing system of Ollagüe has experienced thermal and chemical disequilibria within the system and individual crystals.

The four distinct groups of plagioclase phenocrysts show strong evidence of at least three distinct and separate chambers below the edifice. Beginning with some inheritance into an isolated chamber at deeper crustal levels, then into a larger shallower chamber that is homogenizing through periodic volumetric flux, and an extended branch of the homogenized chamber that receives little to no external interference before being introduced to a more primitive melt likely right before eruption. The proximity of Ollagüe to the APMB suggests that

the intermediate composition of Ollagüe magmas is attributed to a relative balance of crystallization and periodic injection volume from the APMB. Even with the complexities of Ollagüe's plumbing, Ollagüe produced relatively homogenous lavas throughout its lifetime.

Acknowledgements

This project was funded and supported by the National Science Foundation, the NASA-Missouri Space Grant Consortium, and the Missouri State University Graduate College. The authors would like to thank Kenny Horkley of the University of Iowa for use of and assistance with the EPMA analyses and data reduction, and Barry Shaulis of the University of Arkansas for use and assistance with the LA-ICPMS analyses and data reduction.

Literature Cited

Avila-Salinas, W., 1991, Petrologic and tectonic evolution of the Cenozoic volcanism in the Bolivian western Andes. Geologic Society of America Memoir 265, 245-257.

Annen, B.C., J.D., S., R.S.J., 2006. The Genesis of Intermediate and Silicic Magmas in Deep Crustal Hot Zones. J. Petrol. 47, 505-539. https://doi.org/10.1093/petrology/egi084.

Baker, D.R., Alletti, M., 2012. Fluid saturation and volatile partitioning between melts and hydrous fluids in crustal magmatic systems: The contribution of experimental measurements and solubility models. Earth-Sci. Rev. 114, 298-324. https://doi.org/10.1016/j.earscirev.2012.06.005.

Cahill, T., Isacks, B., 1992. Seismicity, and shape of the subducted Nazca Plate. J. Geophys. Res. 97, 503-529. https://doi.org/10.1029/92JB00493.

Claeson, D.T., Meurer, W.P., 2004. Fractional Crystallization of hydrous basaltic "arc-type" magmas and the formation of amphibole-bearing gabbroic cumulates. Contrib. Mineral. Petrol. 147, 288-304. https://doi.org/10.1007/s00410-003-0536-0.

Chmielowski, J., Zandt, G., 1999. The Central Andean Altiplano Puna Magma Body. Geophys. Res. Lett. 26, 783-786. https://doi.org/10.1029/1999GL900078.

Conway, C.E., Chamberlain, K.J., Harigane, Y., Morgan, D.J., Wilson C.J.N., 2020. Rapid assembly of high-Mg andesites and dacites by magma mixing at a continental arc stratovolcano. Geology 48, 1033-1037. https://doi.org/10.1130/G47614.1.

Cooper, K.M., Kent, A.J.R., 2014. Rapid remobilization of magmatic crystals kept in cold storage. Nature 506, 480-483. https://doi.org/10.1038/nature12991.

Coote, A., Shane, P., Stirling, C., Reid, M., 2018. The origin of plagioclase phenocryst in basalts from continental volcanoes of the Kaikohe-Bay of Islands field, New Zealand: implications for magmatic assembly and ascent: Contrib. Minerol. Petrol. 173, 14. https://doi.org/10.1007/s00410-018-1440-y.

Delph, J.R., Ward, K.M., Zandt, G., Ducea, M., Beck, S.L., 2017. Imaging a magma plumbing system from MASH zone to magma reservoir. Earth Planet. Sci. Lett. 457, 313-324. https://doi.org/10.1016/j.epsl.2016.10.008.

Fabbro, G.N., Druitt, T.H., Costa, F., 2017. Storage and Eruption of Silicic Magma across the Transition from Dominantly Effusive to Caldera-forming States at an Arc Volcano (Santorini, Greece). J. Petrol. 58, 2429-2464. https://doi.org/10.1093/petrology/egy013

Feeley, T.C., Davidson, J.P, Armendia, A., 1993. The volcanic and magmatic evolution of Volcán Ollagüe, a high-K, late Quaternary stratovolcano in the Andean Central Volcanic Zone: J. Volcanol. Geotherm. Res. 54, 221-245. https://doi.org/10.1016/0377-0273(93)90065-Y.

Feeley, T.C., Davidson, J.P., 1994. Petrology of Calc-Alkaline Lavas at Volcán Ollagüe and the Origin of Compositional Diversity at Central Andean Stratovolcanoes, J. Petrol. 35, 1295-1340. https://doi.org/10.1093/petrology/35.5.1295.

Feeley, T.C., Hacker, M.D., 1995. Intracrustal Derivation of Na-Rich Andesitic and Dacitic Magmas: An Example from Volcán Ollagüe, Andean Central Volcanic Zone. The Journal of Geology 103, 213-225. https://doi.org/10.1086/629737.

Giacomoni, P.P., Ferlito, C., Coltorti, M., Bonadiman, C., Lanzafame, G., 2014. Plagioclase as an archive of magma ascent dynamics on "open conduit" volcanoes: The 2001-2006 eruptive period at Mt. Etna. Earth-Sci. Rev. 138, 371-393. https://doi.org/10.1016/j.earscirev.2014.06.009.

Godoy, B., Wörner, G., Le Roux, P., de Silva, S., Parada, M., Kojima, S., González-Maurel, D.M., Polanco, E., Martínez, P., 2017. Sr- and Nd-isotope variations along the Pleistocene San Pedro-Linzor volcanic chain, N. Chile: Tracking the influence of the Altiplano-Puna Magma Body. J. Volcanol. Geotherm. Res. 341, 172-186. https://doi.org/10.1016/j.jvolgeores.2017.05.030.

Gregory-Wodzicki, K.M., 2000. Uplift history of the Central and Northern Andes: A review. GSA Bulletin 112, 1091-1105. https://doi.org/10.1130/0016-7606(2000)112<1091:UHOTCA>2.0.CO;2.

Jochum, K.P., Weis, U., Stoll, B., Kuzmin, D., Yang, Q., Raczek, I., Jacob, D.E., Stracke, A., Birbaum, K., Frick, D.A., Günther, D., Enzweiler, J., 2011. Determination of Reference Values for NIST SRM 610-617 Glasses Following ISO Guidelines. Geostand. Geoanal. Res. 35, 397-429. https://doi.org/10.1111/j.1751-908X.2011.00120.x.

Klemetti, E.W., Grunder, A.L., 2008. Volcanic Evolution of Volcán Aucanquilcha: a long-lived dacite volcano in the Central Andes of northern Chile. Bull. Volcano. 70, 633-650. https://doi.org/10.1007/s00445-007-0158-x.

Kent, A.J.R., Ungerer, C.A., 2006. Analysis of light lithophile elements (Li,Be,B) by laser ablation ICP-MS: Comparison between magnetic sector and quadrupole ICP-MS. American Minerologist 91, 1401-1411. https://doi.org/10.2138/am.2006.2030.

Kent, A.J.R., Darr, C., Koleszar, A.M., Salisbury, M.J., Cooper, K.M., 2010. Preferential eruption of andesitic magma through recharge filtering. Nature Geosci. 3, 631-636. https://doi.org/10.1038/ngeo924.

Loewen, M.W., Kent, A.J.R., 2012. Sources of elemental fractionation and uncertainty during the analysis of semi-volatile metals in silicate glasses using LA-ICP-MS. J. Anal. At. Spectrom. 27, 1502-1508. 10.1039/C2JA30075C.

Michelfelder, G.S., Feeley, T.C., Wilder, A.D., Klemetti, E.W., 2013. Modification of the Continental Crust by Subduction Zone Magmatism and Vice-Versa: Across-Strike Geochemical Variations of Silicic Lavas from Individual Eruptive Centers in the Andean Central Volcanic Zone. Geosciences 3, 633-667. https://doi.org/10.3390/geosciences3040633.

Nelson, S.T., Montana, A., 1992. Sieve-textured plagioclase in volcanic rocks produced by rapid decompression. American Minerologist 77, 1242-1249.

Paton, C., Hellstrom, J., Paul, B., Woodhead, J., Hergt, J., 2011. Iolite: Freeware for the visualization and processing of mass spectrometric data. J. Anal. At. Spectrom. 26, 2508-2518. 10.1039/C1JA10172B.

Perkins, J.P., Ward, K.M., de Silva, S.L., Zandt, G., Beck, S.L., Finnegan, N.J., 2016. Surface uplift in the Central Andes driven by growth of the Altiplano Puna Magma Body. Nat. Commun. 7, 13185. https://doi.org/10.1038/ncomms13185.

Renjith, M.L., 2014. Micro-textures in plagioclase from 1994-1995 eruption, Barron Island Volcano: Evidence of dynamic magma plumbing system in the Andaman subduction zone. Geosci. Front. 5, 113-126. https://doi.org/10.1016/j.gsf.2013.03.006.

Scott, E.M., Allen, M.B., Macpherson, C.G., McCaffrey, K.J.W., Davidson, J.P., Saville, C., Ducea, M.N., 2018. Andean surface uplift constrained by radiogenic isotopes of arc lavas. Nat. Commun. 9, 969. https://doi.org/10.1038/s41467-018-03173-4.

Shane, P., 2015. Contrasting plagioclase textures and geochemistry in response to magma dynamics in an intra-caldera rhyolite system, Okataina volcano: J. Volcanol. Geotherm. Res. 297, 1-10. https://doi.org/10.1016/j.jvolgeores.2015.03.013.

Sun, S., McDonough, W.F., 1989. Chemical and isotopic systematics of oceanic basalts: implications for mantle composition and processes. Geological Society, London, Special Publications 42, 313-345. https://doi.org/10.1144/GSL.SP.1989.042.01.19.

Thorpe, R.S., Francis, P.W., 1979. Variations in Andean andesite compositions and their petrogenetic significance. Tectonophysics 57, 53-70. https://doi.org/10.1016/0040-1951(79)90101-X.

Vezzoli, L., Tibaldi, A., Renzulli, A., Menna, M., Flude, S., 2008. Faulting-assisted lateral collapses and influence on shallow magma feeding system at Ollagüe volcano (Central Volcanic Zone, Chile-Bolivia Andes): J. Volcanol. Geotherm. Res. 171, 137-159. https://doi.org/10.1016/j.jvolgeores.2007.11.015.

Viccaro, M., Barca, D., Bohrson, W.A., D'Oriano, C., Giuffrida, M., Nicotra, E., Pitcher, B.W., 2016. Crystal residence times from trace element zoning in plagioclase reveal changes in magma transfer dynamics at Mt. Etna during the last 400 years. Lithos 248-251, 309-323. https://doi.org/10.1016/j.lithos.2016.02.004.

Ward, K., Zandt, G., Beck, S., Christensen, D., McFarlin, H., 2014. Seismic imaging of the magmatic underpinnings beneath the Altiplano-Puna volcanic complex from the joint inversion of surface wave dispersion and receiver functions. Earth Planet. Sci. Lett. 404, 43-53. https://doi.org/10.1016/j.epsl.2014.07.022.

Zandt, G., Leidig, M., Chmielowski, J., Baumont, D., Yuan, X., 2003. Seismic Detection and Characterization of the Altiplano Puna Magma Body, Central Andes. Pure Appl. Geophys. 160, 789-807. https://doi.org/10.1007/PL00012557.

Table 1. Major element analysis of select plagioclase cores (PxA), mantles (PxB), and rims (PxC)

	OLA-9014	Vinta Loma		OLA-9025	EL Azufre		OLA-9002	La Celosa		OLA-9052	Santa Cecilia	
	P13A	P13B	P13C	P9A	P9B	P9C	P8A	P8B	P8C	P7A	P7B	P7C
SiO_2	50.421	53.459	60.153	58.748	55.798	55.416	61.984	59.531	58.998	56.998	57.282	59.31
TiO_2	0.035	0.06	0.023	0.055	0.062	0.062	0	0.014	0.009	0.03	0	0.06
Al_2O_3	31.377	29.302	24.515	25.089	27.491	27.693	23.75	23.353	25.59	26.319	26.061	27.059
FeO	0.61	0.488	0.423	0.327	0.492	0.544	0.24	0.226	0.304	0.434	0.473	0.656
MgO	0.045	0.031	0.049	0.008	0.016	0.033	0.004	0.009	0.018	0.029	0.022	0.044
Na_2O	3.412	4.832	7.132	7.185	5.797	5.871	7.977	7.234	7.101	6.546	6.641	5.753
CaO	13.737	11.387	6.934	7.559	9.6	9.691	5.244	5.439	7.254	8.375	8.055	8.91
K_2O	0.138	0.229	0.579	0.736	0.469	0.416	1.026	1.695	0.634	0.693	0.75	0.54
BaO	0	0.009	0.086	0.056	0.044	0.049	0.056	0.041	0.067	0.024	0.06	0.103
Total	99.775	99.797	99.894	99.763	99.769	99.775	100.281	97.542	99.975	99.448	99.344	102.435

Table 2. Average trace element compositions (ppm) of Groups 1-4 cores, mantles, and rims

	Group 1 Cores	Mantles	Rims	Group 2 Cores	Mantles	Rims	Group 3 Cores	Mantles	Rims	Group 4 Cores	Mantles	Rims
Fe	1541.91	2264.61	2230.87	1215.74	1779.09	1910.11	1666.62	1647.92	1908.24	2186.17	1865.52	1156.51
Mg	400.05	825.56	623.10	342.22	533.54	370.84	421.33	350.50	417.06	401.44	450.09	211.82
Sr	1388.46	1466.58	1504.75	1492.97	1546.61	1740.53	1852.54	1741.49	2215.88	2017.07	1831.46	1819.61
Ba	811.30	1342.65	1472.05	732.05	870.17	616.53	360.03	200.88	801.88	305.75	393.46	289.66
La	22.97	37.56	34.53	22.45	23.35	17.76	7.66	5.56	24.96	8.26	13.88	9.68
Ce	34.62	63.20	56.75	31.10	33.63	24.37	11.77	8.70	36.98	13.37	22.59	13.50
Pr	3.11	6.17	5.26	2.69	2.99	2.19	1.12	0.84	3.42	1.36	2.18	1.19
Nd	9.84	19.72	16.62	8.30	9.08	6.24	3.62	2.60	10.46	4.68	6.92	3.58
Sm	1.22	2.79	2.25	0.88	1.05	0.74	0.44	0.31	1.22	0.66	0.97	0.35
Eu	2.20	2.61	2.75	2.30	2.29	1.79	0.85	0.71	2.34	0.85	1.06	1.20
Gd	0.76	1.84	1.49	0.56	0.62	0.44	0.26	0.21	0.72	0.44	0.61	0.13
Tb	0.08	0.20	0.17	0.05	0.06	0.04	0.03	0.02	0.07	0.04	0.06	0.01
Dy	0.39	0.98	0.80	0.20	0.24	0.17	0.13	0.09	0.43	0.24	0.35	0.05

A.)

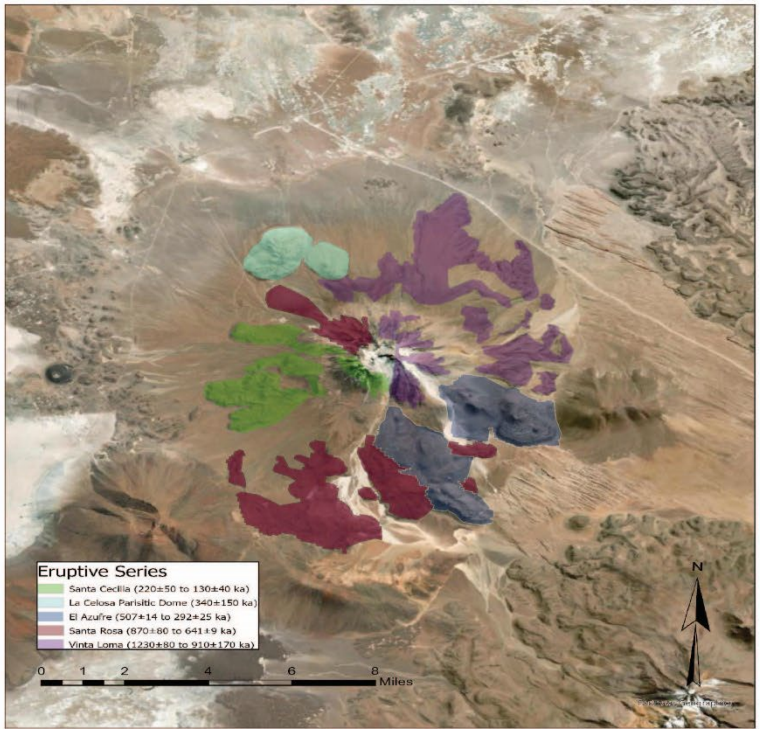

B.)

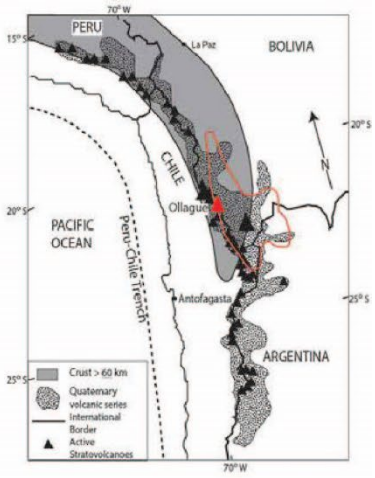

Figure 1A: Geologic map of Ollagüe, a composite volcano primarily active from 1,200ka to 130ka in the arc front of the CVZ drafted in ArcGIS modified from Feeley and Davidson (1994) and Vezzoli et al., (2008). Figure 1B: Location map showing multiple volcanic centers within the CVZ including Ollagüe (red) on the Chile-Bolivian Border. The APMB thought to be affecting magma storage conditions of Ollagüe is outlined in orange.

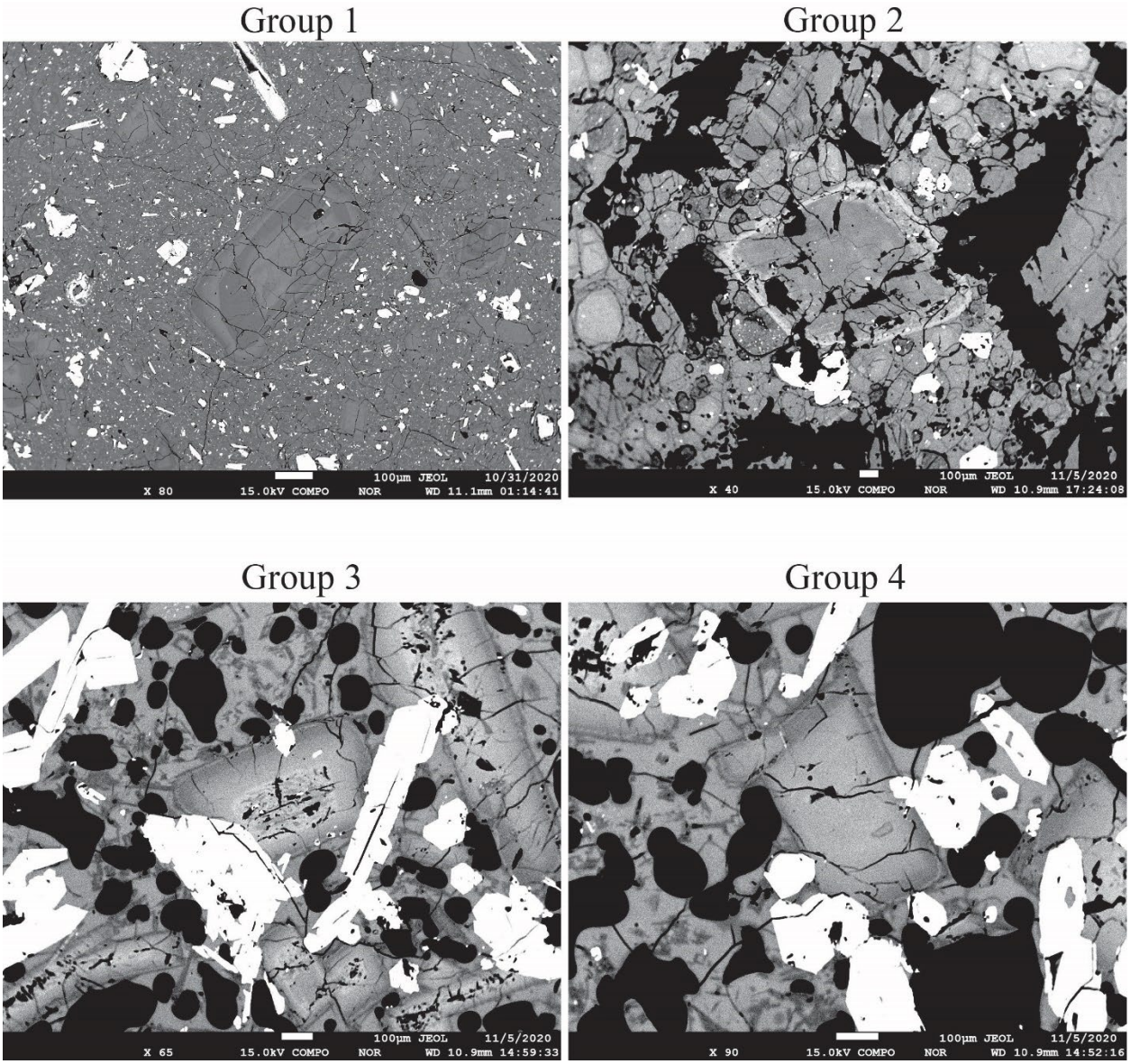

Figure 2: Representative plagioclase from Group 1 exhibiting patchy resorption at the core. Representative plagioclase from Group 2 exhibiting lighter patchy resorption and sieving at the rim. Representative plagioclase from Group 3 exhibiting coarse sieving at the core. Representative plagioclase from Group 4 showing no micro-textures.

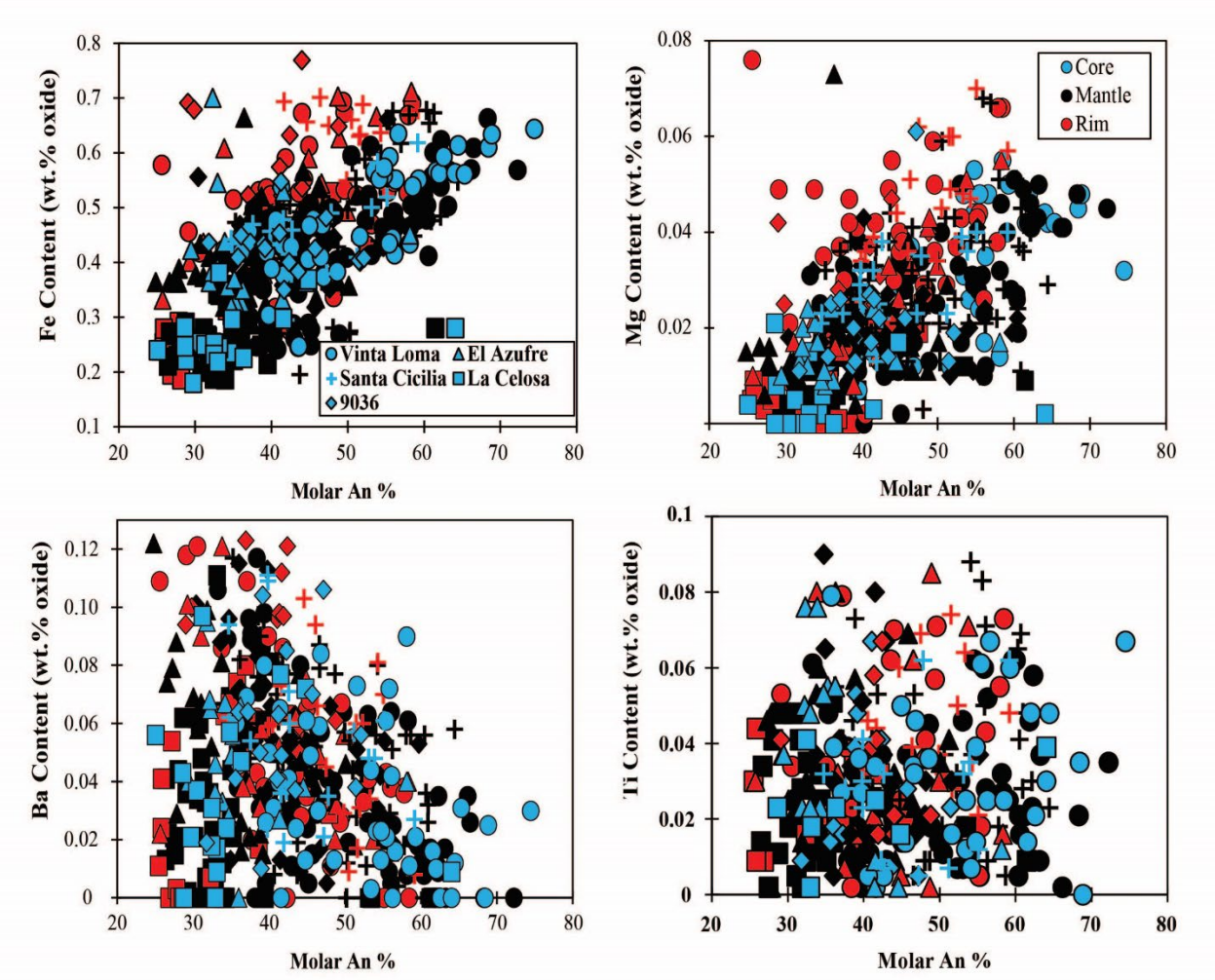

Figure 3: Molar An% vs Fe, Mg, Ba and Ti (wt.% oxide) in plagioclase cores, mantles, and rims from the eruptive series of Ollagüe.

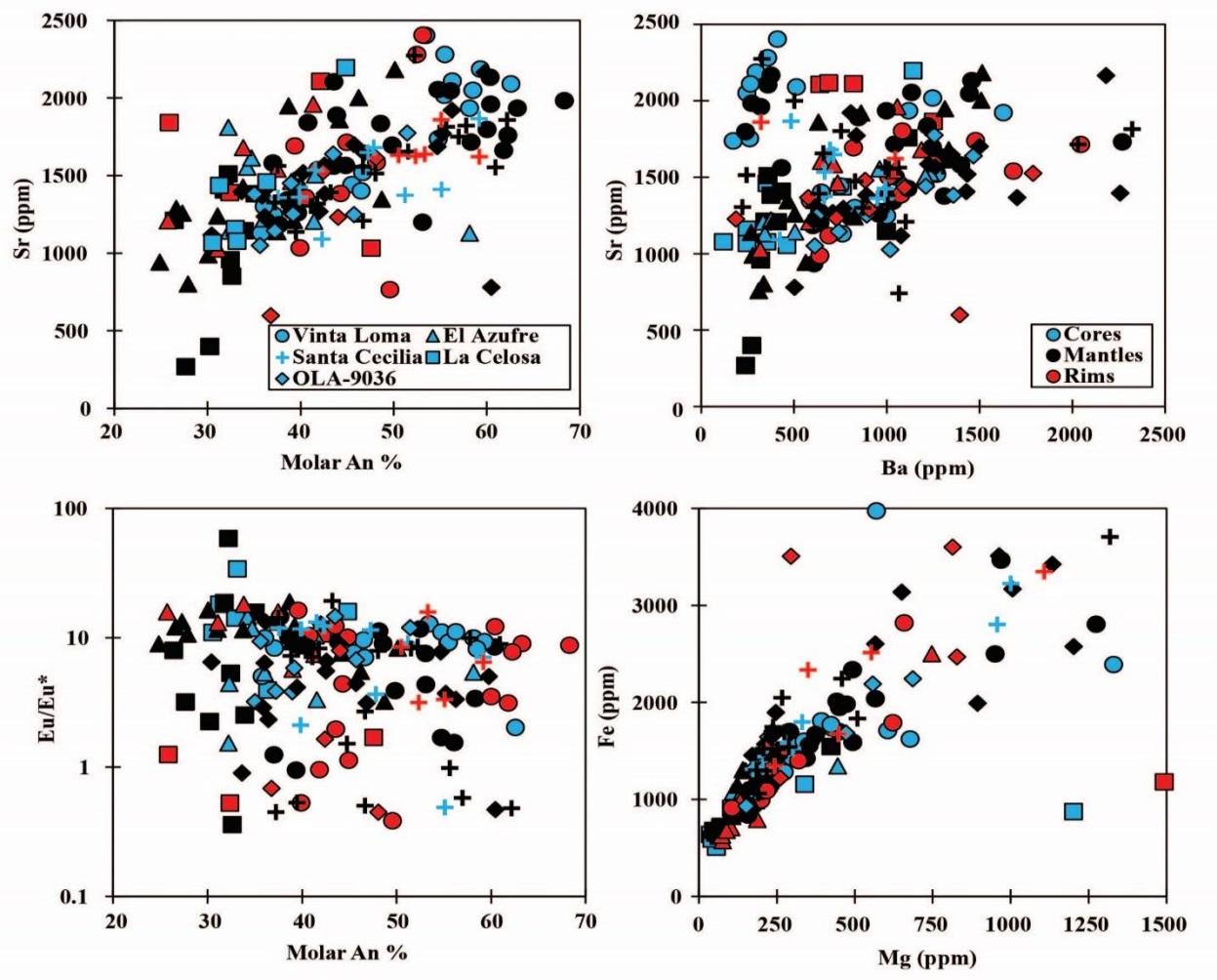

Figure 4: Molar An % versus trace elements (ppm), Ba (ppm) versus Sr (ppm), and Mg (ppm) versus Fe (ppm) in plagioclase cores, mantles, and rims from Ollagüe.

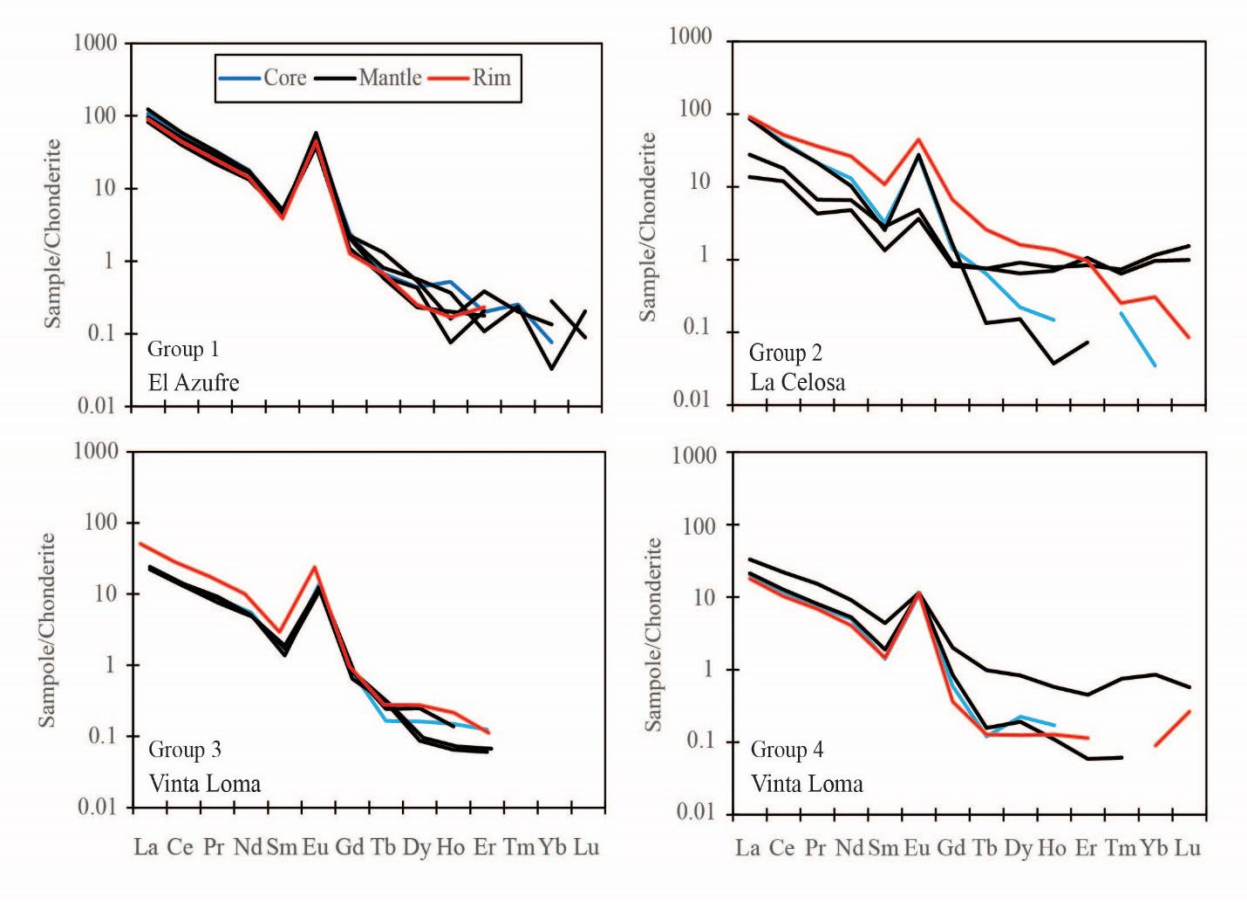

Figure 5: Rare earth element (REE) plots (light to heavy) normalized to chondrite for a representative plagioclase from groups 1 through 4. Chondrite normalized values from Sun and McDonough (1989).

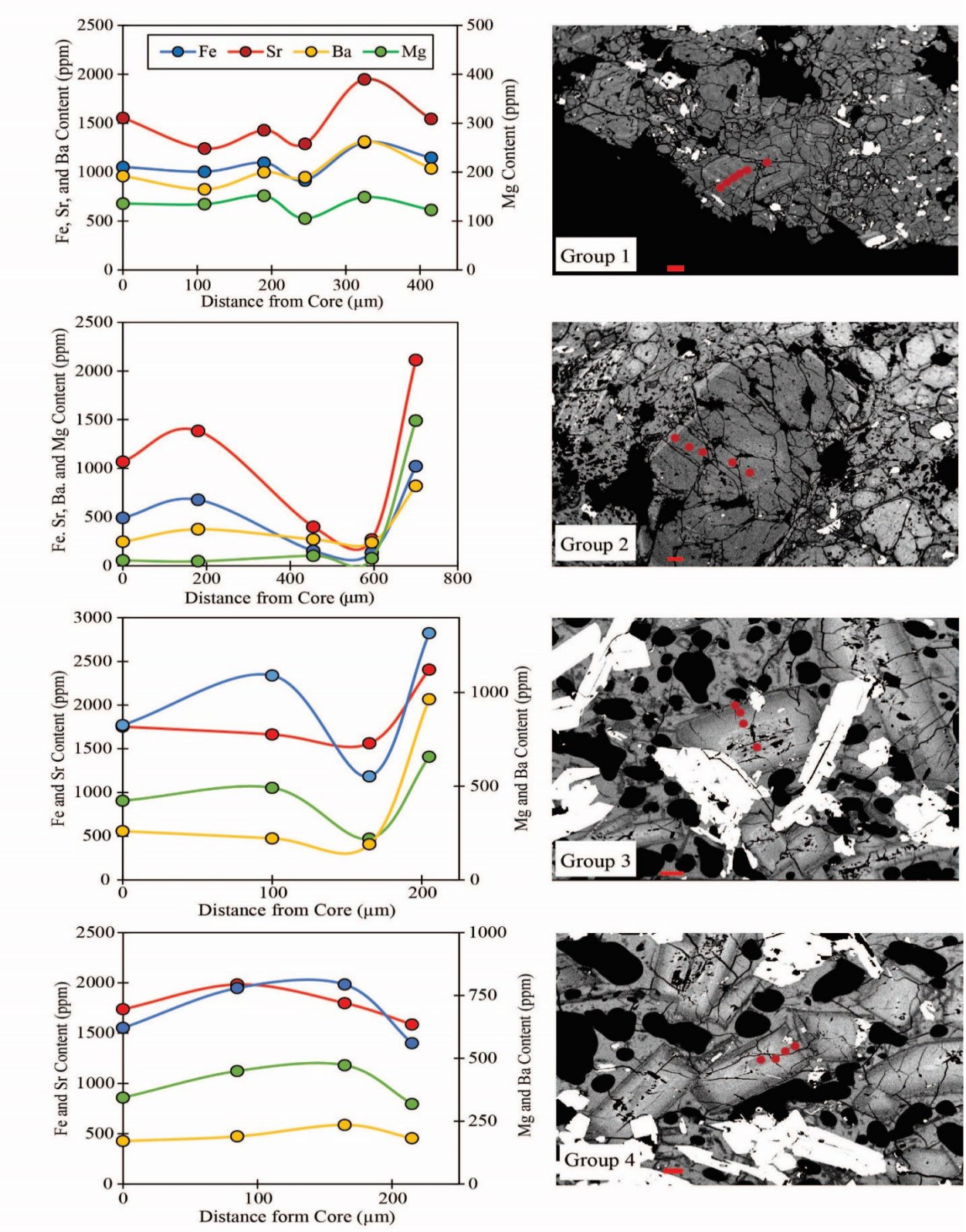

Figure 6: Core-to-rim spot analyses of plagioclase collected by LA-ICPMS showing chemical variations of Fe, Sr, Ba, and Mg contents.

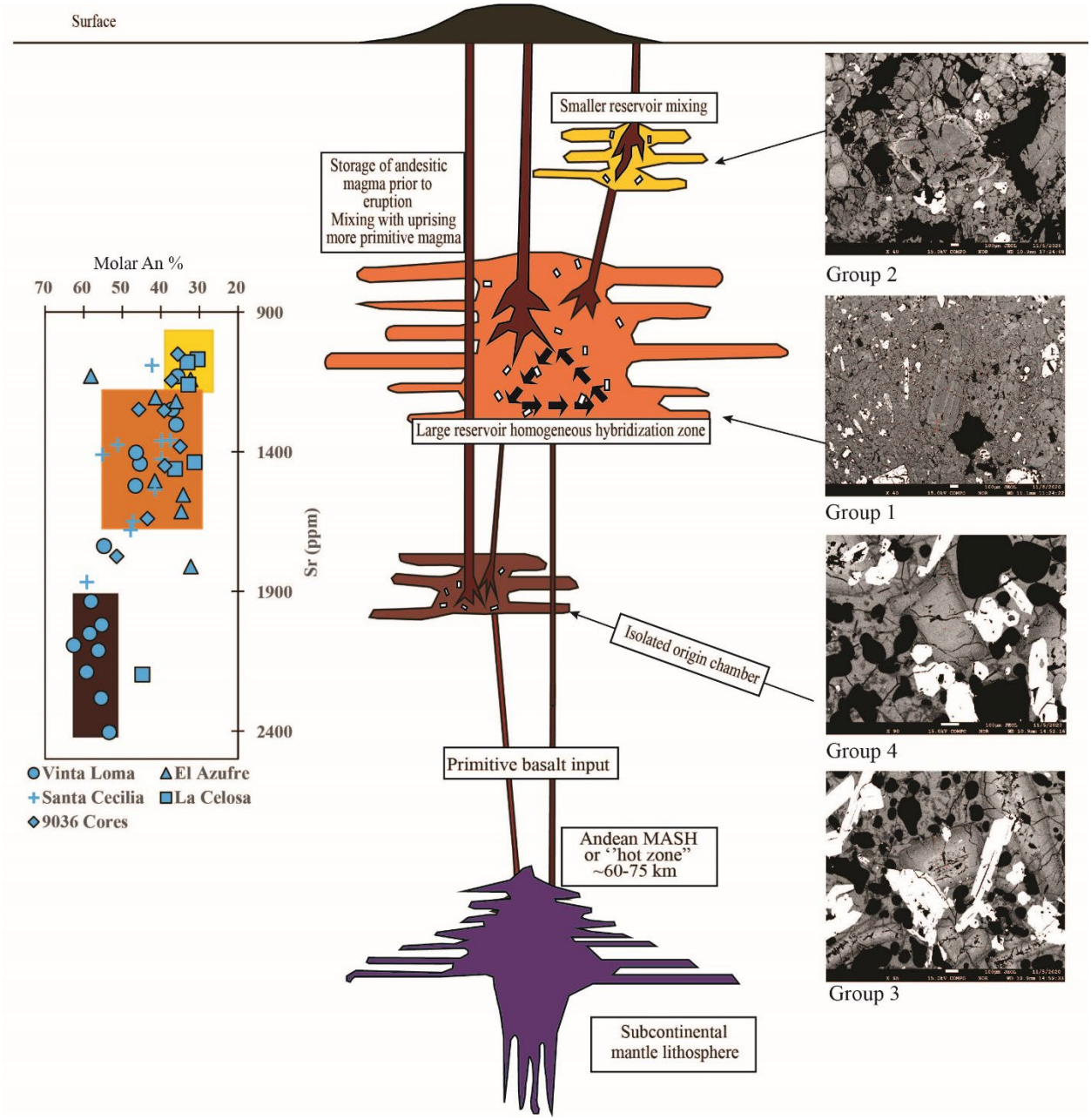

Figure 7: Magmatic plumbing model of Ollague showing three distinct magma chambers originating from the Altiplano Puna Magma Body or "Hot Zone".

CONCLUSIONS

Intermediate-composition magmas from continental-arc composite volcanism are difficult to interpret. It is suggested that stalling through the thick continental crust or the hybridization of magma through mixing events are likely ways to produce these intermediate-composition magmas (Michelfelder et al., 2013; Conway et al., 2020). Eruption ages from $^{40}Ar/^{39}Ar$, U-Pb zircon crystallization ages, and zircon trace element geochemistry combined with plagioclase textural and geochemical analyses have been an essential tool in determining the magma source, storage conditions, and magma plumbing system of Ollagüe. These data have brought a clearer understanding of the plumbing and source material of Ollagüe and a broader understanding of the production of intermediate-composition magma at continental arcs.

Manuscript one, *Rapid Rejuvenation and Magma Storage Conditions Revealed by Zircon Geochronology and Geochemistry at Volcán Ollagüe, Chile-Bolivia, Central Andes*, reviewed two groups of zircons with complex zoning patterns, suggesting the zircons grew in a highly complex melt. The combination of $^{40}Ar/^{39}Ar$ eruption ages and U-Pb zircon crystallization ages suggest shortened (0.005 to 0.05 Ma) crystal residence times. Additionally, a geochemical group of zircons was plotted within a previously defined set of rejuvenation conditions proposed by Klemetti and Clynne (2014). With the short crystal residence time and geochemical data showing rejuvenation, it can be suggested that these rejuvenation periods are happening at a rapid rate within 5,000 to 50,000 years and based on eruption ages, just before an eruption event. Zircon trace element ratios of U/Yb to Gd/Yb and Gd/Yb to Ce/Yb ratios exhibit dense clustering through the influence of zircon crystallization and cooling, amphibole fractionation, and titanite/appetite fractionation. A population of cores did plot within the “garnet signature,”

which is an indicator of zircons originating from a more basaltic melt source, supporting the idea of external influence.

The results of manuscript two, *Geochemical Investigation of Intermediate Lavas: Using Plagioclase to Decipher the Magma Plumbing System of Volcán Ollagüe*, *Chile-Bolivia, Central Andes*, allowed for deciphering the architecture of the magma plumbing system of Ollagüe. Four distinct groups of plagioclases were identified via textural analysis, showing four different crystallization types attributed to three separate chambers beneath the edifice. This is supported geochemically as plagioclase groups 3 and 4 show high concentrations of Sr and Fe acting as a calcic endmember (isolated chamber), whereas group 2 plagioclase shows the lowest concentrations of Sr and Fe acting as the sodic end member (branch off a larger hybridized chamber). Group one is the most dominant (60% of analyses) and forms the largest volume chamber below the edifice. This group displays intense fine-scale oscillatory chemical zoning along with interior resorption, likely pertaining to a convecting magma with periodic injections from a more calcic source. Together, these data help to answer the initial research questions 1) What is the architecture of the magma plumbing system beneath Ollagüe, and how long does magma reside; and 2) What evidence is there for the involvement of regional crustal magma reservoirs controlling the magma compositions at Ollagüe?

The architecture of Ollagüe's plumbing system, revealed by plagioclase textures and trace element geochemistry, can be pieced into at least three distinct chambers during the eruptive series of Ollagüe. A period in the early stages of Ollagüe of an isolated chamber, a likely more voluminous hybridizing chamber observed in all the eruptive series, and a chamber branched off of the hybridized chamber feeding the La Celosa parasitic dome. Further, combining zircon crystallization with eruption ages suggests that the residence time of magma

post zircon crystallization is geologically short (5,000 to 50,000 years). Both plagioclase and zircon data suggest the influence of outsourced magma. Group 1 plagioclase has fine-scale oscillatory chemical zoning seen in the BSE images and core-to-rim analyses attributed to high-to-low volume injections from the regional Altiplano Puna Magma Body. Group 2 phenocrysts exhibit chemical spikes of Fe, Mg, and Sr at the rims attributed to an injection of new melt during a rapid ascent just before an eruption. Plagioclase major element contents of Groups 3 and 4 have cores with a mafic signature exhibiting high (>0.5 wt.%) Fe and Mg (>0.05 wt.%). Further trace element contents of groups 3 and 4 display plagioclase cores with high Sr (>1,800 ppm), suggesting that Ollagüe is sourced from basaltic material. Chemically, a population of zircons plots along a garnet signature while the remaining zircons plot in a dense cluster suggesting the influence of zircon crystallization and cooling, amphibole fractionation, and titanite/apatite fractionation. The smaller population plotting in the mafic garnet signature suggests they are crystallizing in a different source material before being introduced into Ollagüe's system. These data reveal the complexities of the plumbing system of Ollagüe and confirm that the compositional hybridization is being controlled through periodic high-to-low volume injections from an external source. With Ollagüe located on the edge of the APMB and the APMB being such a voluminous reservoir, likely, the complexities and geochemical constraints of Ollagüe's magma plumbing system are linked to the APMB.

REFERENCES

Chmielowski, J., Zandt, G., 1999. The Central Andean Altiplano Puna Magma Body. Geophys. Res. Lett. 26, 783-786. https://doi.org/10.1029/1999GL900078.

Conway, C.E., Chamberlain, K.J., Harigane, Yumiko, M.J., Daniel, W., Colin J.N., 2020. Rapid assembly of high-Mg andesites and dacites by magma mixing at a continental arc stratavolcano. Geology 48, 1033-1037. https://doi.org/10.1130/G47614.1.

Delph, J.R., Ward, K.M., Zandt, G., Ducea, M., Beck, S.L., 2016. Imaging a magma plumbing system from MASH zone to magma reservoir. Earth Planet Sci. Lett. 457, 313-324. https://doi.org/10.1016/j.epsl.2016.10.008.

Feeley, T.C., Davidson, J.P., Armendia, A., 1993. The volcanic and magmatic evolution of Volcán Ollagüe, a high-K, late Quaternary stratovolcano in the Andean Central Volcanic Zone: J. Volcanol. Geotherm. Res. 54, 221-245. https://doi.org/10.1016/0377-0273(93)90065-Y.

Kent, A.J.R., Darr, C., Koleszar, A.M., Salisbury, M.J., Cooper, K.M., 2010. Preferential eruption of andesitic magma through recharge filtering. Nature geosci.3: 631-636. https://doi.org/10.1038/ngeo924.

Kern J.M., de Silva S.L., Schmitt A.K., Kaiser, J.F., Iriarte R.A., Economos, R., 2016. Geochronological imaging of an episodically constructed subvolcanic batholith: U-Pb in zircon chronochemistry of the Altiplano-Puna Volcanic Complex of the Central Andes. GSA Geosphere 12, 1054-1077. https://doi.org/10.1130/GES01258.1.

Klemetti, E.W., Clynne, M.A., 2014. Localized Rejuvenation of a Crystal Mush Recorded in Zircon Temporal and Compositional Variation at the Lassen Volcanic Center, Norther California, PLoS ONE 9(12). https://doi.org/10.1371/journal.pone.0113157.

Michelfelder, G.S., Feeley, T.C., Wilder, A.D., Klemetti, E.W., 2013. Modification of the Continental Crust by Subduction Zone Magmatism and Vice-Versa: Across-Strike Geochemical Variations of Silicic Lavas from Individual Eruptive Centers in the Andean Central Volcanic Zone. Geosciences 3, 633-667. https://doi.org/10.3390/geosciences3040633.

Perkins, J.P., Ward, Kevin M., de Silva, Shanaka L., Zandt, George, Beck, Susan L., Finnegan, Noah J., 2016. Surface uplift in the Central Andes driven by growth of the Altiplano Puna Magma Body. Nat. Commun. 7, 13185. https://doi.org/10.1038/ncomms13185.

Renjith, M.L., 2014. Micro-textures in plagioclase from 1994-1995 eruption, Barron Island Volcano: Evidence of dynamic magma plumbing system in the Andaman subduction zone. Geosci. Front. 5, 113-126. https://doi.org/10.1016/j.gsf.2013.03.006.

Gregory-Wodzicki, K.M., 2000. Uplift history of the Central and Northern Andes. A review: GSA Bull. 112, 1091-1105. https://doi.org/10.1130/0016-7606(2000)112<1091:UHOTCA>2.0.CO;2

Ward, K., Zandt, G., Beck, S., Christensen, D., and McFarlin, H., 2014. Seismic imaging of the magmatic underpinnings beneath the Altiplano-Puna volcanic complex from the joint inversion of surface wave dispersion and receiver functions. Earth Planet. Sci. Lett. 404, 43-53. https://doi.org/10.1016/j.epsl.2014.07.022.

Zandt, G., Leidig, M., Chmielowski, J., Baumont, D., Yuan, X., 2003. Seismic Detection and Characterization of the Altiplano Puna Magma Body, Central Andes. Pure Appl. Geophys. 160, 789-807. https://doi.org/10.1007/PL00012557

APPENDICES

Appendix A: *Manuscript 1.* Trace element data of zircon cores (xx.1) and rims (xx.2) from Ollagüe

Sample	206Pb/238U Age Ma	Uncertainty 1σ	U	Th	*48Ti*	*49Ti*	*Fe*	*Y*	*La*	*Ce*	*Nd*	*Sm*	*Eu*	*Gd*	*Dy*	*Er*	*Yb*	*Yb/Dy*	*Yb/Gd*	*Hf*	*Eu*	*Eu/ Eu**
9006_1.1	0.719	0.16	113	76	5.2	5.2	4.53	627	0.008	13.7	2.00	3.61	1.40	16.0	55	77	152	2.770	10	10583	0.562	2.491
9006_1.2	0.646	0.12	188	92	5.4	5.6	4.21	702	0.004	19.3	1.33	2.06	0.88	11.5	55	96	200	3.669	17	10308	0.548	1.600
9006_2.1	0.729	0.13	135	80	5.9	5.5	4.56	619	0.008	13.8	1.80	3.03	1.02	13.6	52	81	166	3.185	12	11113	0.481	2.111
9006_2.2	0.815	0.05	312	183	6.8	6.6	4.95	978	0.008	28.4	1.61	2.86	0.95	16.7	68	133	291	4.270	17	10971	0.420	2.265
9006_3.1	0.856	0.07	178	125	5.7	5.3	3.79	836	0.016	17.7	3.50	3.85	1.49	19.2	70	116	241	3.420	13	11146	0.529	2.822
9006_3.2	0.814	0.09	144	83	5.9	5.5	4.26	355	0.013	15.4	0.77	1.24	0.41	6.9	29	46	101	3.489	15	12295	0.430	0.964
9006_4.1	0.677	0.05	262	188	4.5	4.6	4.82	1249	0.036	24.5	5.80	7.60	2.79	35.1	115	164	305	2.643	9	10781	0.521	5.360
9006_4.2	0.697	0.06	209	111	4.9	4.9	2.22	724	0.005	21.3	1.61	2.35	0.91	12.2	59	94	199	3.361	16	9443	0.519	1.756
9006_5.1	0.739	0.10	240	182	2.7	2.7	3.51	924	0.037	28.0	6.34	8.98	3.00	36.3	102	105	170	1.665	5	8071	0.507	5.923
9006_6.1	0.551	0.07	249	279	6.4	6.5	4.97	1991	0.250	39.5	12.31	15.37	5.74	64.3	190	264	438	2.303	7	6886	0.557	10.313
9006_7.1	0.699	0.10	244	456	10.9	10.5	4.66	2921	0.068	87.8	20.25	22.51	8.27	102.7	285	344	533	1.869	5	9273	0.524	15.773
9006_7.2	0.752	0.10	331	670	12.1	12.4	4.25	3691	0.027	132.0	12.26	20.77	7.64	110.3	401	464	655	1.634	6	8461	0.487	15.702
9006_8.1	0.837	0.06	376	226	3.9	3.5	4.19	1198	0.006	32.3	4.41	6.64	2.33	33.1	118	155	280	2.364	8	11552	0.479	4.867
9006_8.2	0.731	0.07	203	98	5.3	5.3	4.48	701	0.004	18.2	1.61	2.56	1.02	14.4	63	94	199	3.175	14	10726	0.513	1.993
9006_9.1	0.751	0.06	262	135	3.4	3.1	4.39	780	0.004	22.6	2.86	4.39	1.60	22.2	75	101	184	2.438	8	12503	0.495	3.237
9006_9.2	0.859	0.06	229	122	7.5	7.4	4.13	918	0.124	25.8	2.32	2.66	0.99	14.8	74	121	263	3.545	18	10221	0.480	2.059
9006_10.1	0.713	0.07	170	89	4.6	4.5	4.31	674	0.010	15.5	1.86	2.59	1.01	13.9	52	93	200	3.867	14	10876	0.515	1.965
9006_10.2	0.773	0.07	194	108	5.3	5.3	4.32	502	0.009	19.6	1.06	1.67	0.60	9.6	39	68	147	3.752	15	12044	0.455	1.315
9006_11.1	0.754	0.10	195	138	4.0	4.0	4.12	925	0.014	19.3	4.58	5.66	1.94	25.0	84	121	227	2.694	9	9273	0.496	3.904
9006_11.2	1.039	0.21	149	84	10.0	12.2	11.37	512	0.157	16.7	1.08	1.80	0.60	9.3	43	74	164	3.818	18	11781	0.447	1.343
9006_12.2	0.860	0.06	261	148	8.1	8.4	3.76	762	0.009	27.9	1.24	2.47	0.48	14.0	60	105	209	3.512	15	12344	0.249	1.930
9006_13.1	0.799	0.06	261	142	5.5	5.8	3.89	895	0.003	25.9	1.43	2.43	0.92	13.6	65	127	279	4.303	21	9823	0.490	1.883
9006_14.1	0.647	0.12	194	135	3.6	3.3	20.66	694	0.037	17.4	3.75	4.68	1.68	19.5	59	81	144	2.464	7	5762	0.534	3.137
9006_15.1	0.739	0.06	276	143	3.8	3.5	7.27	720	0.063	23.2	2.13	3.39	1.22	16.7	66	93	172	2.605	10	10688	0.493	2.468
9006_15.2	0.843	0.06	213	125	5.5	5.3	4.26	529	0.004	18.4	1.08	1.75	0.69	9.5	41	73	156	3.823	16	9701	0.517	1.336
9006_16.1	0.634	0.08	169	115	5.6	6.1	4.32	795	0.010	17.3	4.16	5.04	1.61	20.8	70	111	214	3.061	10	10815	0.479	3.360
9006_16.2	0.962	0.09	168	100	6.1	5.9	4.57	666	0.009	16.5	2.24	2.77	1.03	14.2	53	84	178	3.336	13	10328	0.498	2.058
9006_17.1	0.524	0.12	213	143	4.8	5.1	4.84	985	0.012	20.4	5.41	5.87	2.10	24.8	82	128	250	3.062	10	10548	0.530	3.961
9006_17.2	0.922	0.26	157	97	24.0	24.6	45.14	631	0.395	20.6	2.02	2.42	0.72	12.1	54	86	183	3.381	15	10879	0.403	1.777
9006_18.1	0.789	0.17	119	77	7.8	7.5	4.94	559	0.004	15.8	1.31	1.95	0.93	12.1	40	63	125	3.124	10	10425	0.582	1.597
9006_18.2	0.719	0.13	136	80	5.4	5.5	4.55	356	0.010	14.9	0.47	1.22	0.39	6.1	26	48	104	3.928	17	10820	0.441	0.895
9006_19.1	0.833	0.17	210	178	7.2	7.1	4.77	977	0.018	20.4	6.02	6.62	2.46	27.5	91	128	253	2.775	9	10891	0.554	4.430
9006_19.2	0.835	0.08	399	473	10.8	10.2	5.43	2195	0.062	46.4	13.18	15.57	4.94	64.4	215	287	511	2.372	8	10237	0.475	10.386
9006_20.1	0.823	0.10	182	111	4.3	4.1	4.63	698	0.005	18.7	3.10	3.81	1.32	18.9	57	86	161	2.829	9	9579	0.476	2.781
9006_20.2	0.505	0.08	181	87	5.7	5.7	5.28	449	0.004	14.3	1.14	1.57	0.65	7.6	32	60	133	4.208	17	10533	0.574	1.138
9006_21.1	1.031	0.12	636	652	10.1	9.5	11.42	2182	0.108	59.4	3.93	7.24	3.58	45.9	201	271	425	2.109	9	11374	0.598	5.980
9006_21.2	0.779	0.05	359	315	4.2	3.8	5.34	1103	0.005	35.9	1.65	3.79	1.79	24.4	104	144	256	2.460	10	11896	0.567	3.156
9006_22.1	0.884	0.04	561	481	11.0	11.7	5.67	2251	0.071	63.4	5.05	6.49	3.28	45.5	193	302	570	2.946	13	11113	0.581	5.639
9006_22.2	0.630	0.14	207	113	7.7	7.8	10.58	743	0.023	19.9	1.58	2.34	0.79	12.5	57	106	242	4.237	19	10649	0.446	1.773
9007_1.1	0.613	0.12	158	83	5.2	5.1	5.74	664	0.011	20.7	3.31	4.77	1.79	21.3	55	79	136	2.495	6	10349	0.542	3.307

9007_1.2	0.844	0.11	241	160	9.9	11.8	5.59	466	0.105	21.8	1.37	1.91	0.63	9.8	37	64	133	3.569	14	9153	0.440	1.422
9007_2.1	0.780	0.10	152	56	1.9	1.8	4.05	363	0.003	14.9	0.51	1.28	0.54	7.9	32	44	88	2.718	11	10591	0.519	1.047
9007_3.1	0.732	0.15	205	248	13.5	13.3	9.52	1858	0.029	40.9	16.33	22.45	10.55	103.8	220	154	145	0.657	1	8345	0.666	15.833
9007_3.2	0.655	0.04	516	473	6.2	5.9	4.62	910	0.020	46.7	2.51	4.37	1.75	24.4	90	115	202	2.250	8	10786	0.516	3.385
9007_4.1	0.699	0.07	246	132	3.4	3.4	4.06	654	0.007	23.7	1.08	2.14	0.89	12.8	45	79	148	3.264	12	5889	0.516	1.720
9007_5.1	0.746	0.11	192	110	4.3	3.9	5.31	729	0.004	17.0	2.28	3.01	1.08	15.1	55	97	206	3.767	14	11996	0.489	2.209
9007_5.2	0.661	0.13	138	79	6.6	6.3	4.67	362	0.004	15.4	0.82	1.22	0.44	6.6	30	50	107	3.542	16	11864	0.475	0.926
9007_6.1	0.805	0.09	358	202	3.1	3.2	6.16	1010	0.011	31.1	4.40	6.34	2.12	29.7	99	125	215	2.163	7	11583	0.471	4.504
9007_6.2	0.724	0.08	294	216	5.9	5.9	4.69	776	0.037	23.3	1.93	2.19	0.87	13.3	50	81	204	4.044	15	11072	0.494	1.769
9007_7.1	0.677	0.09	661	358	52.6	51.3	285.07	985	0.298	26.8	10.77	18.56	5.48	83.4	149	90	114	0.763	1	12323	0.424	12.910
9007_7.2	0.819	0.05	346	241	6.2	5.9	4.15	782	0.005	29.3	2.01	2.78	1.23	18.2	70	105	197	2.801	11	11019	0.528	2.338
9007_9.1	0.954	0.07	382	258	4.9	5.2	5.99	1212	0.038	55.8	2.94	4.85	1.86	29.3	112	146	270	2.414	9	10840	0.477	3.906
9007_9.2	0.766	0.04	496	399	6.1	6.2	4.36	1345	0.006	52.7	2.83	5.24	1.84	32.2	135	178	314	2.318	10	11430	0.433	4.259
9007_10.1	0.886	0.09	203	131	5.4	5.5	8.34	764	0.051	19.6	3.11	4.37	1.72	21.3	72	92	182	2.544	9	11321	0.544	3.165
9007_10.2	0.835	0.06	279	191	6.0	5.4	4.19	683	0.005	23.9	1.40	2.08	0.85	12.0	54	91	198	3.656	17	11275	0.517	1.638
9007_11.1	0.880	0.08	182	88	2.5	2.7	3.87	596	0.025	17.5	1.35	2.36	0.95	12.8	52	76	142	2.739	11	8932	0.527	1.805
9007_12.2	0.705	0.08	250	167	6.1	6.0	3.42	734	0.006	23.0	1.49	2.48	1.04	14.2	59	98	183	3.090	13	8524	0.536	1.944
9007_13.1	0.657	0.10	205	112	5.2	5.6	3.82	717	0.023	20.8	1.91	2.57	1.04	13.0	56	97	199	3.531	15	9973	0.546	1.896
9007_13.2	0.661	0.06	226	138	6.0	6.7	1.77	562	0.004	21.4	1.76	2.26	0.79	11.3	45	78	168	3.745	15	11203	0.480	1.654
9007_14.1	0.759	0.06	959	1406	10.7	10.5	7.79	3966	0.088	104.1	13.52	21.99	8.58	123.5	369	417	626	1.697	5	11362	0.502	17.097
9007_14.2	0.693	0.10	359	234	8.7	9.2	4.52	1357	0.009	33.2	2.30	3.40	1.72	23.7	93	174	356	3.824	15	10408	0.583	2.947
9034_7.1	0.428	0.13	144	93	9.2	9.7	3.91	699	0.030	16.7	2.32	3.03	0.77	14.8	54	93	165	3.070	11	6477	0.350	2.202
9034_1.1	1.340	0.48	523	484	13.8	14.4	22.92	2365	0.852	76.5	10.76	13.58	4.41	68.5	225	298	488	2.164	7	11045	0.441	10.003
9034_1.2	0.834	0.12	252	123	5.5	5.8	6.52	840	0.004	22.9	1.49	2.77	1.02	14.9	65	118	240	3.684	16	11099	0.482	2.105
9034_2.1	0.648	0.17	108	47	4.0	4.0	5.44	417	0.182	10.5	1.42	1.42	0.56	6.6	34	56	125	3.636	19	8304	0.556	1.002
9034_2.2	0.919	0.16	177	93	6.3	6.7	5.05	571	0.068	16.2	1.66	1.55	0.65	8.4	38	80	171	4.473	20	9890	0.547	1.188
9034_4.2	0.617	0.14	89	40	6.2	6.7	4.23	266	0.006	12.6	0.58	0.95	0.23	5.4	23	33	62	2.718	11	7006	0.303	0.746
9034_5.2	0.170	0.13	91	60	8.8	9.3	4.19	414	0.020	15.0	1.31	1.84	0.46	9.7	35	53	100	2.849	10	6759	0.331	1.384
9034_6.1	0.742	0.15	130	65	4.4	4.6	6.54	427	0.005	13.6	1.12	1.92	0.58	8.3	34	58	123	3.598	15	12829	0.444	1.308
9034_6.2	0.402	0.10	116	61	11.1	12.4	6.30	469	0.040	16.1	0.96	1.75	0.48	10.2	40	65	125	3.083	12	11357	0.345	1.385
9034_8.1	0.757	0.15	117	97	5.6	5.6	7.07	441	0.051	13.0	1.54	2.33	0.65	9.4	39	56	114	2.917	12	7865	0.426	1.535
9034_8.2	0.641	0.09	101	61	7.5	7.2	1.79	397	0.020	13.4	1.07	1.82	0.53	8.4	33	53	106	3.211	13	9255	0.416	1.282
9034_9.1	0.754	0.07	309	290	9.5	9.3	24.96	1707	0.259	32.7	10.83	10.35	2.82	46.9	161	220	380	2.363	8	11055	0.390	7.227
9034_10.1	1.498	1.39	175	141	5.5	5.7	4.01	800	0.014	17.9	2.94	4.18	1.32	19.5	67	102	199	2.950	10	9452	0.443	2.966
9034_10.2	0.610	0.07	179	98	6.1	5.9	4.11	512	0.006	19.7	0.90	1.92	0.43	10.1	39	68	135	3.488	13	9627	0.300	1.445
9041_1.1	0.906	0.12	276	129	3.9	4.0	5.73	733	0.013	27.6	1.79	3.29	1.42	20.5	71	86	157	2.216	8	12039	0.527	2.694
9041_1.2	0.798	0.10	440	287	7.7	8.8	5.85	1365	0.026	46.7	2.21	3.29	1.42	23.0	110	196	398	3.614	17	11132	0.499	2.852
9041_2.1	0.622	0.15	98	116	12.7	13.6	7.07	519	0.253	15.4	19.83	18.46	5.50	54.8	80	47	50	0.619	1	6718	0.527	10.435
9041_2.2	0.943	0.15	197	110	5.2	5.2	3.55	489	0.009	17.4	1.29	1.72	0.64	8.7	35	63	138	3.924	16	9845	0.506	1.273
9041_3.1	0.279	0.24	65	65	14.2	15.1	5.19	1428	0.096	37.3	29.28	32.29	15.62	115.6	203	128	122	0.601	1	8816	0.779	20.044
9041_3.2	0.743	0.06	277	192	4.6	5.7	6.90	551	0.019	24.7	1.50	2.46	0.98	13.4	44	69	130	2.952	10	7691	0.520	1.881
9041_4.1	0.455	0.18	169	87	5.1	5.6	7.57	411	0.049	11.4	1.43	1.76	0.73	10.3	36	47	83	2.294	8	5668	0.521	1.397
9041_4.2	0.967	0.49	164	102	50.2	68.3	74.14	549	0.925	17.3	3.77	3.22	1.19	14.8	46	71	134	2.915	9	6733	0.523	2.268
9041_5.1	0.981	0.08	336	244	5.0	5.6	4.25	2004	0.008	26.9	3.90	6.43	2.41	38.3	194	287	548	2.825	14	11566	0.469	5.150

9041_5.2	0.736	0.05	300	191	5.4	5.7	1.96	1036	0.005	25.6	1.58	3.17	1.04	18.8	84	141	281	3.335	15	8388	0.411	2.530
9041_6.1	1.056	0.10	186	205	11.4	11.7	10.21	1817	0.170	37.6	15.49	20.30	8.78	83.6	217	190	230	1.062	3	7960	0.650	13.515
9041_6.2	1.097	0.08	204	114	4.7	4.7	4.32	443	0.014	16.3	1.02	1.50	0.64	8.4	33	61	125	3.757	15	8965	0.549	1.162
9041_7.1	3.808	1.03	468	107	9.1	9.4	6.33	763	0.015	13.0	6.74	8.28	2.82	32.0	81	91	139	1.727	4	11705	0.528	5.344
9041_7.2	0.909	0.09	251	151	7.1	7.4	14.46	677	0.019	26.3	1.27	2.29	0.75	13.0	56	92	198	3.519	15	11760	0.417	1.792
9041_8.1	0.851	0.09	154	118	4.1	4.0	5.00	820	0.057	24.7	3.69	5.38	2.34	29.2	80	94	144	1.794	5	7913	0.568	4.113
9041_9.1	0.827	0.16	99	43	3.9	4.5	5.65	353	0.017	9.3	0.82	0.95	0.46	5.9	27	47	107	3.999	18	7936	0.591	0.782
9041_10.1	1.481	0.89	294	276	14.3	13.7	46.09	903	0.886	27.3	3.98	4.19	1.40	22.6	73	110	214	2.939	9	10873	0.438	3.189
9041_10.2	0.932	0.06	311	230	6.8	6.6	3.92	731	0.028	28.5	1.54	2.82	0.97	13.4	61	100	207	3.371	15	11970	0.480	2.020
9041_11.1	0.758	0.17	329	277	8.6	9.2	23.74	964	0.198	46.9	4.36	7.48	3.30	40.4	83	106	163	1.968	4	9258	0.579	5.703
9041_11.2	0.953	0.38	163	87	7.5	7.4	10.01	352	6.411	30.2	13.18	2.47	0.62	8.1	25	41	93	3.788	11	9425	0.420	1.469
9041_12.1	0.750	0.06	289	145	4.1	4.1	4.78	902	0.009	24.3	2.83	3.83	1.51	21.6	79	122	230	2.914	11	11552	0.505	2.983
9041_12.2	0.847	0.04	402	295	7.0	7.0	3.79	1184	0.005	46.8	2.53	4.34	1.70	27.2	112	157	272	2.427	10	11663	0.477	3.562
9041_13.1	0.659	0.08	352	202	4.3	4.1	5.04	1029	0.041	41.5	3.03	4.82	1.71	26.4	98	129	223	2.280	8	11766	0.462	3.703
9041_13.2	1.154	0.13	125	69	4.9	5.7	4.47	337	0.247	12.9	0.74	1.24	0.40	6.4	25	41	87	3.478	14	7155	0.431	0.925
9041_14.1	0.827	0.08	842	611	8.4	10.0	21.27	1267	2.583	52.4	16.11	12.97	3.42	50.4	129	148	248	1.930	5	8219	0.408	8.387
9041_14.2	0.718	0.05	377	300	5.6	5.6	3.92	840	0.161	37.5	2.61	3.22	1.35	20.1	76	110	198	2.611	10	9223	0.511	2.636
9041_15.1	1.075	0.17	173	76	5.1	5.1	4.25	594	0.004	13.7	0.88	1.86	0.79	10.7	47	71	173	3.667	16	11219	0.542	1.464
9041_15.2	0.766	0.07	233	122	6.5	6.6	7.51	753	0.007	14.3	1.06	2.02	0.78	12.4	43	96	212	4.900	17	11346	0.477	1.639
9046_2.1	0.781	0.07	520	434	4.6	4.3	4.92	1988	0.008	54.2	5.95	10.36	3.55	54.8	151	256	479	3.176	9	12101	0.454	7.813
9046_2.2	1.224	0.20	214	117	5.7	5.9	5.27	499	0.004	18.9	1.08	1.55	0.58	9.0	38	70	150	3.967	17	12096	0.475	1.223
9046_3.1	0.915	0.08	194	89	2.9	2.6	4.59	645	0.006	20.0	1.70	3.18	1.02	14.8	63	81	147	2.327	10	12780	0.453	2.251
9046_4.1	0.636	0.10	141	138	21.5	20.7	7.27	1322	0.134	51.7	39.80	38.86	17.28	122.1	181	119	128	0.705	1	10752	0.765	22.601
9046_4.2	0.891	0.14	220	131	6.0	6.1	4.82	628	0.006	21.3	1.26	2.10	0.87	11.9	48	84	173	3.618	15	11123	0.531	1.644
9046_5.1	0.730	0.06	716	871	6.4	6.3	4.25	2874	0.086	78.5	20.12	24.24	6.72	100.1	306	327	532	1.737	5	10513	0.416	16.161
9046_5.2	0.945	0.08	246	174	5.6	5.9	4.01	1104	0.018	24.4	4.56	5.37	1.97	25.7	94	147	288	3.053	11	11682	0.512	3.852
9046_6.1	0.723	0.08	190	110	3.5	3.4	4.96	736	0.012	23.8	3.12	4.49	1.54	21.8	62	85	146	2.376	7	12456	0.474	3.243
9046_6.2	1.526	0.48	156	140	11.1	7.9	36.22	923	126.565	245.8	188.59	26.32	4.41	40.5	92	112	185	2.010	5	8323	0.412	10.705

Appendix B: ***Manuscript 2.*** **Major element data of Ollagüe plagioclase (wt.%); core to rim transects**

Sample ID	SiO_2	TiO_2	Al_2O_3	FeO	MgO	Na_2O	CaO	K_2O	BaO	Total	Mol An %
OLA90_36_P1A	57.242	0	25.653	0.426	0.013	6.334	8.045	0.866	0.104	98.683	39.17
OLA90_36_P1B	51.949	0.025	29.441	0.498	0.019	4.361	12.302	0.331	0.053	98.979	59.75
OLA90_36_P1C	56.385	0.041	26.273	0.522	0.025	6.181	8.541	0.777	0.098	98.843	41.36
OLA90_36_P2A	55.633	0.009	27.242	0.482	0.061	5.518	9.571	0.614	0.106	99.236	47.18
OLA90_36_P2B	57.245	0.037	26.023	0.477	0.022	6.249	8.288	0.818	0.055	99.214	40.29
OLA90_36_P2D	62.409	0.126	22.331	0.691	0.042	6.627	5.528	1.259	0.094	99.107	29.07
OLA90_36_P3A	57.066	0.014	27.064	0.383	0.014	5.898	8.91	0.755	0.037	100.141	43.50
OLA90_36_P3B	56.098	0.09	27.567	0.318	0.016	5.7	9.374	0.686	0.042	99.891	45.71
OLA90_36_P3C	63.007	0.115	22.204	0.679	0.025	6.37	5.604	1.376	0.1	99.48	29.86
OLA90_36_P4B	56.017	0.065	26.888	0.447	0.024	5.999	9.256	0.689	0.079	99.464	44.22
OLA90_36_P4C	57.603	0.039	25.499	0.522	0.028	6.51	7.591	0.974	0.123	98.889	36.97
OLA90_36_P5A	58.772	0.018	25.601	0.409	0.014	6.746	7.457	1.073	0.041	100.131	35.61
OLA90_36_P5B	56.843	0.03	27.233	0.402	0.02	5.911	9.081	0.732	0.049	100.301	43.98
OLA90_36_P5C	57.402	0.005	26.632	0.383	0.017	6.196	8.784	0.775	0.05	100.244	41.99
OLA90_36_P5D	56.785	0.058	26.618	0.632	0.031	6.165	8.792	0.653	0.121	99.855	42.42
OLA90_36_P6A	58.222	0.016	25.749	0.436	0.026	6.564	7.726	0.965	0.064	99.768	37.23
OLA90_36_P6B	56.774	0.03	26.23	0.446	0.012	6.064	8.772	0.719	0.049	99.096	42.58
OLA90_36_P6C	55.88	0	27.305	0.448	0.019	5.651	9.644	0.608	0.017	99.572	46.83
OLA90_36_P6D	58.656	0.041	25.387	0.437	0.022	6.708	7.55	1.001	0.072	99.874	36.16
OLA90_36_P6E	56.619	0.016	26.465	0.439	0.016	6.074	8.805	0.756	0.027	99.217	42.54
OLA90_36_P6F	59.453	0.034	24.871	0.389	0.032	6.984	7.078	1.102	0.088	100.031	33.66
OLA90_36_P6G	57.205	0.032	26.834	0.445	0.025	6.152	8.924	0.737	0.053	100.407	42.63
OLA90_36_P6H	55.528	0.028	27.84	0.48	0.027	5.611	9.993	0.539	0.066	100.112	48.07
OLA90_36_P6I	57.853	0	26.555	0.574	0.037	6.265	8.528	0.749	0.096	100.657	41.08
OLA90_36_P7A	58.952	0.039	25.486	0.449	0.025	6.65	7.455	1.011	0.064	100.131	36.03
OLA90_36_P7B	57.727	0.009	26.697	0.42	0.027	6.176	8.582	0.801	0.065	100.504	41.44
OLA90_36_P7C	57.961	0.051	25.873	0.437	0.024	6.499	7.975	0.9	0.086	99.806	38.33
OLA90_36_P7D	57.975	0.016	25.819	0.468	0.027	6.591	7.966	0.885	0.1	99.847	38.03
OLA90_36_P8A	58.145	0.053	26.434	0.431	0.012	6.472	8.128	0.924	0.05	100.649	38.82
OLA90_36_P8B	57.029	0.028	26.98	0.472	0.027	6.024	9.054	0.75	0.063	100.427	43.43
OLA90_36_P9A	54.368	0.048	28.853	0.408	0.019	5.187	10.844	0.479	0.056	100.262	14.61
OLA90_36_P9B	53.451	0.012	29.067	0.428	0.02	4.945	11.22	0.443	0.031	99.617	52.13
OLA90_36_P9C	56.557	0.016	26.842	0.438	0.016	6.169	8.942	0.704	0.055	99.739	54.21
OLA90_36_P9D	54.801	0.016	28.447	0.401	0.01	5.217	10.72	0.517	0.051	100.18	42.70
OLA90_36_P9E	55.516	0.067	27.891	0.648	0.04	5.474	10.111	0.58	0.061	100.388	51.60
OLA90_36_P10B	57.817	0.025	26.283	0.448	0.043	6.19	8.2	0.806	0.066	99.878	48.83
OLA90_36_P10C	62.675	0.08	23.555	0.556	0.018	6.26	6.004	2.021	0.101	101.27	47.07
OLA90_36_P10D	52.83	0.023	28.936	0.428	0.011	4.761	11.029	0.445	0.042	98.505	40.27
OLA90_36_P10E	58.445	0.016	25.868	0.468	0.018	6.705	7.657	0.862	0.062	100.101	30.42
OLA90_36_P11A	55.122	0.067	28.79	0.403	0.013	5.212	10.669	0.533	0.038	100.847	54.67
OLA90_36_P11B	57.704	0	26.495	0.419	0.022	6.362	8.257	0.971	0.073	100.303	36.78
OLA90_36_P12A	60.156	0	24.887	0.436	0.011	7.064	6.678	1.293	0.019	100.544	57.07
OLA90_36_P12B	58.358	0.037	25.941	0.39	0.012	6.384	7.932	0.936	0.083	100.073	51.45
OLA90_36_P13A	56.128	0	27.589	0.425	0.022	5.691	9.375	0.696	0.07	99.996	39.46

OLA90_36_P13B	53.144	0.023	29.39	0.429	0.024	4.745	11.733	0.452	0.019	99.959	54.48
OLA90_36_P13C	58.476	0.021	25.677	0.38	0.02	6.655	7.649	1.089	0.058	100.025	31.80
OLA90_36_P14A	57.721	0.044	26.225	0.434	0.02	6.427	8.161	0.964	0.01	100.006	38.51
OLA90_36_P14B	53.835	0.032	29.336	0.661	0.041	4.842	11.44	0.432	0.054	100.673	49.89
OLA90_36_P15A	57.257	0.032	26.562	0.547	0.017	6.282	8.627	0.768	0.063	100.155	45.73
OLA90_36_P15B	50.069	0	29.455	0.555	0.022	4.014	11.717	0.334	0.017	96.183	56.25
OLA90_36_P15C	56.395	0.021	27.164	0.536	0.021	5.99	9.152	0.672	0.059	100.01	36.44
OLA90_36_P16A	58.958	0.041	25.407	0.458	0.032	6.706	7.206	1.044	0.061	99.913	57.43
OLA90_36_P16B	58.933	0.067	25.559	0.441	0.022	6.757	7.562	0.996	0.115	100.452	38.97
OLA90_36_P16C	58.9	0.03	25.729	0.468	0.021	6.615	7.371	1.014	0.071	100.219	55.22
OLA90_36_P16D	57.869	0	26.261	0.474	0.027	6.369	8.432	0.822	0.055	100.309	45.59
OLA90_36_P16E	57.964	0	26.325	0.484	0.021	6.318	8.239	0.863	0.113	100.327	41.26
OLA90_36_P17A	57.329	0.007	26.82	0.4	0.022	6.116	8.801	0.779	0.085	100.359	60.46
OLA90_36_P17B	57.707	0	26.447	0.399	0.033	6.362	8.352	0.878	0.037	100.215	44.02
OLA90_36_P17C	57.383	0.009	26.792	0.428	0.02	6.192	8.709	0.731	0.097	100.361	35.01
OLA90_36_P18A	57.403	0.028	26.662	0.453	0.027	6.173	8.491	0.855	0.041	100.133	36.05
OLA90_36_P18B	57.09	0.021	27.042	0.421	0.019	6.036	8.893	0.762	0.055	100.339	35.87
OLA90_36_P18C	57.445	0	26.687	0.463	0.025	6.157	8.601	0.753	0.112	100.243	40.27
OLA90_36_P19A	57.497	0.005	26.667	0.35	0.026	6.134	8.588	0.78	0.049	100.096	39.80
OLA90_36_P19B	59.021	0	25.246	0.397	0.02	6.799	7.276	1.047	0.013	99.819	50.97
OLA90_36_P19C	58.654	0.014	26.079	0.554	0.022	6.526	7.864	0.875	0.043	100.631	42.32
OLA90_36_P20A	56.805	0.023	27.019	0.427	0.02	6.041	9.091	0.783	0.029	100.238	39.94
OLA90_36_P20B	56.33	0.016	27.065	0.408	0.011	5.974	9.246	0.765	0.009	99.824	41.90
OLA90_36_P20C	57.69	0.018	26.606	0.358	0.023	6.084	8.557	0.891	0.013	100.24	41.06
OLA90_36_P20D	55.708	0.021	27.932	0.352	0.025	5.576	9.901	0.677	0.005	100.197	42.91
OLA90_36_P20E	58.234	0.03	26.226	0.397	0.018	6.402	8.165	1.045	0.035	100.552	41.67
OLA90_36_P20F	56.066	0.03	27.986	0.445	0.024	5.534	10.047	0.666	0.011	100.809	41.66
OLA90_36_P20G	59.498	0.011	25.446	0.409	0.017	6.689	7.258	1.271	0.096	100.695	34.94
OLA90_36_P20H	58.108	0	25.768	0.43	0.019	5.936	8.203	0.994	0.032	99.49	37.96
OLA90_36_P20I	58.568	0.037	26.157	0.51	0.022	6.401	7.97	1.103	0.054	100.822	43.38
OLA90_36_P20J	56.88	0.06	26.786	0.769	0.047	5.921	8.995	0.621	0.05	100.129	44.10
OLA90_25_P1A	57.11	0.002	26.89	0.333	0.016	6.448	8.709	0.544	0.027	100.079	41.48
OLA90_25_P1B	58.366	0	26.198	0.287	0.018	6.759	7.812	0.671	0.021	100.132	47.61
OLA90_25_P1C	59.971	0.025	25.116	0.377	0.009	7.47	6.27	0.896	0.069	100.203	38.89
OLA90_25_P1D	61.657	0.03	23.985	0.332	0.01	7.968	5.434	1.067	0.022	100.505	48.18
OLA90_25_P2A	53.976	0.076	24.332	0.7	0.02	5.771	5.405	0.746	0.065	91.091	34.77
OLA90_25_P2B	56.06	0.025	27.464	0.539	0.038	5.796	9.47	0.444	0.038	99.874	40.75
OLA90_25_P2C	57.314	0.021	26.743	0.482	0.022	6.338	8.553	0.567	0.042	100.082	38.19
OLA90_25_P2D	55.221	0.035	28.156	0.648	0.032	5.543	10.339	0.389	0.021	100.384	43.99
OLA90_25_P3B	56.592	0.009	27.416	0.566	0.015	6.246	9.337	0.429	0.047	100.657	44.15
OLA90_25_P3C	61.359	0.046	24.281	0.363	0.006	7.822	5.761	1.001	0.079	100.718	27.29
OLA90_25_P4A	58.189	0	25.804	0.327	0.024	6.97	7.558	0.674	0	99.546	36.04
OLA90_25_P4B	58.065	0.057	26.343	0.374	0.012	6.624	8.08	0.61	0.022	100.187	38.86
OLA90_25_P4C	60.726	0.048	24.431	0.388	0.016	7.684	5.836	0.997	0.029	100.155	27.89
OLA90_25_P4D	57.794	0.007	26.739	0.322	0.004	6.682	8.247	0.575	0.015	100.385	39.23
OLA90_25_P4E	59.912	0	24.955	0.436	0.017	7.407	6.527	0.891	0.09	100.235	31.09

OLA90_25_P5A	59.888	0.023	25.04	0.364	0.013	7.43	6.748	0.82	0.095	100.421	31.88
OLA90_25_P5C	56.237	0.002	27.699	0.703	0.041	5.517	9.993	0.455	0.02	100.667	48.70
OLA90_25_P6A	56.359	0.002	27.63	0.364	0.013	6.14	9.363	0.461	0.038	100.37	44.54
OLA90_25_P6B	58.319	0.041	25.84	0.336	0.014	6.92	7.834	0.666	0.041	100.011	37.04
OLA90_25_P6C	61.857	0.119	23.557	0.664	0.073	5.86	6.883	1.189	0.072	100.274	36.41
OLA90_25_P6D	53.416	0.071	28.656	0.666	0.051	4.998	10.967	0.325	0.02	99.17	53.76
OLA90_25_P7A	50.423	0.012	28.993	0.451	0.017	4.578	11.941	0.259	0.04	96.714	58.15
OLA90_25_P7B	56.361	0.08	25.015	0.321	0.014	6.811	7.472	0.658	0.026	96.758	36.31
OLA90_25_P7C	52.927	0	27.476	0.365	0.011	5.537	9.931	0.366	0.033	96.646	48.71
OLA90_25_P7D	55.264	0	25.937	0.379	0.008	6.626	8.107	0.582	0.058	96.961	38.99
OLA90_25_P8A	57.024	0.009	26.936	0.529	0.024	6.402	8.729	0.583	0.078	100.314	41.55
OLA90_25_P9A	58.748	0.055	25.089	0.327	0.008	7.185	7.559	0.736	0.056	99.763	35.26
OLA90_25_P9B	55.798	0.062	27.491	0.492	0.016	5.797	9.6	0.469	0.044	99.769	46.49
OLA90_25_P9C	55.416	0.062	27.693	0.544	0.033	5.871	9.691	0.416	0.049	99.775	46.57
OLA90_25_P10A	59.137	0.076	25.253	0.437	0.021	7.152	7.15	0.85	0.033	100.109	33.88
OLA90_25_P10B	58.843	0.06	25.323	0.408	0.017	7.131	7.123	0.786	0.023	99.714	33.98
OLA90_25_P10C	55.134	0.005	27.278	0.59	0.026	6.08	9.428	0.479	0.075	99.095	44.89
OLA90_25_P11B	56.022	0.069	27.624	0.334	0.016	5.966	9.582	0.441	0.054	100.108	45.84
OLA90_25_P11C	61.127	0.002	24.127	0.363	0.013	7.608	5.782	1.042	0.088	100.152	27.81
OLA90_25_P11D	58.206	0.016	26.089	0.507	0.027	6.499	7.957	0.637	0.031	99.969	38.86
OLA90_25_P12B	54.019	0.035	28.297	0.357	0.017	5.462	10.357	0.354	0.046	98.944	50.12
OLA90_25_P12C	60.654	0	23.34	0.364	0.015	7.949	5.221	1.185	0.122	98.85	24.84
OLA90_25_P12D	58.531	0.08	24.843	0.608	0.022	7.142	7.065	0.752	0.121	99.164	33.83
OLA90_25_P13A	58.08	0.055	25.696	0.35	0.009	7.067	7.727	0.667	0.066	99.717	36.26
OLA90_25_P13B	59.185	0.03	25.184	0.371	0.012	7.323	6.805	0.778	0.052	99.74	32.43
OLA90_25_P13C	56.797	0.037	26.772	0.433	0.018	6.367	8.58	0.548	0.052	99.604	41.34
OLA90_25_P14A	60.603	0.037	24.546	0.423	0.01	7.672	6.245	0.888	0.04	100.464	29.48
OLA90_25_P14B	60.329	0.025	24.649	0.433	0.013	7.515	6.46	0.842	0.058	100.324	30.67
OLA90_25_P14C	53.109	0.085	24.428	0.627	0.043	6.05	11.118	0.557	0.032	96.049	48.91
OLA90_25_P15A	58.545	0.023	25.196	0.355	0.017	7.119	7.156	0.726	0.067	99.204	34.23
OLA90_25_P15B	59.511	0.023	24.94	0.373	0.013	7.48	6.538	0.812	0.067	99.757	31.07
OLA90_25_P15C	58.805	0.053	25.641	0.319	0.016	7.241	7.131	0.732	0.081	100.019	33.79
OLA90_25_P15D	60.773	0.034	24.057	0.364	0.016	7.986	5.706	1.069	0.074	100.079	26.63
OLA90_25_P15E	56.732	0.028	26.545	0.52	0.026	6.258	7.604	0.607	0.074	98.394	38.69
OLA90_25_P15F	59.694	0.014	25.265	0.41	0.009	7.434	6.75	0.814	0.099	100.489	31.88
OLA90_25_P15G	57.961	0.007	26.145	0.504	0.015	6.843	7.863	0.623	0.039	100	37.46
OLA90_25_P16A	58.796	0.053	25.443	0.32	0.009	7.113	7.311	0.737	0.028	99.81	34.71
OLA90_25_P16C	55.04	0.03	28.013	0.493	0.033	5.489	10.353	0.379	0.056	99.886	49.92
OLA90_25_P17A	58.603	0.023	24.77	0.391	0.012	7.116	6.799	0.803	0.046	98.563	32.95
OLA90_25_P17B	51.523	0.016	29.343	0.711	0.055	4.559	11.969	0.249	0.04	98.465	58.34
OLA90_25_P18A	58.892	0	25.573	0.369	0.011	7.088	7.388	0.69	0.049	100.06	35.12
OLA90_25_P18B	54.879	0.041	28.382	0.523	0.029	5.313	10.553	0.359	0.018	100.097	51.24
OLA90_25_P18D	56.765	0	27.263	0.489	0.033	6.195	9.087	0.468	0.062	100.362	43.57
OLA90_25_P19A	59.813	0.05	25.145	0.383	0.016	7.394	6.81	0.798	0.068	100.477	32.21
OLA90_25_P19B	56.386	0.032	27.395	0.39	0.016	6.147	9.187	0.476	0.077	100.106	44.00
OLA90_25_P19C	58.357	0.032	25.936	0.361	0.016	6.892	7.661	0.68	0.038	99.973	36.58

OLA90_25_P20A	58.352	0.048	25.615	0.545	0.024	7.011	6.667	0.74	0.036	99.038	32.95
OLA90_25_P20B	55.319	0.023	27.916	0.395	0.011	5.864	9.7	0.404	0.033	99.665	46.65
OLA90_25_P20C	58.108	0	25.84	0.379	0.016	6.892	7.578	0.665	0.016	99.494	36.36
OLA90_25_P20D	60.027	0.037	24.432	0.401	0.009	7.569	6.157	0.984	0.101	99.717	29.28
OLA90_14_P1A	51.894	0.025	28.731	0.551	0.035	4.668	11.233	0.239	0	97.376	56.26
OLA90_14_P1B	51.385	0	30.012	0.623	0.041	4.114	12.621	0.178	0.009	98.983	62.24
OLA90_14_P1C	58.423	0.039	26.352	0.399	0.016	7.097	8.037	0.341	0.053	100.757	37.76
OLA90_14_P2A	52.825	0.012	28.753	0.563	0.048	5.185	11.061	0.215	0.003	98.665	53.44
OLA90_14_P2B	49.448	0	30.78	0.609	0.041	3.641	13.427	0.152	0.026	98.124	66.48
OLA90_14_P2C	52.146	0.018	28.845	0.553	0.044	4.842	11.246	0.238	0.043	97.975	55.42
OLA90_14_P3A	48.234	0.067	32.018	0.644	0.032	2.775	14.884	0.074	0.03	98.758	74.44
OLA90_14_P3B	53.127	0	28.517	0.613	0.05	5.175	10.879	0.249	0.026	98.636	52.96
OLA90_14_P3D	52.896	0.005	29.097	0.556	0.028	4.939	11.379	0.22	0.02	99.14	55.30
OLA90_14_P3E	57.641	0.062	25.932	0.528	0.049	5.854	8.59	0.454	0.057	99.167	43.55
OLA90_14_P4A	51.396	0.014	30.043	0.566	0.042	4.211	12.524	0.172	0.016	98.984	61.55
OLA90_14_P4B	55.668	0.025	27.316	0.249	0.02	6.087	9.364	0.304	0.053	99.086	45.15
OLA90_14_P4C	55.937	0.018	26.942	0.466	0.036	5.951	9.13	0.341	0.065	98.886	44.96
OLA90_14_P5A	53.309	0.067	29.211	0.635	0.048	4.791	11.648	0.216	0.016	99.941	56.61
OLA90_14_P5B	52.506	0.062	30.019	0.506	0.028	4.444	12.191	0.18	0.018	99.954	59.62
OLA90_14_P5C	58.19	0.002	25.692	0.53	0.047	6.781	7.952	0.422	0.043	99.659	38.37
OLA90_14_P6A	51.005	0.048	30.671	0.614	0.042	3.895	13.119	0.157	0.012	99.563	64.45
OLA90_14_P6B	53.725	0.062	29.102	0.463	0.031	4.981	11.151	0.236	0.028	99.779	54.54
OLA90_14_P6C	56.582	0.016	27.409	0.246	0.015	6.304	9.053	0.292	0.044	99.961	43.51
OLA90_14_P6D	61.339	0.053	24.522	0.456	0.049	7.71	6.041	0.625	0.118	100.913	29.13
OLA90_14_P7A	53.54	0.039	29.164	0.559	0.044	5.033	11.335	0.219	0.013	99.946	54.75
OLA90_14_P7B	50.478	0.021	31.257	0.663	0.048	3.469	13.86	0.128	0	99.924	68.31
OLA90_14_P7C	52.284	0.062	29.769	0.523	0.051	4.411	12.311	0.185	0.012	99.608	60.01
OLA90_14_P7D	55.579	0.041	28.096	0.337	0.029	5.732	9.922	0.27	0.011	100.017	48.13
OLA90_14_P8A	52.613	0.06	29.662	0.551	0.05	4.462	12.083	0.189	0.021	99.691	59.28
OLA90_14_P8B	57.465	0.011	27.047	0.242	0.016	6.602	8.497	0.341	0.063	100.284	40.75
OLA90_14_P8C	58.213	0	26.543	0.25	0.025	6.825	8.092	0.365	0.031	100.344	38.76
OLA90_14_P8D	57.974	0	26.333	0.535	0.041	6.662	8.14	0.409	0.038	100.132	39.36
OLA90_14_P9A	52.954	0.025	29.444	0.539	0.055	4.506	11.855	0.216	0.011	99.605	58.50
OLA90_14_P9B	57.807	0	26.59	0.278	0.011	6.761	8.271	0.334	0.005	100.057	39.57
OLA90_14_P9C	56.05	0.037	27.836	0.471	0.028	6.003	9.453	0.319	0.015	100.212	45.68
OLA90_14_P10A	53.553	0	29.323	0.592	0.048	4.866	11.302	0.22	0.021	99.925	55.48
OLA90_14_P10C	57.81	0.016	26.483	0.317	0.002	6.548	8.323	0.309	0.038	99.846	40.52
OLA90_14_P11A	52.422	0.048	30.239	0.562	0.048	4.149	12.567	0.167	0.01	100.212	61.99
OLA90_14_P11B	49.202	0.035	31.805	0.569	0.045	3.024	14.56	0.106	0	99.346	72.23
OLA90_14_P11C	51.767	0.023	30.225	0.539	0.046	4.151	12.671	0.168	0.011	99.601	62.17
OLA90_14_P11D	58.466	0.023	26.084	0.488	0.042	6.81	7.96	0.376	0.062	100.311	38.40
OLA90_14_P12A	51.93	0.021	30.51	0.593	0.044	4.1	12.773	0.186	0	100.157	62.57
OLA90_14_P12B	56.444	0.025	27.261	0.355	0.016	6.207	8.956	0.318	0.035	99.617	43.55
OLA90_14_P12C	59.122	0.034	25.478	0.515	0.035	7.142	7.284	0.496	0.045	100.151	35.02
OLA90_14_P13A	50.421	0.035	31.377	0.61	0.045	3.412	13.737	0.138	0	99.775	68.43
OLA90_14_P13B	53.459	0.06	29.302	0.488	0.031	4.832	11.387	0.229	0.009	99.797	55.81
OLA90_14_P13C	60.153	0.023	24.515	0.423	0.049	7.132	6.934	0.579	0.086	99.894	33.78

OLA90_14_P14B	52.126	0.046	30.338	0.566	0.042	4.138	12.456	0.176	0	99.888	61.80
OLA90_14_P14C	57.02	0.03	27.257	0.344	0.014	6.201	8.955	0.342	0.029	100.192	43.51
OLA90_14_P14D	54.307	0.018	28.824	0.47	0.043	5.125	10.869	0.276	0.041	99.973	53.09
OLA90_14_P15A	54.154	0.025	28.754	0.568	0.031	5.221	11.163	0.234	0.044	100.194	53.44
OLA90_14_P15B	51.698	0.037	30.567	0.567	0.05	3.995	12.789	0.165	0	99.868	63.27
OLA90_14_P15C	51.753	0.021	29.973	0.504	0.026	4.362	12.35	0.17	0.008	99.167	60.40
OLA90_14_P15D	56.296	0	27.471	0.288	0.011	6.023	9.17	0.329	0.038	99.626	44.82
OLA90_14_P15E	54.506	0	28.691	0.431	0.037	5.216	10.762	0.265	0.033	99.941	52.46
OLA90_14_P16A	50.189	0	31.321	0.634	0.048	3.392	13.887	0.12	0.025	99.616	68.86
OLA90_14_P16B	51.811	0.009	30.709	0.503	0.043	4.026	12.819	0.169	0.017	100.106	63.13
OLA90_14_P16C	57.005	0.037	26.967	0.277	0.013	6.403	8.783	0.316	0	99.801	42.34
OLA90_14_P17A	47.207	0.053	33.916	0.603	0.034	1.88	16.535	0.075	0.029	100.332	82.57
OLA90_14_P17B	51.924	0.058	30.316	0.59	0.041	4.099	12.629	0.184	0.035	99.876	62.32
OLA90_14_P18A	53.987	0.007	28.833	0.553	0.026	4.999	11.006	0.239	0.023	99.673	54.12
OLA90_14_P18B	50.787	0.002	30.967	0.57	0.041	3.73	13.535	0.143	0.035	99.81	66.17
OLA90_14_P18C	52.377	0.025	29.96	0.478	0.04	4.55	12.199	0.181	0.02	99.83	59.08
OLA90_14_P18D	69.19	0.101	19.498	0.578	0.076	6.083	4.335	1.326	0.109	101.296	25.62
OLA90_14_P19A	53.663	0.014	29.101	0.573	0.053	5.023	11.306	0.206	0.023	99.962	54.77
OLA90_14_P19B	52.118	0.021	30.179	0.601	0.049	4.247	12.447	0.168	0.017	99.847	61.22
OLA90_14_P19C	52.739	0.032	29.875	0.465	0.032	4.641	11.985	0.191	0.008	99.968	58.15
OLA90_14_P19E	66.7	0.076	20.365	0.455	0.046	7.663	3.606	1.239	0.072	100.222	19.03
OLA90_14_P20A	51.244	0.03	30.728	0.563	0.044	3.929	12.989	0.154	0	99.681	64.04
OLA90_14_P20B	53.424	0.028	29.498	0.491	0.023	4.894	11.602	0.196	0.005	100.161	56.07
OLA90_14_P20C	56.837	0.023	27.445	0.287	0.012	6.359	8.924	0.322	0.03	100.239	42.87
OLA90_14_P20D	74.786	0.428	12.865	2.082	0.322	2.464	0.592	2.747	0.083	96.369	7.11
OLA90_02_P1A	61.378	0.016	24.141	0.298	0.004	8.087	5.576	0.916	0.031	100.447	26.18
OLA90_02_P1B	59.689	0	25.41	0.253	0	7.581	6.877	0.644	0.036	100.49	32.19
OLA90_02_P1C	61.14	0.011	24.614	0.29	0.009	7.782	6.044	0.773	0.062	100.725	28.72
OLA90_02_P1D	60.372	0.005	25.349	0.279	0.001	7.612	6.591	0.686	0.048	100.943	31.12
OLA90_02_P1E	61.032	0.041	24.572	0.243	0.009	7.786	5.875	0.819	0.044	100.421	28.06
OLA90_02_P1F	61.733	0	24.256	0.196	0.004	7.945	5.669	0.89	0	100.693	26.86
OLA90_02_P2A	60.353	0	25.011	0.18	0	7.58	6.193	0.771	0.021	100.109	29.73
OLA90_02_P2B	59.377	0	25.757	0.343	0.014	7.332	6.896	0.674	0.003	100.396	32.89
OLA90_02_P2C	61.225	0.034	24.291	0.272	0.005	7.995	5.648	0.885	0.022	100.377	26.68
OLA90_02_P2D	60.85	0	24.841	0.231	0	7.732	6.2	0.815	0.002	100.671	29.30
OLA90_02_P2E	58.397	0	25.749	0.321	0.009	7.016	7.494	0.626	0.074	99.686	35.80
OLA90_02_P3A	60.145	0	25.183	0.253	0	7.643	6.417	0.652	0.037	100.33	30.52
OLA90_02_P3B	58.855	0.009	25.828	0.222	0.006	7.127	7.322	0.559	0.044	99.972	35.06
OLA90_02_P3C	60.593	0.018	24.954	0.259	0.001	7.702	6.398	0.711	0.021	100.657	30.20
OLA90_02_P3D	61.275	0	24.386	0.229	0.005	7.932	5.859	0.829	0.015	100.53	27.64
OLA90_02_P3E	57.155	0.009	27.246	0.356	0.014	6.447	8.887	0.458	0.063	100.635	42.12
OLA90_02_P4A	60.592	0	24.89	0.282	0.021	7.978	6.134	0.733	0	100.63	28.60
OLA90_02_P4B	52.371	0.009	30.414	0.28	0.009	4.26	12.685	0.207	0	100.235	61.46
OLA90_02_P4C	60.13	0	24.992	0.233	0.004	7.582	6.745	0.665	0.007	100.358	31.73
OLA90_02_P4D	58.168	0.021	26.833	0.248	0	6.869	8.208	0.503	0.017	100.867	38.65
OLA90_02_P5A	51.844	0.039	30.992	0.28	0.002	3.921	13.035	0.184	0.009	100.306	64.06
OLA90_02_P5B	59.071	0	26.011	0.266	0.017	7.135	7.354	0.647	0.031	100.532	34.96

OLA90_02_P5C	59.889	0	25.121	0.264	0.011	7.46	6.674	0.763	0.033	100.215	31.66
OLA90_02_P5D	60.261	0	25.154	0.244	0	7.49	6.473	0.782	0.06	100.464	30.89
OLA90_02_P5E	59	0.014	26.056	0.251	0.003	7.052	7.603	0.629	0.061	100.669	36.01
OLA90_02_P5G	58.828	0.051	26.248	0.249	0.012	7.042	7.552	0.624	0.049	100.655	35.90
OLA90_02_P5H	59.707	0.041	25.506	0.266	0.005	7.588	6.73	0.733	0.036	100.612	31.55
OLA90_02_P5I	60.346	0.032	24.644	0.291	0.008	7.637	5.769	0.962	0.003	99.692	27.82
OLA90_02_P6A	45.215	0.018	19.54	0.381	0.015	5.254	5.025	0.528	0.017	75.993	33.14
OLA90_02_P6B	60.311	0.028	23.81	0.206	0	6.91	6.198	0.68	0	98.143	31.76
OLA90_02_P6C	61.378	0	24.194	0.212	0.005	7.979	5.576	0.928	0.013	100.285	26.40
OLA90_02_P6D	61.852	0.034	24.05	0.252	0.009	8.096	5.496	0.948	0.024	100.761	25.83
OLA90_02_P7A	60.006	0	22.554	0.222	0.008	7.202	5.656	0.793	0	96.441	28.81
OLA90_02_P7B	59.039	0	25.909	0.259	0	7.217	7.332	0.549	0.069	100.374	34.84
OLA90_02_P7C	61.008	0.048	25.175	0.248	0.003	7.569	6.435	0.742	0.034	101.262	30.62
OLA90_02_P7D	59.133	0	25.654	0.313	0	7.222	7.175	0.645	0.063	100.205	34.15
OLA90_02_P8A	61.984	0	23.75	0.24	0.004	7.977	5.244	1.026	0.056	100.281	25.09
OLA90_02_P8B	59.531	0.014	23.353	0.226	0.009	7.234	5.439	1.695	0.041	97.542	26.47
OLA90_02_P8C	58.998	0.009	25.59	0.304	0.018	7.101	7.254	0.634	0.067	99.975	34.78
OLA90_02_P9A	56.983	0.025	27.209	0.297	0.003	6.521	8.735	0.414	0.077	100.264	41.54
OLA90_02_P9B	59.078	0.032	25.654	0.34	0.012	7.281	7.215	0.62	0.064	100.296	34.15
OLA90_02_P9C	59.15	0	26.058	0.333	0.02	6.89	7.526	0.583	0.042	100.602	36.38
OLA90_02_P10A	60.204	0	25.327	0.249	0.005	7.539	6.566	0.67	0.097	100.657	31.26
OLA90_02_P10B	58.177	0.039	26.777	0.222	0.005	6.835	8.21	0.503	0.017	100.785	38.77
OLA90_02_P11A	59.251	0	25.761	0.235	0.002	7.232	7.253	0.633	0.024	100.391	34.38
OLA90_02_P11B	59.057	0	26.145	0.298	0.006	6.907	7.653	0.575	0.055	100.696	36.73
OLA90_02_P11C	59.78	0.012	25.687	0.341	0.006	7.432	7.044	0.631	0.111	101.044	33.16
OLA90_02_P11D	70.819	0.12	16.423	0.571	0.017	5.78	2.234	2.513	0.143	98.62	14.24
OLA90_02_P12A	59.703	0	25.514	0.244	0.002	7.45	7.029	0.591	0.009	100.542	33.13
OLA90_02_P12B	60.31	0.018	25.035	0.261	0	7.748	6.517	0.684	0.062	100.635	30.52
OLA90_02_P12C	59.942	0	25.154	0.246	0.005	7.628	6.652	0.635	0.04	100.302	31.36
OLA90_02_P12D	60.53	0.048	24.731	0.232	0.004	7.856	6.194	0.72	0.036	100.351	29.12
OLA90_02_P12E	58.988	0.016	26.22	0.277	0.002	7.288	7.544	0.553	0.021	100.909	35.27
OLA90_02_P12F	61.676	0	23.645	0.24	0.005	8.184	5.422	0.877	0.011	100.06	25.48
OLA90_02_P13A	60.88	0.023	24.414	0.247	0	7.982	6.183	0.819	0.043	100.591	28.62
OLA90_02_P13B	59.372	0.025	25.578	0.229	0.003	7.263	7.247	0.603	0	100.32	34.33
OLA90_02_P13C	57.752	0.03	26.864	0.287	0.014	6.685	8.295	0.529	0.061	100.517	39.46
OLA90_02_P13D	61.919	0.018	23.849	0.279	0.006	8.063	5.481	0.926	0.041	100.582	25.88
OLA90_02_P14B	60.295	0	24.814	0.202	0.01	7.654	6.567	0.746	0	100.288	30.82
OLA90_02_P14C	59.991	0.03	24.956	0.211	0.001	7.416	6.826	0.716	0.007	100.154	32.35
OLA90_02_P15A	59.696	0	25.564	0.252	0	7.578	6.957	0.635	0.031	100.713	32.47
OLA90_02_P15B	54.185	0.018	29.144	0.202	0.012	5.158	11.12	0.286	0	100.125	53.48
OLA90_02_P15C	59.519	0.021	25.835	0.205	0.011	7.365	7.191	0.642	0	100.789	33.79
OLA90_02_P15D	61.24	0.044	24.343	0.233	0.003	7.942	5.752	0.858	0.054	100.469	27.20
OLA90_02_P16A	56.54	0.016	27.4	0.369	0.017	6.065	9.341	0.445	0.072	100.265	44.81
OLA90_02_P16B	60.091	0.035	24.947	0.2	0.006	7.313	6.784	0.669	0.023	100.068	32.59
OLA90_02_P16C	56.129	0.016	27.904	0.367	0.019	5.808	9.905	0.347	0.03	100.525	47.56
OLA90_02_P17A	58.795	0	25.056	0.296	0.006	7.105	7.304	0.671	0.057	99.29	34.85
OLA90_02_P17B	59.686	0.002	25.079	0.201	0.002	7.682	6.865	0.664	0.006	100.187	31.85

OLA90_02_P17C	58.568	0	25.686	0.359	0.001	6.895	7.742	0.618	0.08	99.949	36.95
OLA90_02_P18A	59.711	0.041	25.402	0.231	0	7.41	6.806	0.632	0.018	100.251	32.46
OLA90_02_P18B	57.495	0.037	26.738	0.215	0.007	6.677	8.227	0.444	0	99.84	39.48
OLA90_02_P18C	60.6	0.002	24.622	0.269	0.006	8.004	5.853	0.814	0.021	100.191	27.47
OLA90_02_P18D	60.523	0	24.424	0.187	0.005	7.766	5.89	0.831	0	99.626	28.14
OLA90_02_P19A	59.741	0.002	25.321	0.218	0	7.421	6.99	0.675	0	100.368	32.94
OLA90_02_P19B	59.543	0.014	25.568	0.187	0.001	7.408	7.25	0.601	0.012	100.584	33.92
OLA90_02_P20A	58.801	0.023	26.162	0.226	0	7.07	7.67	0.542	0.047	100.541	36.33
OLA90_02_P20B	59.999	0.009	25.294	0.188	0.004	7.418	6.821	0.665	0.01	100.408	32.42
OLA90_02_P20C	55.616	0.018	27.886	0.528	0.025	5.75	10	0.376	0.029	100.228	47.95
OLA90_52_P1A	55.95	0.007	26.402	0.459	0.038	6.084	8.779	0.646	0.06	98.425	42.70
OLA90_52_P1C	56.651	0.009	26.358	0.437	0.03	6.339	8.5	0.667	0.033	99.024	40.93
OLA90_52_P1D	57.861	0.055	25.338	0.434	0.023	6.739	7.489	0.847	0.082	98.868	36.19
OLA90_52_P1E	55.363	0.03	27.193	0.524	0.036	5.783	9.528	0.554	0.094	99.105	46.13
OLA90_52_P2A	56.634	0.041	25.879	0.457	0.026	6.306	8.148	0.746	0.111	98.348	39.85
OLA90_52_P2B	52.821	0.088	28.602	0.439	0.021	4.996	11.211	0.403	0.056	98.637	54.08
OLA90_52_P2C	56.476	0	26.287	0.407	0.019	6.272	8.529	0.655	0.061	98.706	41.29
OLA90_52_P2D	55.737	0	26.702	0.448	0.038	6.018	8.982	0.605	0.077	98.607	43.62
OLA90_52_P2E	56.955	0.032	26.107	0.448	0.034	6.503	8.383	0.7	0.059	99.221	39.95
OLA90_52_P3A	55.888	0.032	26.416	0.38	0.022	5.97	8.785	0.858	0.071	98.422	42.62
OLA90_52_P3B	52.64	0.009	28.823	0.416	0.021	4.629	11.539	0.498	0.051	98.626	56.26
OLA90_52_P3C	54.629	0.009	27.866	0.428	0.03	5.422	10.051	0.651	0.077	99.163	48.70
OLA90_52_P3D	53.975	0.074	27.995	0.63	0.06	5.231	10.53	0.38	0.06	98.935	51.50
OLA90_52_P4A	53.9	0.007	28.16	0.409	0.023	5.219	10.606	0.555	0.057	98.936	51.21
OLA90_52_P4B	54.494	0.009	27.633	0.497	0.021	5.577	10.018	0.629	0.042	98.92	48.03
OLA90_52_P4C	56.612	0.041	26.198	0.536	0.032	6.329	8.625	0.762	0.066	99.201	41.10
OLA90_52_P4D	52.304	0.048	29.199	0.678	0.057	4.42	12.153	0.32	0.008	99.187	59.19
OLA90_52_P5A	57.957	0.032	25.125	0.442	0.021	6.857	7.24	1.01	0.094	98.778	34.72
OLA90_52_P5B	56.472	0.053	26.48	0.481	0.033	6.226	8.666	0.665	0.084	99.16	41.82
OLA90_52_P6A	52.067	0.062	29.533	0.618	0.04	4.43	12.232	0.358	0.027	99.367	59.16
OLA90_52_P6B	51.18	0.03	30.114	0.484	0.04	4.106	12.75	0.276	0	98.98	62.17
OLA90_52_P6C	52.549	0	29.346	0.617	0.067	4.68	11.731	0.329	0.004	99.323	56.97
OLA90_52_P6D	51.506	0.065	29.896	0.677	0.051	4.325	12.465	0.317	0	99.302	60.31
OLA90_52_P6E	53.442	0.016	28.424	0.608	0.038	5.116	10.978	0.453	0.011	99.086	52.84
OLA90_52_P6F	53.228	0.021	28.741	0.661	0.07	4.907	11.384	0.337	0.07	99.419	55.09
OLA90_52_P7A	56.998	0.03	26.319	0.434	0.029	6.546	8.375	0.693	0.024	99.448	39.79
OLA90_52_P7B	57.282	0	26.061	0.473	0.022	6.641	8.055	0.75	0.06	99.344	38.42
OLA90_52_P7C	59.31	0.06	27.059	0.656	0.044	5.753	8.91	0.54	0.103	102.435	44.63
OLA90_52_P8A	56.748	0	26.466	0.295	0.013	6.2	8.664	0.635	0.019	99.04	41.98
OLA90_52_P8B	54.382	0.018	28.323	0.274	0.013	5.405	10.407	0.42	0.012	99.254	50.30
OLA90_52_P8C	55.139	0.009	27.615	0.28	0.003	5.616	9.959	0.494	0.034	99.149	48.09
OLA90_52_P8D	55.908	0	26.943	0.195	0.016	6.126	9.128	0.556	0.008	98.88	43.73
OLA90_52_P8E	54.268	0.014	27.924	0.27	0.021	5.344	10.29	0.438	0	98.569	50.24
OLA90_52_P8F	56.609	0.028	26.501	0.27	0.027	6.323	8.524	0.621	0.047	98.95	41.17
OLA90_52_P9A	52.597	0.012	28.932	0.519	0.04	4.891	11.404	0.363	0.061	98.819	55.13
OLA90_52_P9B	51.572	0.041	29.904	0.543	0.024	4.302	12.485	0.301	0.056	99.228	60.52
OLA90_52_P9C	55.336	0.053	27.253	0.455	0.032	5.752	9.659	0.532	0.087	99.159	46.66

OLA90_52_P9D	50.763	0.023	30.266	0.548	0.029	3.861	13.15	0.228	0.058	98.926	64.43
OLA90_52_P9E	53.41	0	28.502	0.514	0.038	4.962	11.173	0.356	0.08	99.035	54.30
OLA90_52_P9F	57.969	0.069	28.412	0.65	0.062	5.705	9.872	0.486	0.045	103.27	47.52
OLA90_52_P10B	57.586	0.032	25.868	0.433	0.026	6.581	8.021	0.704	0.097	99.348	38.62
OLA90_52_P10C	51.713	0.048	29.88	0.542	0.045	4.268	12.598	0.285	0.032	99.411	60.98
OLA90_52_P10D	54.657	0.012	27.97	0.496	0.034	5.421	10.319	0.428	0.057	99.394	50.00
OLA90_52_P10E	51.623	0.069	29.648	0.654	0.037	4.257	12.411	0.283	0.036	99.018	60.69
OLA90_52_P10F	52.354	0.028	29.432	0.669	0.051	4.593	12.001	0.298	0.056	99.482	58.07
OLA90_52_P10G	53.365	0.035	28.593	0.637	0.047	4.991	11.247	0.36	0.081	99.356	54.31
OLA90_52_P11A	53.191	0.035	28.061	0.582	0.036	5.058	11.241	0.387	0.048	98.639	53.90
OLA90_52_P11B	56.407	0.018	26.686	0.492	0.044	5.992	8.979	0.586	0.019	99.223	43.76
OLA90_52_P11C	53.665	0.037	28.638	0.598	0.039	4.923	11.131	0.376	0.021	99.428	54.33
OLA90_52_P11D	53.913	0.028	28.121	0.633	0.049	5.266	10.712	0.42	0.017	99.159	51.65
OLA90_52_P12A	55.062	0.062	27.761	0.49	0.035	5.594	9.823	0.497	0.035	99.359	47.83
OLA90_52_P12B	51.751	0.014	30.019	0.673	0.036	4.238	12.694	0.297	0.016	99.738	61.27
OLA90_52_P12C	53.863	0.028	28.508	0.588	0.043	5.234	10.864	0.392	0	99.52	52.23
OLA90_52_P12D	52.753	0.071	28.911	0.644	0.038	4.805	11.602	0.34	0.013	99.177	56.04
OLA90_52_P12E	54.404	0.016	28.08	0.552	0.043	5.315	10.567	0.433	0.044	99.454	51.05
OLA90_52_P12F	55.065	0.039	27.108	0.701	0.051	5.768	9.595	0.552	0.066	98.945	46.37
OLA90_52_P13A	53.422	0.032	28.585	0.5	0.039	5.081	10.947	0.385	0.048	99.039	53.14
OLA90_52_P13B	52.191	0.005	29.87	0.448	0.028	4.56	12.234	0.307	0.056	99.699	58.67
OLA90_52_P13C	56.707	0	26.783	0.505	0.023	6.236	8.819	0.591	0.04	99.704	42.38
OLA90_52_P13D	55.082	0.037	28.106	0.549	0.034	5.507	10.415	0.424	0.029	100.183	49.87
OLA90_52_P14A	56.374	0.009	26.56	0.415	0.025	6.035	8.832	0.948	0.037	99.235	42.30
OLA90_52_P14B	55.761	0	27.192	0.466	0.013	5.647	9.562	0.836	0.052	99.529	46.02
OLA90_52_P14C	57.67	0	25.515	0.449	0.02	6.344	7.758	1.209	0.048	99.013	37.52
OLA90_52_P14D	53.035	0.032	28.189	0.463	0.026	4.991	10.717	0.641	0.043	98.137	52.25
OLA90_52_P14E	55.456	0	27.237	0.52	0.041	5.786	9.713	0.529	0.079	99.361	46.67
OLA90_52_P14F	57.121	0.044	25.838	0.693	0.039	6.173	8.547	0.677	0.073	99.205	41.64
OLA90_52_P15A	57.796	0.028	25.959	0.469	0.023	6.728	7.868	0.761	0.054	99.686	37.56
OLA90_52_P15B	53.317	0.083	29.114	0.451	0.01	4.848	11.539	0.359	0.041	99.762	55.64
OLA90_52_P15C	56.044	0.025	26.978	0.431	0.021	5.919	9.232	0.575	0.045	99.27	44.76
OLA90_52_P15D	55.603	0.005	27.36	0.455	0.025	5.73	9.584	0.537	0.057	99.356	46.54
OLA90_52_P15E	57.454	0.046	25.829	0.406	0.038	6.538	7.961	0.714	0.076	99.062	38.57
OLA90_52_P15F	54.144	0.05	28.383	0.616	0.038	5.175	10.823	0.409	0.06	99.698	52.35
OLA90_52_P16A	57.357	0.023	26.394	0.432	0.032	6.4	8.41	0.925	0.109	100.082	39.87
OLA90_52_P16B	56.42	0	26.871	0.444	0.013	5.966	8.935	0.803	0.055	99.507	43.19
OLA90_52_P16C	54.359	0.03	28.484	0.441	0.02	5.224	10.738	0.54	0.028	99.864	51.54
OLA90_52_P16D	57.209	0.073	26.061	0.444	0.027	6.405	8.095	0.961	0.09	99.365	38.86
OLA90_52_P16E	52.079	0.028	30.046	0.476	0.011	4.217	12.575	0.365	0.026	99.823	60.92
OLA90_52_P16F	57.236	0.023	26.116	0.467	0.028	6.506	8.322	0.893	0.096	99.687	39.33
OLA90_52_P16G	54.213	0.032	27.874	0.66	0.045	5.38	10.451	0.422	0.009	99.086	50.51
OLA90_52_P17A	56.837	0	26.525	0.478	0.032	6.278	8.702	0.735	0.036	99.623	41.56
OLA90_52_P17B	57.693	0.041	25.728	0.462	0.036	6.652	7.758	0.872	0.064	99.306	37.24
OLA90_52_P17C	57.713	0.011	25.831	0.46	0.021	6.325	8.06	0.764	0.077	99.262	39.48
OLA90_52_P17D	54.021	0.124	27.874	0.688	0.06	5.206	10.741	0.425	0.031	99.17	51.97
OLA90_52_P18A	55.263	0.005	27.485	0.379	0.023	5.675	9.712	0.483	0.021	99.046	47.25

OLA90_52_P18B	52.372	0.018	29.371	0.46	0.022	4.621	11.967	0.319	0.018	99.168	57.79
OLA90_52_P18C	56.896	0.009	26.647	0.441	0.023	6.29	8.702	0.63	0.078	99.716	41.77
OLA90_52_P18D	54.024	0.064	28.246	0.611	0.048	5.054	10.934	0.358	0.034	99.373	53.32
OLA90_52_P19B	54.177	0.037	27.978	0.583	0.059	5.378	10.502	0.436	0.054	99.204	50.60
OLA90_52_P19C	53.098	0.05	29.003	0.675	0.068	4.824	11.569	0.329	0.029	99.645	55.92
OLA90_52_P20A	58.659	0	25.357	0.434	0.023	6.993	7.334	0.905	0.062	99.767	34.81
OLA90_52_P20B	56.619	0	26.622	0.452	0.02	6.269	8.786	0.717	0.047	99.532	41.87
OLA90_52_P20C	56.42	0.014	26.427	0.5	0.022	6.379	8.519	0.73	0.008	99.019	40.70
OLA90_52_P20D	56.303	0.025	27.081	0.455	0.024	6.138	9.076	0.616	0.044	99.762	43.39
OLA90_52_P20E	56.83	0.041	26.694	0.415	0.037	6.284	8.783	0.666	0.032	99.782	41.93
OLA90_52_P20F	57.09	0.007	26.753	0.415	0.024	6.204	8.774	0.64	0.04	99.947	42.26
OLA90_52_P20G	58.321	0.021	25.628	0.473	0.032	7.038	7.471	0.812	0.117	99.913	35.28
OLA90_52_P20H	56.857	0	26.977	0.498	0.027	6.467	8.646	0.593	0.07	100.135	41.06
OLA90_52_P20I	58.256	0.046	26.998	0.516	0.036	6.198	8.157	0.641	0.06	100.908	40.51
OLA90_22_P1A	56.348	0.014	27.379	0.478	0.028	5.98	9.642	0.623	0.049	100.541	45.47
OLA90_22_P1B	58.692	0	25.803	0.497	0.033	6.715	7.958	0.86	0.091	100.649	37.66
OLA90_22_P1C	54.713	0.046	28.537	0.502	0.018	5.128	11.013	0.4	0.063	100.42	53.03
OLA90_22_P1D	57.189	0	26.883	0.552	0.03	6.084	9.277	0.562	0.028	100.605	44.27
OLA90_22_P2A	53.915	0	29	0.444	0.026	4.78	11.626	0.453	0.072	100.316	55.85
OLA90_22_P2B	53.969	0.052	29.232	0.473	0.012	4.766	11.708	0.388	0.025	100.625	56.30
OLA90_22_P2D	55.739	0	27.758	0.533	0.036	5.429	10.141	0.418	0.067	100.121	49.56
OLA90_22_P3A	56.193	0.046	27.196	0.374	0.012	5.784	9.819	0.577	0.084	100.085	46.82
OLA90_22_P3B	54.643	0.03	28.369	0.523	0.033	5.16	11.017	0.459	0.038	100.272	52.71
OLA90_22_P4A	56.807	0	26.917	0.406	0.029	5.735	9.201	0.811	0.013	99.919	44.79
OLA90_22_P4B	53.492	0.073	29.345	0.691	0.066	4.652	12.145	0.182	0	100.646	58.45
OLA90_22_P5A	57.5	0.034	26.56	0.431	0.015	6.212	8.758	0.951	0.065	100.526	41.44
OLA90_22_P5B	53.166	0.055	29.241	0.669	0.066	4.702	12.042	0.206	0.038	100.185	57.91
OLA90_22_P6A	56.295	0.034	27.604	0.41	0.037	5.737	9.769	0.729	0.03	100.645	46.48
OLA90_22_P6B	52.75	0.005	29.702	0.479	0.027	4.275	12.502	0.402	0.014	100.156	60.35
OLA90_22_P6C	53.68	0.005	28.8	0.529	0.043	4.992	11.455	0.23	0	99.734	55.17
OLA90_22_P7A	57.23	0.002	26.641	0.377	0.025	6.304	8.753	0.747	0	100.079	41.58
OLA90_22_P7B	58.249	0.007	26.318	0.351	0.015	6.68	8.321	0.845	0.06	100.846	38.86
OLA90_22_P7C	58.749	0.009	25.789	0.377	0.027	6.638	8.015	0.931	0.043	100.578	37.92
OLA90_22_P7D	58.543	0	25.809	0.441	0.021	6.538	7.907	0.861	0.055	100.175	38.08
OLA90_22_P7E	55.335	0.03	28.352	0.522	0.029	5.359	10.706	0.45	0.055	100.838	51.13
OLA90_22_P8A	58.289	0.036	26.114	0.419	0.015	6.639	8.348	0.711	0.08	100.651	39.36
OLA90_22_P8B	55.823	0.02	27.591	0.435	0.017	5.883	9.917	0.498	0.057	100.241	46.88
OLA90_22_P8C	60.329	0.034	24.624	0.419	0.021	7.446	6.453	1.005	0.121	100.452	30.55
OLA90_22_P9A	57.642	0.005	26.396	0.429	0.019	5.92	8.756	0.907	0.041	100.115	42.61
OLA90_22_P10A	58.253	0.005	26.129	0.477	0.024	6.271	8.447	0.859	0.031	100.496	40.58
OLA90_22_P11A	56.343	0.032	27.311	0.469	0.022	5.763	9.729	0.591	0.059	100.319	46.64
OLA90_22_P11B	53.213	0.027	29.349	0.505	0.046	4.563	12.126	0.351	0.061	100.241	58.29
OLA90_22_P11C	58.185	0.002	26.3	0.468	0.038	6.714	8.448	0.59	0.031	100.776	39.66
OLA90_22_P11D	55.665	0.071	27.856	0.674	0.05	5.554	10.356	0.41	0.028	100.664	49.56
OLA90_22_P12A	56.741	0.05	27.212	0.467	0.035	5.852	9.294	0.671	0.061	100.383	44.94
OLA90_22_P12B	56.9	0.02	26.793	0.479	0.031	6.013	9.276	0.725	0.08	100.317	44.13
OLA90_22_P12C	54.466	0.007	28.275	0.477	0.012	5.151	10.894	0.509	0.045	99.836	52.32

OLA90_22_P12D	56.592	0	27.307	0.464	0.022	5.69	9.59	0.642	0.058	100.365	46.44
OLA90_22_P12E	55.001	0.011	28.157	0.595	0.04	5.561	10.606	0.301	0.019	100.291	50.44
OLA90_22_P12F	55.469	0.057	27.639	0.693	0.059	5.564	10.26	0.381	0.026	100.148	49.37
OLA90_22_P13A	55.008	0.016	28.482	0.447	0.012	5.229	10.74	0.519	0.073	100.526	51.58
OLA90_22_P13B	58.481	0.005	26.214	0.478	0.028	6.498	8.324	0.886	0.098	101.012	39.38
OLA90_22_P14A	58.788	0.027	25.687	0.457	0.023	6.811	7.83	0.81	0.069	100.502	37.07
OLA90_22_P14B	54.74	0.007	28.379	0.414	0.017	5.09	11	0.435	0.059	100.141	53.07
OLA90_22_P14C	58.413	0.011	25.906	0.423	0.009	6.61	8.078	0.754	0.071	100.275	38.58
OLA90_22_P14D	55.379	0.014	27.965	0.409	0.025	5.458	10.339	0.449	0.064	100.102	49.83
OLA90_22_P14E	56.998	0.023	27.088	0.484	0.015	6.038	9.286	0.548	0.054	100.534	44.51
OLA90_22_P14F	57.151	0.07	27.094	0.673	0.055	6.159	9.262	0.545	0.043	101.052	43.99
OLA90_22_P15A	58.37	0.027	26.145	0.304	0.007	6.47	8.26	0.741	0.026	100.35	39.62
OLA90_22_P15B	58.974	0	25.662	0.362	0.029	6.637	7.814	0.794	0.089	100.361	37.62
OLA90_22_P15C	59.902	0.052	25.224	0.359	0.025	7.018	7.281	0.915	0.089	100.865	34.56
OLA90_22_P15D	58.577	0.023	25.911	0.455	0.03	6.794	8.205	0.728	0.117	100.84	38.40
OLA90_22_P15E	60.442	0.061	24.956	0.406	0.031	7.202	7.017	0.886	0.106	101.107	33.25
OLA90_22_P15F	58.806	0.079	25.846	0.457	0.037	6.953	7.896	0.672	0.109	100.855	37.11
OLA90_22_P16A	51.67	0	30.652	0.561	0.042	3.816	13.545	0.245	0.031	100.562	65.30
OLA90_22_P17A	53.259	0	29.651	0.435	0.014	4.596	12.197	0.394	0.09	100.636	58.13
OLA90_22_P17B	58.711	0.02	25.548	0.356	0.014	6.702	7.771	0.922	0.061	100.105	37.01
OLA90_22_P17C	55.742	0.036	27.771	0.491	0.027	5.746	10.196	0.465	0.032	100.506	48.21
OLA90_22_P18A	58.745	0.079	25.202	0.443	0.013	6.648	7.413	1.093	0.06	99.696	35.73
OLA90_22_P18B	55.79	0.045	27.664	0.404	0.028	5.612	10.217	0.559	0.04	100.359	48.56
OLA90_22_P18D	57.663	0.014	26.215	0.523	0.027	6.527	8.376	0.676	0.09	100.111	39.90
OLA90_22_P19A	53.721	0	29.19	0.415	0.017	4.72	11.6	0.443	0.042	100.148	56.12
OLA90_22_P19B	52.923	0.016	29.926	0.412	0.019	4.261	12.487	0.356	0.012	100.412	60.55
OLA90_22_P19C	56.653	0.018	27.273	0.42	0.031	5.824	9.668	0.603	0.029	100.519	46.20
OLA90_22_P19D	56.215	0	27.53	0.499	0.034	5.822	10.107	0.427	0.041	100.675	47.78
OLA90_22_P19E	53.925	0.043	29.2	0.547	0.026	4.852	11.757	0.371	0.038	100.759	56.04
OLA90_22_P20A	57.216	0	27.018	0.247	0.011	6.212	9.177	0.545	0.024	100.45	43.56
OLA90_22_P20B	55.812	0.018	27.866	0.268	0.013	5.598	10.196	0.45	0.03	100.251	48.87
OLA90_22_P20C	58.838	0.016	25.784	0.299	0.014	6.757	7.769	0.732	0.042	100.251	37.23
OLA90_22_P20D	57.567	0.009	26.867	0.261	0.01	6.173	8.937	0.577	0.011	100.412	42.98
OLA90_22_P20E	58.442	0.005	26.296	0.265	0	6.444	8.399	0.661	0.081	100.593	40.29
OLA90_22_P20F	56.96	0.025	27.244	0.277	0.002	5.917	9.335	0.518	0.005	100.283	45.19
OLA90_22_P20G	59.191	0.023	26.056	0.247	0.008	6.648	7.931	0.699	0	100.803	38.14
OLA90_22_P20H	59.463	0	25.473	0.293	0.006	6.827	7.439	0.803	0.038	100.342	35.85
OLA90_22_P20I	59.69	0.048	25.509	0.296	0.014	6.868	7.331	0.835	0.023	100.614	35.32
OLA90_22_P20J	58.637	0	25.842	0.494	0.03	6.689	7.812	0.671	0.02	100.195	37.71
OLA90_22_P21A	58.788	0.039	25.502	0.418	0.021	6.848	7.548	0.837	0.046	100.047	36.05
OLA90_22_P21B	53.643	0	29.139	0.461	0.01	4.743	11.507	0.36	0.064	99.927	56.08
OLA90_22_P21C	58.721	0	25.811	0.411	0.022	6.751	7.794	0.722	0.096	100.328	37.34
OLA90_22_P21D	56.901	0.025	27.2	0.613	0.04	6.006	9.315	0.46	0.035	100.595	44.93
OLA90_22_P22A	54.415	0.061	29.04	0.435	0.024	4.827	11.393	0.363	0.061	100.619	55.41
OLA90_22_P22B	58.408	0.018	26.088	0.419	0.021	6.572	8.201	0.747	0.086	100.56	39.08
OLA90_22_P22C	54.384	0	28.818	0.448	0.029	4.895	11.252	0.379	0.022	100.227	54.72
OLA90_22_P22D	57.4	0.12	26.53	0.59	0.042	6.247	8.655	0.619	0.086	100.289	41.82

OLA90_22_P23A	56.126	0.036	27.773	0.383	0.026	5.434	10.023	0.65	0.013	100.464	48.58
OLA90_22_P23B	56.946	0.02	26.951	0.436	0.023	5.907	9.055	0.766	0.039	100.143	43.84
OLA90_22_P23C	55.974	0	27.754	0.487	0.035	5.502	10.024	0.667	0.035	100.478	48.25
OLA90_22_P23D	58.308	0.034	26.12	0.447	0.015	6.366	8.261	0.97	0.046	100.567	39.46
OLA90_22_P24A	57.6	0	26.427	0.538	0.02	6.373	8.699	0.702	0.04	100.399	41.29
OLA90_22_P24B	56.968	0.014	27.048	0.506	0.034	5.942	9.373	0.574	0.024	100.483	45.04
OLA90_22_P24C	56.692	0.02	27.576	0.466	0.038	5.975	9.513	0.541	0.068	100.889	45.37
OLA90_22_P25A	58.375	0	26.306	0.389	0.018	6.48	8.324	0.647	0.05	100.589	39.98
OLA90_22_P25B	53.726	0	29.637	0.527	0.038	4.574	11.845	0.317	0.036	100.7	57.78

Appendix C: *Manuscript 2.* Trace element data of Ollagüe plagioclase; core to rim transects

Sample	Li	Mg	Si	Ca	Sc	Ti	Cr	Fe	Zn	Rb	Sr	Y	Zr	Nb
OLA9002.P1.S1	21.21	6735.41	350932.11	55760.00	10.38	93.79	68.49	643.62	20.35	10.08	1055.18	0.38	33.39	0.14
OLA9002.P1.S2	29.61	68.51	444584.93	68770.00	11.94	55.53	5.24	711.59	17.65	1.62	1511.43	0.03	0.03	0.00
OLA9002.P1.S3	599.07	5947.96	4892843.72	60440.00	149.56	10178.16	12.64	23302.74	735.27	2554.75	1318.03	86.56	1182.66	161.85
OLA9002.P1.S4	347.56	26989.12	3202263.49	65910.00	95.87	8065.26	176.54	20420.95	251.76	1669.60	853.68	63.72	918.14	112.27
OLA9002.P1.S5	17.18	2665.13	2822519.88	58750.00	84.13	5471.16	6.50	7768.24	347.37	167.73	1034.02	28.06	597.75	88.62
OLA9002.P3.S1	28.12	54.67	329170.42	64170.00	9.20	82.56	1.88	508.85	15.64	0.98	1068.48	0.19	0.38	0.06
OLA9002.P3.S2	35.14	46.23	437839.81	73220.00	12.26	73.88	-0.46	682.86	14.28	1.43	1383.97	0.14	0.01	0.00
OLA9002.P3.S3	14.70	27009.59	483377.02	63980.00	13.78	257.24	37.74	761.88	29.73	37.34	400.21	1.53	121.03	0.85
OLA9002.P3.S4	9.58	24611.77	413638.00	58590.00	11.56	91.82	22.50	319.37	15.49	28.26	269.90	1.07	113.48	0.33
OLA9002.P3.S5	27.46	1491.54	403405.12	88870.00	11.29	134.79	5.78	1183.20	22.59	4.23	2112.93	1.58	6.66	0.17
OLA9002.P6.S1	23.71	69.88	321693.55	50250.00	8.75	331.36	0.61	724.41	22.28	1.25	1079.26	0.09	0.63	0.64
OLA9002.P6.S2	28.24	2139.96	414527.59	61980.00	11.41	100.31	6.27	1103.28	24.07	6.18	1212.35	0.51	9.54	0.18
OLA9002.P6.S3	22.50	62.81	406052.40	55760.00	10.80	45.71	2.33	621.04	15.44	1.98	1209.26	0.08	0.10	0.01
OLA9002.P6.S4	471.54	4577.81	4114255.16	54960.00	121.11	8098.95	10.25	18812.02	597.80	2035.05	1579.01	67.74	856.17	129.77
OLA9002.P9.S1	21.95	1710.49	3379416.21	87350.00	103.39	6258.03	6.07	14224.99	556.21	202.16	1763.94	56.14	829.26	88.69
OLA9002.P9.S2	28.10	6024.28	1629733.44	72150.00	48.70	15010.71	81.12	21828.90	343.98	106.86	1528.02	93.59	1186.73	506.91
OLA9002.P9.S3	20.68	3625.47	3679187.71	75260.00	107.58	5423.37	14.33	8019.62	347.89	237.65	1938.98	28.25	722.75	28.00
OLA9002.P10.S1	28.66	41.05	369138.82	65660.00	10.22	71.50	2.00	592.76	15.19	1.17	1437.30	0.09	0.14	0.02
OLA9002.P10.S2	31.25	11224.07	665890.57	82100.00	19.32	586.50	95.74	1837.29	35.08	19.17	1758.17	2.41	59.36	1.79
OLA9002.P10.S3	26.33	422.25	491912.96	65660.00	14.04	419.76	1.12	1548.16	46.56	76.86	1631.49	8.85	45.67	5.92
OLA9002.P10.S4	107.91	1573.70	1351484.21	65660.00	40.87	2177.96	12.73	5497.71	164.19	484.15	1842.11	19.03	261.01	34.38
OLA9002.P14.S1	26.40	35.78	318598.07	65670.00	9.62	338.23	1.73	640.38	12.88	0.64	1079.02	0.45	0.43	0.48
OLA9002.P14.S2	223.45	2103.53	2294681.30	68260.00	69.35	4131.99	9.66	8915.68	374.64	987.26	1948.13	34.39	473.58	64.11
OLA9002.P14.S3	14.09	150.38	415244.87	66970.00	11.43	175.46	1.83	900.92	30.58	25.01	1866.50	1.07	14.27	1.97
OLA9002.P16.S1	21.29	338.23	515858.21	93410.00	13.88	128.89	4.47	1159.07	72.58	6.44	2196.84	0.48	5.12	0.35
OLA9002.P16.S2	30.07	53.65	399878.18	67840.00	10.47	72.07	2.22	653.47	18.48	1.50	1409.18	0.07	0.14	0.04
OLA9002.P16.S3	46.39	103.78	615193.94	99050.00	17.14	109.45	3.53	909.91	25.10	2.10	2117.84	0.04	0.02	0.00
OLA9002.P19.S1	32.03	45.44	407841.84	69900.00	11.90	122.84	3.14	596.23	13.04	1.34	1159.96	0.17	0.01	0.00
OLA9002.P19.S2	29.73	16184.68	543153.79	72500.00	16.31	459.32	18.02	1810.88	24.42	108.44	1145.80	3.91	111.01	5.89
OLA9002.P19.S3	491.03	14491.75	3956023.17	71200.00	114.20	8414.21	63.31	17601.17	489.92	1964.60	1392.38	72.86	999.15	120.14
OLA9002.P20.S1	18.25	1200.39	338854.82	76700.00	9.89	135.52	3.53	875.63	21.90	7.50	1460.86	1.22	8.73	0.43
OLA9002.P20.S2	14.66	11955.10	333499.90	68210.00	9.92	346.07	10.99	1253.68	17.42	15.60	959.92	0.82	53.86	1.07
OLA9002.P20.S3	22.70	180.98	396101.75	100000.00	11.35	124.60	-0.20	989.12	24.60	1.16	2107.82	0.38	0.42	0.06
OLA9014.P1.S1	9.90	392.22	359205.31	112330.00	7.75	203.57	0.13	1811.39	12.64	0.52	2110.58	0.13	0.02	0.00
OLA9014.P1.S2	7.77	441.36	331530.90	126210.00	7.22	158.15	0.54	2012.49	12.53	2.30	1761.27	0.40	4.94	0.45
OLA9014.P1.S3	22.82	46818.39	432740.57	80370.00	26.95	5614.57	8.41	38888.53	166.83	39.28	1118.67	32.54	207.63	6.66
OLA9014.P5.S1	382.57	43599.60	4855130.54	116480.00	139.17	29866.08	232.99	61108.21	439.05	1848.71	1553.40	183.31	4605.86	198.41
OLA9014.P5.S2	467.63	46312.19	6107423.80	121910.00	159.35	34964.01	11.42	85986.79	1407.79	2238.29	2168.24	211.40	5863.54	245.99
OLA9014.P5.S3	291.31	23183.56	3425328.43	79520.00	82.87	23437.76	2620.33	40827.54	264.13	1585.23	987.88	168.70	4325.62	159.52
OLA9014.P7.S1	9.30	343.42	314970.52	113350.00	6.85	139.15	2.08	1552.41	11.47	0.30	1737.75	0.15	0.02	0.01
OLA9014.P7.S2	9.86	449.47	367662.42	138600.00	8.29	164.78	1.60	1949.09	13.15	0.32	1984.38	0.16	0.03	0.00
OLA9014.P7.S3	8.75	472.42	343526.05	123110.00	7.54	350.23	0.11	1983.54	15.99	12.22	1798.19	1.21	22.18	1.18
OLA9014.P7.S4	7.26	318.49	274964.73	99220.00	5.99	117.35	1.27	1400.05	9.99	0.25	1586.52	0.17	1.69	0.00
OLA9014.P8.S1	10.35	358.33	340352.66	120830.00	7.36	152.41	0.76	1612.04	13.09	0.35	2188.10	0.20	0.01	0.00
OLA9014.P8.S2	9.63	157.31	332600.21	84970.00	7.12	128.62	1.26	840.58	9.27	1.88	1842.74	0.35	4.05	0.13
OLA9014.P8.S3	61.03	4251.79	1079631.46	80920.00	26.39	4914.64	1.45	11037.82	198.32	281.10	1693.20	22.98	703.73	31.10
OLA9014.P9.S1	9.20	335.78	331029.63	118550.00	7.51	147.62	0.46	1603.43	13.55	0.34	2050.44	0.18	0.02	0.00
OLA9014.P9.S2	7.30	203.17	246662.09	82710.00	5.55	102.20	1.05	1086.38	8.60	0.30	1426.46	0.16	0.04	0.00
OLA9014.P9.S3	10.96	105.14	387887.46	94530.00	8.51	111.02	2.18	912.97	8.00	0.54	2052.70	0.23	0.16	0.00
OLA9014.P10.S1	11.21	1329.14	351081.34	113020.00	7.76	365.54	2.33	2392.41	17.23	1.86	2282.04	0.49	1.68	0.14
OLA9014.P10.S2	6.93	343.15	253650.80	98125.00	5.60	128.09	1.05	1425.40	8.13	0.67	1376.92	0.18	1.17	0.04
OLA9014.P10.S3	6.75	216.77	236847.89	83230.00	5.05	94.38	0.22	1091.56	8.43	0.27	1359.39	0.11	0.02	0.00

OLA9014.P12.S1	11.79	568.22	445730.13	127730.00	10.28	646.34	1.05	3976.80	26.39	54.62	2092.00	3.91	84.27	3.06
OLA9014.P12.S2	21.65	968.07	578858.32	89560.00	13.86	1406.55	1.32	3468.01	44.38	76.01	2105.53	8.31	250.89	9.13
OLA9014.P12.S3	58.41	75004.35	471647.19	72840.00	37.24	11386.35	3.05	39061.34	285.66	115.59	242.46	74.49	422.39	21.94
OLA9014.P14.S2	7.07	491.73	333003.54	124560.00	7.55	332.83	0.43	2338.96	15.76	12.10	1663.60	1.77	32.15	1.53
OLA9014.P14.S3	8.07	220.38	262634.82	89550.00	5.85	105.09	0.57	1183.94	9.47	0.32	1562.02	0.14	0.11	0.00
OLA9014.P14.S4	17.30	657.73	545353.71	108690.00	12.36	706.15	2.35	2821.95	36.91	42.91	2405.47	3.41	107.06	4.89
OLA9014.P15.S1	11.16	425.47	338151.81	111630.00	7.77	204.95	0.93	1738.36	13.47	0.61	2404.05	0.15	0.01	0.00
OLA9014.P15.S2	9.83	373.38	326142.31	127890.00	7.52	147.84	0.07	1671.46	12.09	0.46	1935.15	0.18	0.12	0.00
OLA9014.P15.S3	10.28	352.68	339492.37	123500.00	7.54	146.69	1.59	1559.63	11.85	0.46	1961.17	0.19	0.05	0.00
OLA9014.P15.S4	7.65	223.47	263172.51	91700.00	5.69	111.13	1.67	1121.08	9.77	0.27	1565.75	0.15	0.02	0.00
OLA9014.P15.S5	10.60	189.78	364673.28	107620.00	7.75	148.53	1.00	1145.70	11.51	0.46	2282.01	0.26	0.05	0.00
OLA9022.P1.S1	17.13	604.59	418421.74	96420.00	10.80	221.86	-0.01	1711.55	26.07	12.94	1443.33	1.51	6.47	0.72
OLA9022.P1.S2	17.50	229.58	348455.02	79580.00	9.32	91.10	1.27	1159.09	16.98	2.01	1185.59	0.24	0.03	0.00
OLA9022.P1.S3	36.13	26018.04	346772.29	110130.00	42.27	25722.41	2.61	31511.95	151.56	20.83	934.46	27.44	81.38	59.05
OLA9022.P1.S4	17.63	233.96	400645.69	92770.00	10.99	176.95	1.39	1415.67	19.64	2.29	1504.68	0.57	0.19	0.15
OLA9022.P6.S1	15.74	220.92	331125.88	97690.00	8.67	183.19	1.02	1160.61	14.64	1.75	1402.44	0.71	0.72	0.04
OLA9022.P6.S2	21.23	1273.56	567018.74	125020.00	14.83	489.30	1.78	2806.97	39.93	9.34	2133.60	1.59	8.48	0.62
OLA9022.P6.S3	137.64	850694.37	2202970.40	114550.00	231.74	75463.79	371.01	423072.19	6184.22	326.95	766.72	156.12	741.82	81.15
OLA9022.P11.S1	19.41	295.50	443001.96	97290.00	10.85	188.71	4.45	1437.41	20.80	5.09	1521.38	0.96	1.11	0.05
OLA9022.P11.S2	17.81	565.12	465301.47	121260.00	11.80	329.94	1.78	2041.16	35.16	23.62	1716.70	4.21	15.98	0.91
OLA9022.P11.S3	14.04	223.04	365316.52	84480.00	9.38	159.49	3.31	1203.29	15.72	2.75	1260.83	0.77	0.63	0.03
OLA9022.P11.S4	20.74	265.09	491097.71	103560.00	12.04	201.38	5.47	1518.63	20.44	3.74	1739.22	0.76	0.04	0.00
OLA9022.P13.S1	49.27	4977.51	769739.60	107400.00	23.12	4613.63	2.29	8528.97	118.66	193.26	1923.90	22.00	304.96	18.84
OLA9022.P13.S2	88.27	13739.41	1366159.37	83240.00	44.31	11028.52	7.04	19132.45	278.16	475.61	1498.30	52.07	799.41	48.98
OLA9022.P13.S3	35.56	5904.11	689895.19	95320.00	21.07	5977.11	6.69	9514.70	122.43	145.94	1714.56	22.57	260.76	18.26
OLA9022.P14.S1	13.62	272.40	365525.68	78300.00	9.68	200.18	2.16	1283.67	18.94	11.95	1248.07	1.59	11.73	0.84
OLA9022.P14.S2	15.45	187.10	337921.15	110000.00	9.08	172.90	0.64	1059.69	14.54	1.61	1200.53	1.29	0.39	0.04
OLA9022.P14.S3	16.47	197.94	389575.09	80780.00	10.08	156.34	0.95	1157.15	16.97	2.37	1344.20	0.63	0.32	0.04
OLA9022.P14.S4	23.01	949.25	521381.24	103390.00	14.08	439.18	3.36	2501.92	42.17	68.85	1696.93	5.14	51.99	4.06
OLA9022.P14.S5	68.40	13272.61	1154104.34	92860.00	36.15	8455.76	6.24	13895.19	215.33	343.69	1538.71	40.24	567.37	34.99
OLA9022.P17.S1	22.16	210.29	533150.16	121970.00	14.43	188.33	1.35	1451.61	20.16	3.12	1935.24	0.98	0.01	0.00
OLA9022.P17.S2	25.54	3507.84	547974.73	77710.00	17.12	2801.03	3.48	5409.14	81.63	112.60	1581.08	11.54	173.50	11.26
OLA9022.P17.S3	173.06	465145.74	3009396.10	101960.00	147.86	27801.33	57.10	193185.64	2659.42	958.85	1035.38	128.37	1467.01	92.48
OLA9022.P18.S1	12.72	676.57	336810.03	74130.00	9.55	212.62	5.80	1624.20	27.81	22.63	1130.24	2.34	16.36	1.47
OLA9022.P18.S2	20.72	290.12	545712.25	102170.00	15.12	209.38	4.58	1703.25	23.89	4.96	1837.18	0.91	1.19	0.06
OLA9022.P18.S3	18.98	250.32	453372.46	86690.00	12.02	195.30	2.91	1453.11	18.34	4.49	1502.63	0.61	1.16	0.12
OLA9022.P18.S4	15.72	221.41	410771.18	83760.00	10.67	165.36	0.63	1286.41	17.31	3.03	1385.84	2.52	0.62	0.06
OLA9022.P21.S1	15.64	191.21	355745.65	75480.00	9.41	99.91	0.38	1115.30	16.01	3.05	1302.19	0.57	0.52	0.06
OLA9022.P21.S2	26.94	6479.22	595045.59	115070.00	17.41	2320.56	3.11	6340.88	82.35	71.59	2047.93	12.30	131.13	7.84
OLA9022.P21.S3	63.66	32264.62	1072069.46	77940.00	38.25	14303.80	26.78	33828.41	493.41	348.14	1259.51	48.01	587.36	40.05
OLA9022.P21.S4	16.15	621.21	421058.68	93150.00	10.97	441.60	1.75	1792.09	27.66	12.21	1802.98	1.78	17.52	1.17
OLA9022.P22.S1	23.29	279.38	489441.29	113930.00	12.60	284.54	0.48	1443.38	21.90	2.42	2019.08	0.66	1.02	0.07
OLA9022.P22.S2	13.29	175.45	302503.87	82010.00	7.72	250.40	0.89	944.10	13.79	1.36	1273.74	0.60	0.66	0.05
OLA9022.P22.S3	24.08	449.25	507921.18	112520.00	13.05	1046.73	5.87	1700.38	23.18	3.65	2055.63	9.84	190.68	10.10
OLA9022.P22.S4	13.48	198.74	301897.43	86550.00	7.83	117.81	-0.30	995.68	14.61	1.34	1347.86	10.77	0.78	0.03
OLA9022.P23.S1	99.45	50890.70	1579148.43	100230.00	56.48	14739.23	15.38	33885.54	470.82	546.70	1561.46	66.82	887.40	58.09
OLA9022.P23.S2	42.97	31929.31	787241.16	90550.00	29.73	12595.23	7.61	35110.97	510.22	212.35	1732.87	28.87	377.06	23.78
OLA9022.P23.S3	16.77	492.48	399137.69	100240.00	10.31	256.86	-0.33	1589.80	18.83	2.77	1890.54	0.46	1.04	0.12
OLA9022.P23.S4	41.81	35402.94	774526.68	82610.00	40.00	6812.03	13.63	16531.31	198.92	221.36	804.56	34.32	364.52	22.22
OLA9022.P23.S5	33.05	35511.42	599076.34	93410.00	29.36	10838.33	18.65	23874.46	286.46	130.10	1541.74	23.37	243.89	16.92
OLA9025.P1.S1	29.63	133.83	391626.60	87090.00	9.84	114.16	0.42	853.63	12.76	6.84	1205.82	0.85	7.89	0.58
OLA9025.P1.S2	27.79	102.69	376641.58	78120.00	9.63	51.66	1.02	711.46	11.22	2.08	1138.82	0.43	40.54	0.76
OLA9025.P1.S3	21.66	75.64	317673.23	62700.00	7.94	45.63	2.32	570.44	8.57	1.66	988.95	0.40	0.84	0.08
OLA9025.P1.S4	24.13	103.65	357988.09	54340.00	9.11	132.09	0.88	863.20	17.38	2.90	1207.88	0.27	2.97	0.27

OLA9025.P2.S1	14.18	444.86	249473.91	54050.00	6.40	344.81	0.14	1345.08	23.57	24.09	1141.87	1.52	22.61	2.35
OLA9025.P2.S2	26.30	9809.91	500082.51	94700.00	12.84	3224.24	2.30	4945.13	72.65	66.57	2002.79	2.37	33.08	6.19
OLA9025.P2.S3	28.09	403.66	516357.36	85530.00	12.62	430.46	0.67	1757.09	31.20	26.30	1960.14	1.99	23.21	2.40
OLA9025.P3.S1	52.52	2382.09	549157.46	75490.00	14.88	1389.66	2.51	3776.81	78.42	134.00	1527.31	8.67	118.69	12.37
OLA9025.P3.S2	28.62	746.21	369235.53	93370.00	9.55	501.50	1.90	2287.90	35.67	9.77	1859.79	0.79	37.64	2.35
OLA9025.P3.S3	16.42	187.08	262179.73	57610.00	6.54	127.06	0.16	839.77	14.26	1.95	1258.40	0.18	2.37	0.22
OLA9025.P3.S4	19.72	165.21	324349.79	75490.00	7.97	179.62	0.85	984.77	16.64	4.21	1604.40	0.44	6.14	0.48
OLA9025.P4.S1	27.08	176.73	369953.95	75580.00	9.07	209.00	1.34	1080.49	18.02	16.19	1220.36	1.67	12.37	1.61
OLA9025.P4.S2	29.92	129.59	402322.85	80800.00	9.65	86.60	0.89	1016.71	16.74	1.59	1345.68	0.46	0.19	0.04
OLA9025.P4.S3	19.94	87.89	257254.83	58360.00	6.31	75.47	0.83	670.83	10.47	1.04	802.01	0.43	0.32	0.06
OLA9025.P4.S4	26.44	115.53	369970.83	82470.00	8.72	102.14	1.64	949.74	14.03	1.85	1210.85	0.48	0.40	0.06
OLA9025.P4.S5	18.46	106.00	299909.85	65270.00	7.16	82.83	0.24	824.55	13.64	2.59	1026.54	0.45	1.42	0.20
OLA9025.P7.S1	21.45	109.07	336937.28	119410.00	8.08	167.68	0.02	1077.64	12.57	0.56	1129.11	0.94	0.09	0.14
OLA9025.P7.S2	66.47	18869.66	239192.11	74720.00	30.97	113791.97	300.17	477144.80	3891.88	1.46	757.52	38.12	194.49	37.54
OLA9025.P7.S3	33.11	131.70	417230.10	99310.00	10.02	227.93	2.69	994.72	15.29	1.68	1348.10	4.92	29.89	1.18
OLA9025.P7.S4	29.83	3330.35	410179.50	81070.00	10.35	255.06	1.80	2520.28	35.91	1.75	1461.64	1.50	1.52	0.49
OLA9025.P8.S1	16.42	9179.74	360353.06	87290.00	9.78	3815.69	0.66	9111.67	107.95	45.53	1504.77	2.34	25.43	5.24
OLA9025.P8.S2	23.36	10235.36	427381.92	87290.00	11.89	3250.10	2.20	6120.67	103.89	64.64	1679.93	2.66	46.97	6.41
OLA9025.P8.S3	16.69	3836.51	338014.05	87290.00	8.75	1030.08	2.01	3951.58	69.66	25.33	1581.14	1.37	23.55	2.44
OLA9025.P12.S1	115.64	117696.69	933729.09	75000.00	33.21	35260.78	45.83	48791.10	652.06	760.32	577.77	66.71	293.61	78.38
OLA9025.P12.S2	38.91	204.02	544141.12	103570.00	13.93	353.25	3.15	1553.87	25.73	12.08	2183.40	1.43	24.71	2.33
OLA9025.P12.S3	19.29	73.43	236230.11	52210.00	5.83	125.02	1.38	645.17	11.52	0.98	943.19	0.33	1.16	0.12
OLA9025.P12.S4	36.22	140.52	465447.46	70650.00	11.65	176.13	3.89	1305.39	24.20	3.52	1679.69	0.42	2.18	0.32
OLA9025.P15.S1	25.43	135.70	381232.57	71560.00	9.37	164.95	2.31	1052.45	20.16	2.01	1554.33	0.46	1.55	0.25
OLA9025.P15.S2	28.41	134.54	349589.01	65380.00	8.85	224.14	0.65	1004.43	18.49	2.31	1240.37	0.49	3.69	0.93
OLA9025.P15.S3	29.94	151.55	369654.11	71310.00	9.14	196.51	2.61	1096.09	18.46	2.31	1427.48	0.58	1.98	0.30
OLA9025.P15.S4	23.18	105.16	332539.30	57060.00	7.94	136.70	1.44	915.19	14.82	1.73	1288.62	0.30	0.70	0.06
OLA9025.P15.S5	34.05	149.06	476463.24	76040.00	11.47	189.84	2.49	1303.22	24.46	3.02	1948.40	0.40	2.25	0.31
OLA9025.P15.S6	26.62	122.76	376458.66	67500.00	9.62	168.13	2.26	1146.44	19.08	2.04	1542.27	0.31	0.77	0.05
OLA9025.P16.S1	24.51	207.27	418397.05	73110.00	9.99	229.21	-0.05	1183.63	19.01	8.75	1614.23	0.91	6.44	0.62
OLA9025.P16.S2	25.41	2600.02	417395.04	88320.00	10.83	632.14	0.06	2855.80	52.71	48.34	1919.79	2.97	45.76	4.27
OLA9025.P16.S3	152.03	14363.08	1374239.35	103530.00	42.11	24981.20	88.40	125887.07	1317.40	531.09	2178.02	50.05	559.36	62.95
OLA9025.P19.S1	70.13	1715.88	909691.37	68100.00	24.47	2536.43	3.86	5107.54	109.78	301.15	1811.48	15.18	235.04	25.52
OLA9025.P19.S2	440.06	13510.04	3896925.14	91870.00	104.24	14581.64	23.23	28977.84	650.56	1893.09	2123.93	90.96	1445.42	159.20
OLA9025.P19.S3	153.98	3581.20	1625292.58	76610.00	40.96	5293.45	0.51	9762.25	232.73	653.62	1961.16	30.76	498.89	57.88
OLA9036.P1.S1	19.01	167.65	313325.09	80450.00	7.40	159.11	1.37	1090.75	14.48	1.35	1252.80	1.55	0.74	0.05
OLA9036.P1.S2	33.37	962.18	723023.94	123020.00	18.33	1201.66	3.15	3513.20	55.46	79.62	2165.31	6.89	86.60	5.69
OLA9036.P1.S3	291.15	17398.93	3068559.18	85410.00	100.96	22582.82	9.72	35458.86	501.88	1787.62	1613.28	150.87	1911.86	134.30
OLA9036.P3.S1	15.20	234.42	434203.66	89100.00	9.92	188.30	1.90	1503.91	20.95	5.03	1639.18	0.73	1.57	0.11
OLA9036.P3.S2	12.82	1717.05	481276.55	93740.00	12.27	787.88	3.46	2983.21	39.64	42.59	1700.59	4.75	48.84	8.55
OLA9036.P3.S3	37.06	11976.44	582129.46	56040.00	18.69	3308.72	287.35	18098.65	12372.34	245.41	598.45	15.74	171.62	27.66
OLA9036.P5.S1	21.19	151.39	306001.29	74570.00	7.49	115.40	0.35	932.02	11.26	1.47	1050.80	0.44	0.03	0.00
OLA9036.P5.S2	28.30	212.77	481598.62	90810.00	11.15	206.97	1.13	1568.07	18.86	13.75	1585.98	1.75	28.88	1.71
OLA9036.P5.S3	26.28	172.60	373456.44	87840.00	8.69	141.85	-0.61	1147.03	14.93	2.10	1269.65	0.47	0.14	0.00
OLA9036.P5.S4	23.72	204.94	408352.52	87920.00	9.64	184.07	0.54	1317.06	16.34	6.77	1289.04	0.88	4.06	0.34
OLA9036.P6.S1	19.11	184.66	339353.48	77260.00	8.18	165.25	1.23	1262.09	16.32	1.84	1145.10	1.92	0.25	0.03
OLA9036.P6.S2	21.52	236.15	400520.41	87720.00	9.64	207.98	2.98	1658.77	20.09	4.17	1382.91	0.93	1.56	0.18
OLA9036.P6.S3	40.23	649.94	612275.29	96440.00	15.73	727.57	3.43	3139.02	45.24	96.63	1646.39	6.42	59.12	4.59
OLA9036.P6.S4	19.83	191.47	351859.33	75500.00	8.41	144.43	1.24	1217.54	15.84	2.70	1237.81	0.44	0.18	0.05
OLA9036.P6.S5	17.51	246.40	426958.54	88050.00	10.16	194.39	2.49	1897.25	19.55	3.31	1567.61	0.85	0.47	0.04
OLA9036.P6.S6	28.10	5971.90	660185.66	70780.00	20.49	2831.12	22.69	12897.05	136.56	189.14	1396.69	18.48	207.59	13.69
OLA9036.P6.S7	22.43	215.07	371417.55	89240.00	8.29	250.51	2.06	1527.69	20.03	1.86	1232.43	1.07	0.15	0.04
OLA9036.P10.S1	11.70	471.40	400523.28	82220.00	9.43	291.21	1.14	1685.68	21.86	12.21	1440.88	1.41	8.68	0.63
OLA9036.P10.S1	28.54	222.57	489321.97	106690.00	11.33	201.04	4.44	1643.30	22.25	3.58	1774.86	0.70	0.11	0.01

OLA9036.P10.S2	23.60	206.86	416276.86	82000.00	9.96	176.74	0.40	1477.48	19.25	4.24	1518.92	0.56	0.75	0.05
OLA9036.P10.S2	19.10	171.51	373512.18	82570.00	9.03	153.08	2.33	1455.69	17.05	2.75	1295.56	0.80	0.27	0.03
OLA9036.P10.S3	14.56	150.18	303745.97	60040.00	7.08	135.18	1.38	1096.39	14.31	2.49	1117.60	0.40	0.25	0.04
OLA9036.P10.S3	23.06	295.01	437461.84	94630.00	10.91	2525.78	5.39	3506.78	28.78	3.08	1479.45	0.65	10.96	3.57
OLA9036.P10.S4	27.67	236.44	459117.24	110290.00	10.96	236.40	3.35	1704.75	23.29	2.41	1685.76	1.39	0.28	0.05
OLA9036.P10.S5	18.07	227.38	376226.63	76570.00	9.23	175.49	0.76	1318.49	17.95	2.97	1432.50	0.53	0.10	0.00
OLA9036.P13.S1	18.72	175.90	360198.57	93750.00	8.42	116.69	1.66	1323.71	16.97	2.25	1248.53	1.01	0.24	0.00
OLA9036.P13.S2	10.70	1005.77	590426.75	117330.00	14.36	925.90	1.38	3168.69	39.72	36.29	1922.26	6.55	56.17	3.34
OLA9036.P13.S3	4.30	565.41	325121.14	76490.00	8.31	584.22	4.16	2604.59	23.29	11.80	1216.08	2.27	23.43	1.78
OLA9036.P13.S4	329.27	30213.23	3750599.80	95850.00	125.93	29234.24	12.78	43137.07	3981.12	2105.97	1883.06	200.93	2555.10	165.95
OLA9036.P14.L1	40.05	1372.14	835315.58	196005.00	20.42	844.43	17.92	5071.54	180.93	33.05	2944.90	3.83	39.29	3.58
OLA9036.P14.S1	16.60	685.49	427754.06	81610.00	10.10	469.24	0.48	2245.08	28.55	28.86	1450.67	2.89	31.65	1.46
OLA9036.P14.S2	9.41	1133.10	457912.90	114400.00	11.29	797.52	2.30	3423.46	40.76	35.77	1772.04	3.72	46.18	3.33
OLA9036.P14.S3	4.65	827.09	321588.26	98000.00	7.55	572.25	1.21	2470.62	25.51	10.14	1366.21	2.42	32.24	2.23
OLA9036.P15.S1	17.41	12778.66	315592.62	86270.00	11.21	12708.52	10.10	82297.98	818.41	13.99	1026.43	9.39	75.73	4.19
OLA9036.P15.S2	22.05	39428.05	291399.01	117170.00	26.59	4035.99	1.02	12407.63	102.38	2.03	779.39	34.13	75.65	9.64
OLA9036.P15.S3	13.94	259.85	242282.39	91520.00	5.61	143.27	1.09	1222.17	10.99	0.75	1226.45	0.28	0.21	0.02
OLA9036.P16.S1	19.60	557.32	417995.28	72060.00	10.67	853.85	1.08	2189.53	29.85	53.42	1382.04	4.88	59.67	4.20
OLA9036.P16.S2	19.48	893.18	407239.59	75620.00	10.17	528.21	2.45	1990.79	28.08	27.45	1405.33	2.68	28.97	2.12
OLA9036.P16.S3	24.05	1201.64	459038.78	73710.00	12.49	1139.54	1.86	2577.12	36.01	70.44	1367.54	5.97	76.54	5.54
OLA9036.P16.S4	27.84	813.71	527809.51	84320.00	14.21	1598.09	0.77	3600.86	47.14	102.46	1524.94	13.47	111.17	8.47
OLA9052.P2.S1	18.47	1000.21	417888.43	81480.00	10.71	1362.33	1.35	3227.30	40.07	69.00	1360.96	6.78	97.61	6.23
OLA9052.P2.S1	14.22	330.58	387645.02	122320.00	9.19	234.51	0.78	1798.32	14.25	2.13	1866.65	0.53	1.83	0.06
OLA9052.P2.S2	250.44	64019.49	2866902.14	112110.00	106.07	23551.07	11.05	57321.68	683.68	1298.62	1908.35	145.86	2029.18	123.45
OLA9052.P2.S2	16.54	458.16	376440.10	127500.00	8.78	313.34	2.02	2244.88	17.01	3.05	1858.82	0.49	4.51	0.36
OLA9052.P2.S3	171.95	22209.79	1962706.23	85290.00	65.19	15973.16	8.18	33225.72	410.43	919.24	1420.80	97.00	1375.34	85.49
OLA9052.P2.S3	16.15	508.29	339075.02	117310.00	7.51	214.17	1.06	1834.96	12.53	0.59	1751.13	0.22	0.10	0.00
OLA9052.P2.S4	18.46	349.56	440290.03	89820.00	10.34	544.48	1.20	2335.93	33.39	17.72	1622.19	2.06	29.59	1.86
OLA9052.P2.S4	17.76	552.12	366000.58	124650.00	8.74	358.43	0.94	2513.85	17.91	3.19	1860.05	1.54	4.70	0.44
OLA9052.P4.S1	17.14	240.87	367062.76	106060.00	8.60	161.22	1.37	1448.20	16.21	1.54	1374.93	0.81	0.07	0.01
OLA9052.P4.S2	22.54	273.61	433559.99	100180.00	10.20	146.37	1.72	1693.67	18.56	2.83	1514.65	0.61	0.04	0.00
OLA9052.P4.S3	19.77	252.22	384839.39	86250.00	8.69	135.49	2.69	1516.99	16.43	2.49	1304.24	0.55	0.02	0.01
OLA9052.P4.S4	101.47	10319.21	1431562.05	121530.00	44.44	12427.63	5.18	27939.49	331.39	558.56	2221.59	62.06	896.12	53.78
OLA9052.P9.S1	272.45	160867.06	3038652.71	114040.00	129.38	27377.38	32.08	110142.74	1260.81	1388.15	1410.81	153.37	1948.10	127.73
OLA9052.P9.S2	146.83	707518.11	2253568.05	124850.00	161.32	13950.69	406.86	254238.93	2498.98	536.05	740.55	123.37	850.90	50.04
OLA9052.P9.S3	96.87	23441.32	1323423.59	96590.00	41.17	8788.59	2.92	22499.14	279.95	518.12	1566.84	67.76	743.35	46.73
OLA9052.P9.S4	342.57	15567.48	3920593.53	131500.00	118.53	30562.47	20.29	48191.81	655.43	1890.98	2238.75	174.84	2618.42	170.05
OLA9052.P12.S1	18.81	956.65	381907.27	98230.00	9.12	722.80	0.13	2803.12	39.92	23.71	1680.45	3.01	37.33	2.31
OLA9052.P12.S2	114.25	17102.11	1524445.78	108640.00	68.26	70301.35	53.84	49277.57	413.43	600.42	1999.63	72.88	1240.01	115.14
OLA9052.P12.S3	83.17	7434.53	1090146.46	116020.00	31.89	7592.71	4.47	15442.78	201.25	352.42	2273.28	42.35	607.81	35.37
OLA9052.P12.S4	51.75	2531.44	593345.06	105670.00	19.14	6455.73	220.39	29191.44	135.12	62.57	1998.71	15.63	189.11	15.31
OLA9052.P14.S1	13.70	173.79	292092.82	88320.00	6.54	141.70	1.65	1311.49	13.40	1.93	1090.92	0.35	1.74	0.12
OLA9052.P14.S2	60.04	3462.92	785517.10	95620.00	22.37	4417.56	1.34	9071.13	109.98	256.82	1563.22	24.08	351.40	22.41
OLA9052.P14.S3	257.24	9433.69	2731265.81	77580.00	87.09	22230.81	5.71	36055.45	444.97	1386.07	1209.37	136.38	2041.06	125.62
OLA9052.P14.S4	273.36	38892.66	3216533.68	107170.00	106.89	26116.91	10.31	52053.15	628.80	1569.63	1714.90	154.20	2294.55	141.72
OLA9052.P14.S5	51.58	4916.40	804195.12	97130.00	23.23	4500.81	0.93	9183.11	111.94	251.00	1621.63	25.33	375.29	23.74
OLA9052.P14.S6	25.29	2430.67	483197.53	85470.00	13.40	2001.90	1.24	5169.88	58.57	96.92	1556.65	10.08	154.80	9.34
OLA9052.P14.S7	216.54	45307.20	2437711.14	91880.00	83.32	18756.77	22.57	41646.96	528.31	1120.62	1439.53	118.21	1689.52	105.12
OLA9052.P15.S1	18.51	214.47	365478.66	78680.00	7.96	195.93	1.06	1441.64	16.75	2.56	1358.51	0.54	2.61	0.18
OLA9052.P15.S2	24.02	294.79	478963.93	115390.00	10.74	212.29	0.81	1686.18	21.03	2.00	1814.61	0.70	0.30	0.07
OLA9052.P15.S3	19.52	287.82	400899.42	92320.00	8.88	194.86	0.97	1541.21	20.39	2.24	1568.81	0.67	2.47	0.14
OLA9052.P15.S4	21.13	1107.04	432528.96	95840.00	10.70	1019.85	2.84	3348.94	40.71	42.62	1625.70	5.13	68.09	4.08
OLA9052.P16.S1	19.93	206.31	388248.32	84100.00	8.37	158.86	0.62	1336.84	15.69	3.12	1426.39	0.61	1.05	0.05
OLA9052.P16.S2	21.41	235.78	382533.74	89350.00	8.65	161.64	1.78	1414.15	17.70	2.33	1392.14	1.05	0.95	0.05

OLA9052.P16.S3	24.60	266.38	455490.46	107380.00	10.86	286.40	0.85	2048.16	27.26	3.80	1655.58	1.00	4.20	0.35
OLA9052.P16.S4	16.62	184.95	352492.12	80950.00	7.73	156.21	1.93	1304.03	15.26	2.06	1299.39	0.44	0.06	0.00
OLA9052.P16.S5	20.04	237.86	415717.12	125750.00	9.57	248.95	2.03	1748.27	23.71	1.97	1554.12	1.53	1.41	0.12
OLA9052.P16.S6	17.02	207.17	408835.95	83220.00	8.97	106.11	2.76	1524.68	16.80	3.12	1471.64	0.41	0.26	0.02
OLA9052.P16.S7	18.41	1318.57	484612.31	104510.00	11.98	874.42	6.96	3708.64	43.42	29.19	1801.83	5.73	40.66	2.71
OLA9052.P16.S8	12.97	447.34	301204.27	96460.00	6.73	221.32	1.05	1674.11	14.70	0.69	1631.34	0.34	1.48	0.07
OLA9052.P17.S1	21.39	276.19	440697.30	87020.00	10.02	112.43	2.25	1587.07	17.98	3.71	1534.76	0.17	0.66	0.05
OLA9052.P17.S2	19.83	241.03	389078.19	77580.00	8.77	93.86	3.47	1450.53	14.72	2.74	1327.82	0.18	0.03	0.00
OLA9052.P17.S3	16.89	216.67	327955.36	80600.00	7.48	141.21	0.00	1296.38	13.64	1.42	1137.14	0.42	0.01	0.01
OLA9052.P17.S4	149.13	20167.00	2112400.31	107410.00	65.39	16547.09	5.97	32248.75	370.45	875.28	1798.81	104.44	1408.93	84.60
OLA9052.P18.S1	20.82	300.54	402245.95	97120.00	8.96	144.31	-0.08	1527.61	17.41	1.88	1648.86	0.47	1.62	0.26
OLA9052.P18.S2	25.88	256.08	490086.87	119670.00	11.15	117.72	0.69	1441.50	17.93	1.72	1822.96	0.37	0.00	0.00
OLA9052.P18.S3	19.66	190.41	349174.10	87020.00	7.80	85.05	1.05	1062.55	11.22	1.32	1319.61	0.68	0.01	0.00
OLA9052.P18.S4	24.04	242.06	455504.92	109340.00	9.94	115.15	1.41	1346.54	15.10	1.69	1638.70	0.33	0.04	0.00

Appendix C: Manuscript 2. Trace element data of Ollagüe plagioclase; core to rim transects (Continued)

Sample	Cs	Ba	La	Ce	Pr	Nd	Sm	Eu	Gd	Tb	Dy	Ho	Er	Tm	Yb	Lu	Hf	Pb	Th	U
OLA9002.P1.S1	0.29	461.31	13.96	15.40	1.24	3.30	0.15	1.24	0.27	0.01	0.13	0.02	0.06	0.00	0.03	0.00	1.09	13.25	0.15	0.14
OLA9002.P1.S2	0.02	359.12	12.20	10.47	0.63	1.37	0.06	0.97	0.10	0.00	0.03	0.00	0.00	0.00	0.00	0.00	0.00	17.86	0.00	0.01
OLA9002.P1.S3	109.82	15388.28	488.39	960.49	95.59	318.76	50.43	8.22	35.55	4.58	21.41	3.02	8.84	0.87	7.49	1.06	37.23	341.94	202.37	93.79
OLA9002.P1.S4	71.54	8359.49	331.18	641.66	70.69	207.35	39.98	4.39	25.30	3.05	14.41	1.59	3.68	0.84	3.90	0.57	31.03	190.66	140.36	53.64
OLA9002.P1.S5	42.78	9181.07	154.69	286.97	25.72	80.76	12.30	6.48	9.17	1.06	5.52	0.97	2.46	0.26	2.50	0.36	23.29	201.26	109.48	36.67
OLA9002.P3.S1	0.02	246.61	20.10	25.95	1.93	6.03	0.48	1.55	0.28	0.03	0.06	0.01	0.00	0.00	0.01	0.00	0.00	14.97	0.01	0.01
OLA9002.P3.S2	0.01	374.93	20.42	24.46	1.92	4.72	0.38	1.65	0.33	0.01	0.04	0.00	0.01	0.00	0.00	0.00	0.00	20.08	0.00	0.00
OLA9002.P3.S3	0.56	271.71	6.54	11.18	0.60	3.02	0.43	0.29	0.18	0.03	0.23	0.04	0.13	0.01	0.19	0.03	2.92	11.63	0.60	0.36
OLA9002.P3.S4	0.37	238.52	3.24	7.40	0.39	2.21	0.20	0.22	0.16	0.03	0.16	0.04	0.17	0.01	0.15	0.02	2.96	9.11	0.47	0.26
OLA9002.P3.S5	0.13	819.15	21.66	32.06	3.27	12.11	1.62	2.69	1.34	0.10	0.40	0.07	0.15	0.01	0.05	0.00	0.20	13.35	0.25	0.07
OLA9002.P6.S1	0.02	352.79	17.32	19.93	1.50	3.67	0.18	1.72	0.12	0.01	0.02	0.00	0.00	0.00	0.00	0.00	0.03	14.95	0.04	0.01
OLA9002.P6.S2	0.14	341.49	17.71	20.75	1.78	5.10	0.57	1.29	0.49	0.02	0.08	0.01	0.02	0.00	0.03	0.01	0.23	17.02	0.13	0.09
OLA9002.P6.S3	0.02	410.37	9.21	9.22	0.61	1.60	0.09	1.03	0.11	0.00	0.03	0.00	0.00	0.00	0.01	0.00	0.00	15.45	0.01	0.01
OLA9002.P6.S4	95.56	13101.44	348.33	713.42	73.75	231.48	38.80	6.66	28.92	3.04	14.93	2.22	4.91	0.63	5.25	0.60	29.48	279.43	146.81	70.50
OLA9002.P9.S1	21.17	12840.56	404.33	851.30	91.29	304.95	43.59	9.04	29.42	3.03	12.95	1.81	4.24	0.71	3.98	0.53	26.57	224.18	132.22	65.53
OLA9002.P9.S2	5.81	8603.60	110.46	189.55	20.78	88.01	28.92	7.21	23.40	3.58	19.49	3.47	8.40	1.04	7.82	1.06	24.30	98.28	97.66	93.03
OLA9002.P9.S3	23.21	12682.71	173.81	275.00	22.95	67.33	10.10	8.81	8.41	1.16	6.12	0.89	1.95	0.48	2.26	0.52	28.70	220.93	111.48	27.06
OLA9002.P10.S1	0.01	759.31	19.25	22.74	1.61	4.14	0.35	1.71	0.23	0.00	0.03	0.00	0.00	0.00	0.00	0.00	0.00	16.08	0.00	0.00
OLA9002.P10.S2	0.33	1112.97	13.63	17.95	1.34	3.34	0.58	2.04	0.23	0.05	0.17	0.08	0.42	0.01	0.10	0.05	1.98	21.92	0.61	0.21
OLA9002.P10.S3	3.88	1309.03	51.68	108.80	12.25	46.71	7.70	3.15	5.59	0.55	2.31	0.34	0.50	0.08	0.51	0.07	1.40	20.96	8.47	3.45
OLA9002.P10.S4	24.50	4238.07	111.29	226.45	22.80	74.67	11.59	4.42	7.21	0.88	4.07	0.72	1.77	0.17	1.30	0.20	8.64	77.73	43.21	20.34
OLA9002.P14.S1	-0.01	119.33	21.95	27.82	2.31	6.99	0.80	1.07	0.46	0.05	0.14	0.02	0.01	0.00	0.03	0.00	0.03	14.87	0.11	0.04
OLA9002.P14.S2	50.72	8880.37	201.06	390.45	38.88	126.92	19.43	6.37	13.55	1.37	8.20	1.22	3.22	0.49	3.32	0.28	14.55	139.42	79.47	34.41
OLA9002.P14.S3	1.37	1250.73	17.45	25.78	2.34	6.82	0.85	2.56	0.45	0.06	0.28	0.05	0.09	0.01	0.09	0.00	0.51	14.78	2.55	1.01
OLA9002.P16.S1	0.18	1140.28	21.20	25.82	2.11	6.56	0.64	2.93	0.34	0.03	0.08	0.01	0.02	0.00	0.03	0.01	0.19	22.28	0.97	0.26
OLA9002.P16.S2	0.01	432.03	17.13	19.47	1.36	3.46	0.26	1.40	0.14	0.01	0.01	0.00	0.00	0.00	0.00	0.00	0.00	18.32	0.01	0.00
OLA9002.P16.S3	0.01	686.91	25.12	26.24	1.97	4.01	0.20	1.92	0.32	0.01	0.00	0.00	0.02	0.00	0.00	0.00	0.00	30.01	0.00	0.00
OLA9002.P19.S1	0.00	246.83	24.96	31.27	2.40	6.92	0.50	1.98	0.39	0.01	0.07	0.00	0.00	0.00	0.00	0.00	0.00	19.45	0.00	0.00
OLA9002.P19.S2	3.72	996.41	24.69	45.28	4.39	14.70	1.82	1.44	1.19	0.17	0.78	0.07	0.42	0.05	0.21	0.06	3.28	18.50	6.80	3.18
OLA9002.P19.S3	132.13	11655.66	397.51	739.97	77.55	264.54	44.23	7.08	27.75	3.23	15.32	2.40	7.23	0.75	5.64	0.76	35.91	255.90	159.35	63.04
OLA9002.P20.S1	0.21	355.01	14.76	22.25	2.23	7.70	1.12	1.35	0.82	0.09	0.35	0.06	0.10	0.01	0.06	0.00	0.24	11.24	0.56	0.17
OLA9002.P20.S2	0.33	319.23	7.14	10.42	0.78	3.23	0.46	0.73	0.21	0.03	0.13	0.02	0.07	0.01	0.09	0.01	1.36	8.38	0.38	0.14
OLA9002.P20.S3	0.05	637.64	16.24	23.33	2.13	6.25	0.74	2.26	0.31	0.03	0.14	0.02	0.03	0.00	0.02	0.02	0.03	9.07	0.11	0.03
OLA9014.P1.S1	0.00	263.68	5.20	7.54	0.72	2.09	0.22	0.70	0.14	0.01	0.05	0.01	0.00	0.00	0.00	0.00	0.00	2.49	0.00	0.00
OLA9014.P1.S2	0.07	201.35	4.81	7.88	0.79	2.36	0.30	0.70	0.25	0.02	0.09	0.02	0.04	0.01	0.02	0.00	0.07	2.46	0.18	0.08
OLA9014.P1.S3	1.35	692.92	27.66	55.18	7.50	32.58	8.31	2.39	8.33	1.28	6.21	1.25	3.28	0.38	2.55	0.35	6.64	9.57	6.63	1.09
OLA9014.P5.S1	56.81	17287.66	571.41	1106.79	117.15	405.46	52.80	8.78	35.26	6.36	28.60	6.45	16.70	2.93	18.81	2.98	106.47	278.52	136.94	37.11
OLA9014.P5.S2	62.55	20652.77	659.09	1300.71	141.01	458.41	65.37	10.10	57.67	7.01	36.98	7.32	19.31	3.37	22.69	4.17	138.28	375.77	175.21	48.40
OLA9014.P5.S3	48.00	13458.69	460.73	914.14	98.16	296.16	47.52	2.97	30.82	3.67	15.68	6.12	12.59	1.36	10.83	2.81	97.94	192.51	110.36	33.20
OLA9014.P7.S1	0.01	171.03	4.77	7.26	0.68	2.29	0.21	0.65	0.12	0.00	0.06	0.01	0.00	0.00	0.00	0.00	0.00	2.25	0.00	0.00
OLA9014.P7.S2	0.00	189.63	5.01	7.84	0.72	2.44	0.28	0.69	0.17	0.01	0.05	0.01	0.01	0.00	0.00	0.00	0.00	2.51	0.00	0.00
OLA9014.P7.S3	0.27	235.06	7.78	13.64	1.37	4.18	0.66	0.69	0.40	0.04	0.21	0.03	0.07	0.01	0.14	0.01	0.64	3.28	0.72	0.22
OLA9014.P7.S4	0.00	182.56	4.23	6.36	0.62	1.88	0.22	0.68	0.07	0.01	0.03	0.01	0.02	0.00	0.01	0.01	0.00	2.04	0.00	0.00
OLA9014.P8.S1	0.00	294.69	6.31	9.04	0.89	2.51	0.29	0.80	0.15	0.02	0.05	0.00	0.00	0.00	0.00	0.00	0.00	2.78	0.00	0.00
OLA9014.P8.S2	0.05	344.91	13.51	18.99	1.53	4.47	0.45	1.34	0.17	0.02	0.07	0.00	0.01	0.00	0.01	0.00	0.11	5.90	0.17	0.03
OLA9014.P8.S3	8.47	2832.97	88.11	170.40	17.20	54.34	8.38	2.46	5.44	0.71	4.52	0.80	2.21	0.40	2.73	0.33	17.63	49.75	20.84	6.28

OLA9014.P9.S1	0.01	245.54	5.97	9.14	0.82	2.70	0.36	0.87	0.20	0.02	0.07	0.01	0.01	0.00	0.00	0.00	0.00	2.77	0.00	0.00
OLA9014.P9.S2	0.00	168.84	4.79	6.99	0.67	2.14	0.13	0.64	0.10	0.01	0.04	0.00	0.01	0.00	0.00	0.00	0.00	2.34	0.01	0.00
OLA9014.P9.S3	0.00	396.75	15.14	20.63	1.76	5.28	0.48	1.73	0.19	0.01	0.07	0.01	0.01	0.00	0.01	0.00	0.00	7.49	0.01	0.00
OLA9014.P10.S1	0.01	356.63	5.63	8.71	0.87	2.73	0.32	0.90	0.16	0.02	0.12	0.03	0.04	0.00	0.04	0.00	0.02	3.03	0.03	0.02
OLA9014.P10.S2	0.01	129.16	3.57	5.50	0.57	1.99	0.18	0.51	0.12	0.01	0.04	0.01	0.04	0.00	0.02	0.00	0.03	1.69	0.07	0.02
OLA9014.P10.S3	0.00	152.09	4.76	7.00	0.66	2.15	0.24	0.59	0.10	0.01	0.04	0.00	0.00	0.00	0.00	0.00	0.00	2.17	0.00	0.01
OLA9014.P12.S1	2.36	511.73	16.00	28.04	3.04	11.23	1.76	1.09	1.31	0.14	0.80	0.15	0.38	0.05	0.42	0.04	2.59	8.14	2.97	0.67
OLA9014.P12.S2	2.49	1028.84	38.30	65.51	6.63	21.39	3.33	1.96	2.19	0.22	1.37	0.27	0.79	0.11	0.81	0.15	5.95	16.58	8.07	1.79
OLA9014.P12.S3	3.46	1232.30	50.66	132.05	18.95	89.31	21.82	4.50	19.41	2.90	16.44	3.12	7.49	0.85	6.13	0.81	12.17	18.92	11.59	2.76
OLA9014.P14.S2	0.64	221.68	7.01	11.76	1.23	4.13	0.65	0.63	0.41	0.06	0.30	0.04	0.13	0.03	0.19	0.03	0.68	4.76	1.04	0.26
OLA9014.P14.S3	-0.01	190.72	5.37	7.87	0.74	2.27	0.20	0.73	0.13	0.01	0.05	0.00	0.00	0.00	0.02	0.00	0.00	2.74	0.01	0.00
OLA9014.P14.S4	1.45	964.69	30.29	46.26	4.51	13.93	1.68	2.19	1.03	0.11	0.86	0.13	0.34	0.05	0.31	0.06	2.31	14.46	3.22	1.01
OLA9014.P15.S1	0.01	410.32	5.75	8.54	0.79	2.55	0.22	0.81	0.16	0.01	0.04	0.01	0.02	0.00	0.00	0.00	0.00	2.93	0.00	0.00
OLA9014.P15.S2	0.01	199.15	5.23	8.06	0.79	2.28	0.28	0.73	0.16	0.01	0.06	0.01	0.00	0.00	0.00	0.00	0.00	2.46	0.01	0.01
OLA9014.P15.S3	0.00	214.99	5.66	8.64	0.83	2.35	0.21	0.74	0.13	0.01	0.02	0.00	0.01	0.00	0.01	0.00	0.00	2.64	0.01	0.00
OLA9014.P15.S4	0.00	177.39	5.29	8.00	0.68	2.21	0.24	0.72	0.15	0.01	0.02	0.00	0.01	0.00	0.00	0.00	0.00	2.44	0.00	0.00
OLA9014.P15.S5	0.01	384.34	11.97	17.41	1.57	4.61	0.44	1.43	0.19	0.01	0.07	0.01	0.02	0.00	0.00	0.00	0.00	5.60	0.01	0.00
OLA9022.P1.S1	0.52	747.91	24.00	36.79	3.24	9.43	1.25	2.81	0.78	0.06	0.35	0.05	0.10	0.02	0.15	0.01	0.13	18.40	0.74	0.25
OLA9022.P1.S2	0.02	601.28	19.50	24.82	1.92	5.54	0.54	2.25	0.20	0.02	0.06	0.01	0.02	0.00	0.00	0.00	0.00	13.94	0.00	0.00
OLA9022.P1.S3	1.38	606.24	37.58	78.61	9.91	40.95	9.44	3.14	7.98	1.13	6.13	1.14	2.76	0.35	2.38	0.33	2.94	12.50	5.48	1.98
OLA9022.P1.S4	0.03	1008.87	19.98	29.22	2.59	7.62	0.85	2.70	0.42	0.04	0.12	0.02	0.04	0.00	0.00	0.00	0.00	15.75	0.01	0.09
OLA9022.P6.S1	0.02	647.11	16.65	23.84	2.21	6.69	0.82	2.28	0.47	0.04	0.28	0.03	0.07	0.01	0.04	0.00	0.03	11.92	0.01	0.02
OLA9022.P6.S2	0.20	1456.99	32.70	44.89	4.06	12.60	1.42	3.59	0.66	0.08	0.36	0.07	0.07	0.00	0.08	0.01	0.21	18.34	0.18	0.11
OLA9022.P6.S3	12.68	2963.29	207.79	465.39	59.73	255.94	51.72	6.35	43.78	5.37	30.60	5.53	16.33	2.22	16.56	2.72	21.91	53.57	38.58	10.63
OLA9022.P11.S1	0.01	1268.27	26.52	39.44	3.30	11.00	1.26	2.57	0.61	0.06	0.24	0.05	0.04	0.01	0.01	0.01	0.02	16.44	0.09	0.01
OLA9022.P11.S2	0.66	1040.78	35.04	58.50	5.60	20.36	3.05	3.03	2.22	0.16	0.99	0.15	0.40	0.03	0.30	0.03	0.41	17.58	0.94	0.25
OLA9022.P11.S3	0.04	955.45	21.31	29.79	2.68	8.49	0.86	2.24	0.60	0.06	0.15	0.02	0.05	0.01	0.01	0.00	0.02	13.87	0.02	0.00
OLA9022.P11.S4	0.02	1477.29	29.38	40.32	3.43	11.23	1.01	3.34	0.57	0.04	0.12	0.05	0.03	0.01	0.00	0.01	0.00	17.41	0.00	0.00
OLA9022.P13.S1	6.77	1627.26	57.32	121.89	13.55	51.50	8.99	2.39	6.41	0.87	4.43	0.76	1.90	0.26	2.03	0.27	8.24	30.86	16.76	5.59
OLA9022.P13.S2	16.28	4388.03	129.07	270.70	31.72	115.37	21.55	4.68	17.07	2.01	10.16	1.97	5.35	0.70	4.39	0.69	23.24	68.30	43.86	13.81
OLA9022.P13.S3	5.07	2043.21	61.48	125.64	14.66	58.22	9.82	3.48	6.95	0.91	4.35	0.75	2.10	0.25	1.74	0.28	7.37	27.12	13.56	4.25
OLA9022.P14.S1	0.43	998.61	23.75	36.56	3.04	9.80	0.98	2.48	0.74	0.07	0.34	0.05	0.15	0.01	0.04	0.01	0.32	17.15	1.01	0.34
OLA9022.P14.S2	0.02	638.32	10.05	18.89	1.69	6.08	0.95	2.15	0.48	0.06	0.32	0.04	0.08	0.00	0.09	0.01	0.00	13.11	0.04	0.02
OLA9022.P14.S3	0.01	1031.56	22.38	30.96	2.62	7.31	0.70	2.19	0.43	0.06	0.11	0.02	0.05	0.00	0.03	0.00	0.00	15.52	0.01	0.01
OLA9022.P14.S4	3.12	1244.98	33.38	54.29	5.03	17.36	2.31	2.73	1.50	0.17	1.04	0.17	0.41	0.06	0.54	0.06	1.18	22.98	4.17	1.41
OLA9022.P14.S5	11.66	3536.57	100.48	201.72	23.68	89.43	15.98	4.76	11.58	1.44	8.83	1.55	3.53	0.52	2.95	0.49	15.09	53.02	30.64	10.10
OLA9022.P17.S1	0.01	1117.76	33.21	47.30	3.88	12.03	1.22	3.53	1.08	0.06	0.18	0.03	0.08	0.00	0.00	0.01	0.00	23.94	0.00	0.00
OLA9022.P17.S2	3.79	1397.68	33.74	71.03	8.05	27.25	4.92	1.93	3.30	0.47	2.48	0.45	1.09	0.17	1.15	0.16	5.06	19.02	9.49	3.19
OLA9022.P17.S3	32.44	9155.51	256.64	586.89	70.63	246.45	46.84	7.92	36.84	4.92	24.72	4.48	13.39	1.77	13.47	2.18	44.66	138.58	79.63	29.09
OLA9022.P18.S1	0.89	759.82	20.79	34.80	3.00	10.01	1.47	2.27	0.87	0.11	0.55	0.08	0.21	0.03	0.18	0.02	0.51	16.46	1.46	0.42
OLA9022.P18.S2	0.02	1217.76	32.84	47.29	3.98	11.02	1.19	3.19	0.82	0.07	0.16	0.02	0.04	0.00	0.03	0.00	0.04	20.40	0.02	0.01
OLA9022.P18.S3	0.03	1044.72	27.07	39.10	3.40	9.51	0.97	2.53	0.60	0.03	0.14	0.01	0.04	0.00	0.02	0.01	0.05	16.77	0.02	0.01
OLA9022.P18.S4	0.03	1074.16	26.46	42.24	3.84	12.79	1.81	2.37	1.21	0.11	0.55	0.07	0.19	0.02	0.18	0.01	0.00	14.61	0.07	0.02
OLA9022.P21.S1	0.05	827.15	26.61	36.00	2.95	8.33	0.91	2.59	0.65	0.03	0.13	0.02	0.03	0.00	0.02	0.00	0.02	14.62	0.06	0.02
OLA9022.P21.S2	2.51	1444.19	36.81	71.52	8.48	30.98	5.68	2.73	4.19	0.48	2.87	0.39	1.11	0.15	1.02	0.15	3.52	16.02	6.73	2.37
OLA9022.P21.S3	11.41	3338.95	113.60	244.58	28.88	109.79	20.14	3.87	15.93	2.08	10.14	1.68	4.64	0.55	3.97	0.59	16.31	50.58	31.60	9.93
OLA9022.P21.S4	0.42	1082.88	26.45	38.39	3.41	10.69	1.16	3.54	0.90	0.08	0.43	0.06	0.21	0.01	0.16	0.01	0.44	16.77	0.78	0.26
OLA9022.P22.S1	0.02	1246.26	20.98	30.23	2.82	8.84	0.97	2.56	0.52	0.05	0.11	0.03	0.05	0.01	0.00	0.00	0.05	16.78	0.01	0.01

OLA9022.P22.S2	0.04	636.45	11.93	18.56	1.78	5.61	0.63	1.73	0.30	0.02	0.09	0.03	0.02	0.00	0.02	0.01	0.03	10.06	0.01	0.01
OLA9022.P22.S3	0.33	1132.77	27.20	79.45	11.21	28.45	6.60	3.19	1.70	0.25	1.54	0.12	1.09	0.19	2.00	0.15	16.18	20.00	1.36	2.39
OLA9022.P22.S4	0.01	587.23	33.86	66.56	8.04	32.75	5.85	2.23	4.60	0.52	2.51	0.43	0.96	0.10	0.59	0.06	0.03	9.90	0.30	0.08
OLA9022.P23.S1	17.65	4506.40	162.88	358.98	40.29	153.16	28.33	5.69	22.17	2.71	14.43	2.55	6.21	0.89	6.10	0.86	25.31	80.24	47.51	15.94
OLA9022.P23.S2	6.87	2268.15	68.58	144.63	16.74	62.31	10.53	2.81	9.26	1.27	5.88	1.11	2.90	0.36	2.45	0.38	11.02	33.04	19.72	7.35
OLA9022.P23.S3	0.03	846.39	13.23	19.93	1.78	5.45	0.62	1.65	0.34	0.02	0.15	0.01	0.06	0.00	0.00	0.00	0.03	9.26	0.06	0.02
OLA9022.P23.S4	7.13	2538.30	66.47	145.97	17.58	68.59	13.29	3.48	10.81	1.52	7.70	1.35	3.14	0.47	2.96	0.39	10.17	35.19	18.42	6.19
OLA9022.P23.S5	4.42	1680.82	43.26	92.95	11.15	44.46	9.64	2.55	7.44	0.90	4.75	0.82	2.12	0.31	2.00	0.27	7.15	21.38	11.92	3.70
OLA9025.P1.S1	0.34	334.05	12.14	17.41	1.63	5.17	0.62	1.88	0.39	0.03	0.15	0.03	0.08	0.01	0.04	0.00	0.17	23.97	0.75	0.31
OLA9025.P1.S2	0.06	268.74	9.12	12.26	1.03	3.38	0.48	1.91	0.43	0.03	0.15	0.02	0.04	0.03	0.20	0.00	0.03	22.41	0.01	0.03
OLA9025.P1.S3	0.05	278.56	8.55	11.49	0.98	3.01	0.34	1.71	0.31	0.03	0.09	0.02	0.04	0.00	0.00	0.00	0.01	17.99	0.03	0.03
OLA9025.P1.S4	0.09	582.83	20.95	25.00	1.96	5.63	0.50	2.29	0.28	0.02	0.05	0.00	0.00	0.00	0.00	0.00	0.07	20.03	0.09	0.09
OLA9025.P2.S1	1.39	505.58	13.70	20.90	1.94	6.65	0.84	1.19	0.50	0.09	0.24	0.05	0.15	0.02	0.13	0.02	0.74	9.67	2.64	1.25
OLA9025.P2.S2	3.68	1507.20	30.04	44.53	4.13	12.89	1.65	2.68	1.03	0.10	0.49	0.07	0.21	0.03	0.23	0.02	0.71	21.62	3.74	1.61
OLA9025.P2.S3	1.75	1056.62	32.62	47.28	4.19	12.85	1.55	3.40	0.94	0.09	0.37	0.09	0.16	0.04	0.16	0.02	0.46	24.44	2.65	1.26
OLA9025.P3.S1	8.29	1233.28	40.00	75.20	7.71	25.06	4.37	1.99	2.60	0.44	1.71	0.27	0.80	0.10	0.77	0.13	4.16	30.60	15.00	7.26
OLA9025.P3.S2	0.69	631.36	13.73	21.82	1.96	6.40	0.79	1.73	0.35	0.04	0.24	0.02	0.06	0.01	0.09	0.01	1.26	18.33	2.25	1.13
OLA9025.P3.S3	0.07	503.49	9.98	13.96	1.27	3.58	0.27	1.08	0.19	0.02	0.04	0.01	0.02	0.00	0.00	0.00	0.07	8.92	0.12	0.06
OLA9025.P3.S4	0.22	646.79	13.77	19.42	1.70	5.12	0.51	1.57	0.29	0.02	0.09	0.02	0.04	0.00	0.03	0.00	0.19	11.15	0.40	0.21
OLA9025.P4.S1	1.58	375.14	24.38	36.21	3.05	9.43	1.13	1.81	0.65	0.08	0.35	0.06	0.19	0.02	0.18	0.02	0.48	19.78	2.83	1.51
OLA9025.P4.S2	0.04	466.20	20.49	28.68	2.34	7.46	0.95	2.48	0.51	0.03	0.12	0.01	0.03	0.00	0.04	0.00	0.00	20.52	0.03	0.05
OLA9025.P4.S3	0.02	335.79	14.77	19.44	1.60	4.99	0.56	1.71	0.30	0.02	0.10	0.02	0.03	0.00	0.03	0.00	0.00	13.65	0.04	0.06
OLA9025.P4.S4	0.03	389.63	20.10	27.30	2.31	6.09	0.57	2.07	0.40	0.03	0.14	0.01	0.02	0.00	0.00	0.01	0.00	18.80	0.03	0.02
OLA9025.P4.S5	0.15	318.44	12.18	17.02	1.38	3.79	0.40	1.57	0.23	0.02	0.08	0.01	0.05	0.01	0.02	0.00	0.05	15.38	0.21	0.12
OLA9025.P7.S1	0.00	342.77	17.55	32.12	3.14	10.18	1.38	2.15	0.73	0.06	0.32	0.02	0.02	0.01	0.01	0.00	0.00	14.82	0.01	0.12
OLA9025.P7.S2	0.12	310.16	67.26	166.52	21.67	94.46	18.98	3.00	14.56	1.76	8.02	1.40	3.23	0.31	1.94	0.26	8.00	13.13	3.98	0.85
OLA9025.P7.S3	0.10	609.25	27.10	47.27	4.72	16.66	2.56	2.52	1.78	0.21	1.23	0.18	0.42	0.03	0.32	0.04	0.53	19.63	4.31	1.73
OLA9025.P7.S4	0.03	734.56	30.43	45.71	4.20	12.71	1.70	2.88	0.87	0.10	0.33	0.06	0.14	0.01	0.07	0.01	0.07	21.03	0.09	0.04
OLA9025.P8.S1	2.01	1207.40	18.76	34.67	3.82	11.75	1.71	1.72	1.04	0.12	0.50	0.08	0.19	0.02	0.23	0.02	0.77	15.04	2.25	1.44
OLA9025.P8.S2	3.32	1332.89	23.20	37.34	3.69	11.50	1.72	1.70	0.99	0.09	0.52	0.10	0.28	0.05	0.30	0.03	1.16	21.87	3.89	2.03
OLA9025.P8.S3	1.25	714.70	13.90	22.18	2.09	7.04	0.78	1.54	0.62	0.07	0.25	0.04	0.13	0.02	0.07	0.02	0.64	13.26	1.96	1.09
OLA9025.P12.S1	27.63	8750.31	230.23	551.56	67.48	263.59	44.71	5.44	31.64	3.14	15.58	2.39	5.70	0.71	4.05	0.58	8.32	58.37	38.31	18.97
OLA9025.P12.S2	1.18	1513.30	37.01	58.07	4.63	14.49	1.59	3.85	0.72	0.08	0.41	0.03	0.13	0.02	0.08	0.02	0.52	26.11	3.04	1.11
OLA9025.P12.S3	0.03	564.08	13.40	19.61	1.75	5.10	0.67	1.72	0.32	0.03	0.07	0.01	0.02	0.00	0.00	0.00	0.03	11.18	0.08	0.04
OLA9025.P12.S4	0.10	1186.54	28.40	37.75	3.08	7.96	0.69	3.66	0.49	0.04	0.12	0.01	0.04	0.00	0.03	0.00	0.09	24.26	0.20	0.13
OLA9025.P15.S1	0.05	960.99	25.28	34.02	3.00	8.29	0.70	2.90	0.49	0.03	0.11	0.03	0.03	0.01	0.01	0.00	0.06	18.21	0.12	0.08
OLA9025.P15.S2	0.14	824.69	21.18	29.41	2.48	7.61	0.69	2.34	0.42	0.03	0.14	0.02	0.02	0.00	0.01	0.00	0.02	19.45	0.54	0.74
OLA9025.P15.S3	0.08	999.05	22.53	31.05	2.61	8.09	0.76	2.65	0.45	0.05	0.13	0.01	0.06	0.00	0.02	0.00	0.08	17.76	0.16	0.11
OLA9025.P15.S4	0.01	948.70	19.46	24.69	1.99	6.14	0.66	2.28	0.30	0.02	0.11	0.00	0.03	0.00	0.02	0.00	0.00	15.43	0.04	0.05
OLA9025.P15.S5	0.10	1312.24	29.12	36.36	2.96	7.94	0.65	3.50	0.42	0.02	0.06	0.01	0.03	0.00	0.05	0.00	0.07	23.72	0.15	0.10
OLA9025.P15.S6	0.04	1038.15	21.29	27.35	2.26	6.60	0.58	2.67	0.26	0.03	0.06	0.01	0.04	0.00	0.00	0.00	0.00	18.30	0.05	0.02
OLA9025.P16.S1	0.49	685.76	27.32	38.76	3.28	9.80	0.79	2.89	0.81	0.07	0.23	0.02	0.08	0.01	0.05	0.01	0.17	21.86	0.65	0.30
OLA9025.P16.S2	2.99	861.57	22.43	35.68	3.46	11.30	1.63	1.63	1.14	0.12	0.49	0.09	0.23	0.03	0.30	0.02	1.25	15.34	5.16	2.45
OLA9025.P16.S3	32.85	3925.64	183.32	366.96	41.36	161.34	28.78	4.70	19.47	2.38	10.31	1.83	5.13	0.59	3.96	0.54	16.44	97.30	67.14	29.97
OLA9025.P19.S1	18.84	2665.29	79.03	149.20	14.66	51.59	7.15	3.35	5.22	0.57	2.63	0.58	1.26	0.22	1.63	0.25	7.33	54.02	32.93	16.72
OLA9025.P19.S2	113.58	10634.94	368.96	749.49	77.90	253.93	41.24	6.87	27.33	3.13	17.34	2.93	9.18	1.44	8.63	1.08	49.71	255.00	202.22	104.16
OLA9025.P19.S3	41.19	4267.54	142.22	276.85	28.31	94.00	14.34	4.33	9.26	1.21	6.62	1.03	2.68	0.48	3.34	0.56	14.44	98.59	68.04	35.50
OLA9036.P1.S1	0.01	891.12	22.81	36.10	3.35	11.39	1.44	2.53	0.97	0.10	0.41	0.06	0.18	0.01	0.06	0.00	0.02	13.31	0.14	0.02

OLA9036.P1.S2	2.78	2181.49	58.70	92.85	8.17	26.36	3.53	5.35	2.44	0.25	1.57	0.26	0.77	0.06	0.74	0.11	2.61	35.51	6.99	2.01
OLA9036.P1.S3	62.71	10738.10	370.16	796.01	82.18	303.07	53.39	7.71	39.47	5.89	30.45	5.73	15.84	2.10	14.50	2.22	56.68	219.01	156.74	54.67
OLA9036.P3.S1	1.17	1465.96	32.66	41.44	3.60	10.06	0.79	3.40	0.71	0.05	0.15	0.02	0.04	0.01	0.03	0.00	0.05	17.98	0.16	0.05
OLA9036.P3.S2	1.29	1500.11	35.57	54.89	5.05	16.65	2.21	3.03	1.51	0.19	0.87	0.16	0.34	0.06	0.35	0.06	1.37	19.51	3.78	1.22
OLA9036.P3.S3	9.25	1393.18	43.22	91.60	8.95	35.56	5.20	1.12	4.85	0.50	3.35	0.42	1.82	0.25	1.74	0.12	3.27	12749.69	12.77	4.84
OLA9036.P5.S1	-0.01	611.78	19.11	27.81	2.39	7.45	0.74	2.00	0.46	0.03	0.13	0.01	0.04	0.00	0.03	0.00	0.00	13.63	0.00	0.00
OLA9036.P5.S2	1.26	1224.18	27.75	42.17	3.44	10.37	1.11	3.04	0.95	0.08	0.46	0.06	0.18	0.02	0.18	0.02	0.84	22.51	2.66	1.12
OLA9036.P5.S3	0.01	708.47	22.35	31.68	2.56	7.74	0.67	2.50	0.43	0.03	0.12	0.03	0.02	0.00	0.01	0.00	0.00	16.72	0.00	0.00
OLA9036.P5.S4	0.17	905.57	25.86	37.20	3.10	9.22	0.86	2.84	0.61	0.06	0.24	0.05	0.06	0.01	0.03	0.01	0.13	18.74	0.41	0.17
OLA9036.P6.S1	0.01	740.21	27.77	45.10	4.57	14.66	2.08	2.35	1.02	0.11	0.52	0.06	0.14	0.02	0.11	0.00	0.00	14.15	0.17	0.08
OLA9036.P6.S2	0.07	890.31	27.28	41.00	3.60	11.25	1.39	2.67	0.86	0.07	0.22	0.03	0.08	0.01	0.04	0.01	0.05	17.82	0.11	0.10
OLA9036.P6.S3	3.27	1348.03	45.41	74.72	7.02	22.74	3.38	3.25	2.00	0.28	1.35	0.24	0.55	0.06	0.51	0.08	1.85	32.32	5.60	2.02
OLA9036.P6.S4	0.01	786.98	19.45	28.15	2.55	7.48	0.68	2.62	0.54	0.03	0.13	0.02	0.04	0.00	0.01	0.00	0.00	15.74	0.01	0.02
OLA9036.P6.S5	0.02	1261.13	38.22	64.61	6.31	21.17	2.19	3.45	1.19	0.08	0.37	0.03	0.09	0.01	0.05	0.01	0.00	19.76	0.29	0.18
OLA9036.P6.S6	6.71	2256.88	104.19	197.14	30.83	86.85	13.45	3.53	7.85	0.67	3.89	0.70	1.67	0.19	1.45	0.17	5.58	120.38	16.56	5.57
OLA9036.P6.S7	0.02	728.49	22.81	33.57	3.09	9.49	0.97	2.35	0.58	0.07	0.27	0.05	0.07	0.01	0.12	0.01	0.00	16.47	0.04	0.02
OLA9036.P10.S1	0.39	1210.18	27.21	39.55	3.50	11.49	1.17	2.86	0.90	0.06	0.32	0.07	0.13	0.02	0.12	0.01	0.25	17.18	0.64	0.27
OLA9036.P10.S1	0.02	1255.68	31.68	43.06	3.72	11.48	0.90	3.19	0.58	0.05	0.20	0.03	0.08	0.01	0.02	0.00	0.00	22.57	0.01	0.00
OLA9036.P10.S2	0.06	1432.63	27.87	39.07	3.40	10.15	1.29	3.29	0.48	0.04	0.16	0.02	0.03	0.01	0.05	0.00	0.01	17.72	0.11	0.05
OLA9036.P10.S2	0.01	765.72	29.79	48.06	4.52	13.67	2.02	2.37	0.95	0.07	0.24	0.04	0.10	0.00	0.00	0.00	0.00	16.77	0.13	0.08
OLA9036.P10.S3	0.03	1075.37	23.71	34.23	3.00	10.03	1.24	2.30	0.50	0.05	0.15	0.02	0.05	0.00	0.00	0.00	0.00	12.63	0.09	0.06
OLA9036.P10.S3	-0.01	882.93	27.85	40.08	3.67	9.86	1.10	2.68	0.60	0.03	0.13	0.04	0.03	0.00	0.04	0.00	0.30	19.16	0.04	0.04
OLA9036.P10.S4	0.03	1232.23	33.12	50.47	4.53	14.31	1.61	3.69	0.93	0.09	0.25	0.06	0.09	0.01	0.13	0.01	0.00	21.20	0.06	0.01
OLA9036.P10.S5	0.00	1095.81	25.50	33.51	2.72	8.53	0.98	2.89	0.47	0.04	0.13	0.01	0.09	0.00	0.00	0.00	0.00	15.94	0.00	0.00
OLA9036.P13.S1	0.02	622.95	21.15	33.69	3.18	10.14	1.20	2.37	0.74	0.06	0.29	0.04	0.08	0.01	0.03	0.00	0.00	16.93	0.02	0.01
OLA9036.P13.S2	2.62	805.11	39.94	62.67	6.12	20.48	3.05	3.14	2.40	0.25	1.50	0.18	0.61	0.11	0.49	0.07	1.53	24.73	3.59	1.74
OLA9036.P13.S3	0.59	604.56	26.11	42.43	4.57	15.72	2.38	1.64	1.24	0.14	0.61	0.07	0.21	0.03	0.25	0.03	0.62	60.25	1.48	0.56
OLA9036.P13.S4	77.30	12836.43	487.88	985.43	110.72	396.10	73.03	9.39	51.48	6.67	37.36	6.57	20.11	2.60	16.93	2.66	72.21	307.45	193.80	64.69
OLA9036.P14.L1	1.23	1438.04	51.32	76.30	7.70	21.69	3.14	4.68	1.92	0.16	1.00	0.12	0.39	0.05	0.28	0.04	1.11	163.71	2.89	1.18
OLA9036.P14.S1	0.83	1090.49	27.86	42.44	3.87	12.87	2.07	2.35	0.99	0.12	0.42	0.11	0.27	0.02	0.27	0.02	0.76	19.00	1.39	0.48
OLA9036.P14.S2	2.41	836.15	24.46	40.60	4.08	13.18	1.91	2.17	1.12	0.15	0.76	0.15	0.30	0.04	0.29	0.03	1.02	17.42	3.08	1.06
OLA9036.P14.S3	1.25	577.61	13.03	22.08	2.29	7.80	1.31	1.24	0.78	0.10	0.50	0.07	0.28	0.04	0.24	0.05	0.90	10.15	2.64	0.83
OLA9036.P15.S1	0.65	1017.67	16.42	33.23	3.88	14.72	3.25	1.36	2.18	0.37	2.14	0.33	0.94	0.15	1.10	0.15	2.64	18.96	2.80	0.95
OLA9036.P15.S2	0.05	502.71	16.45	42.49	6.75	32.49	9.30	1.47	7.62	1.31	7.24	1.34	3.42	0.45	3.57	0.51	2.17	7.53	0.85	0.21
OLA9036.P15.S3	0.01	186.97	3.72	6.26	0.58	2.09	0.23	0.49	0.10	0.03	0.06	0.01	0.02	0.00	0.02	0.00	0.00	4.35	0.02	0.01
OLA9036.P16.S1	1.96	1358.16	32.39	51.65	4.98	16.60	2.62	2.53	1.61	0.18	1.03	0.18	0.41	0.06	0.34	0.08	1.61	18.17	4.46	1.48
OLA9036.P16.S2	0.98	1427.97	30.06	44.09	3.97	12.88	1.36	2.73	0.95	0.13	0.65	0.09	0.23	0.03	0.22	0.02	0.87	18.05	2.36	0.79
OLA9036.P16.S3	2.47	1701.79	37.55	61.53	5.95	19.13	2.91	2.60	1.90	0.25	1.40	0.22	0.51	0.09	0.50	0.05	2.09	21.51	6.22	2.10
OLA9036.P16.S4	3.64	1787.03	54.05	103.67	10.74	39.65	6.16	3.19	4.48	0.60	2.63	0.49	1.33	0.17	1.07	0.12	2.82	25.91	8.59	2.85
OLA9052.P2.S1	2.55	950.79	25.25	46.72	4.51	17.03	2.37	1.61	1.76	0.26	1.55	0.26	0.65	0.09	0.54	0.09	2.46	16.80	5.56	2.06
OLA9052.P2.S1	0.02	483.30	10.42	16.46	1.53	5.03	0.55	1.11	0.32	0.02	0.15	0.02	0.06	0.01	0.02	0.01	0.05	5.87	0.06	0.03
OLA9052.P2.S2	52.14	9245.11	334.42	694.01	75.22	280.25	47.80	7.30	38.40	4.84	26.15	4.84	15.28	1.97	12.97	2.11	54.50	190.95	115.66	41.48
OLA9052.P2.S2	0.29	244.64	4.79	8.00	0.76	2.68	0.26	0.65	0.20	0.02	0.09	0.02	0.01	0.01	0.02	0.01	0.13	3.81	0.07	0.06
OLA9052.P2.S3	35.67	6716.36	233.16	487.61	52.05	191.67	34.81	6.30	25.93	3.28	18.71	3.72	9.48	1.27	8.80	1.46	37.92	135.43	80.51	28.17
OLA9052.P2.S3	-0.01	222.04	4.74	7.32	0.65	2.34	0.28	0.59	0.15	0.02	0.06	0.01	0.02	0.00	0.02	0.00	0.00	3.03	0.00	0.00
OLA9052.P2.S4	0.76	1046.47	24.33	36.32	3.21	9.95	1.23	2.38	0.73	0.08	0.37	0.09	0.18	0.02	0.17	0.03	0.84	16.28	1.36	0.66
OLA9052.P2.S4	0.11	321.94	11.86	12.08	2.01	6.97	0.80	0.84	0.51	0.08	0.40	0.05	0.12	0.01	0.10	0.01	0.11	5.16	0.24	0.10
OLA9052.P4.S1	0.02	660.75	17.92	26.53	2.47	7.56	0.75	2.06	0.54	0.06	0.19	0.03	0.05	0.00	0.00	0.00	0.00	13.68	0.00	0.00

OLA9052.P4.S2	0.00	1065.91	22.32	31.19	2.72	7.81	0.64	2.57	0.59	0.03	0.12	0.03	0.03	0.00	0.03	0.01	0.01	15.86	0.01	0.00
OLA9052.P4.S3	0.02	993.76	20.85	29.51	2.53	7.69	0.77	2.14	0.42	0.03	0.12	0.02	0.02	0.01	0.01	0.00	0.00	13.80	0.00	0.00
OLA9052.P4.S4	20.88	4194.35	153.53	309.49	33.96	126.07	21.88	4.11	16.59	2.46	12.58	2.20	5.89	0.79	5.45	0.90	23.65	81.83	51.17	17.60
OLA9052.P9.S1	50.82	10344.95	337.45	788.94	81.62	304.09	55.25	8.59	42.15	5.69	31.10	5.70	13.98	2.31	16.03	1.96	51.03	221.12	118.80	44.41
OLA9052.P9.S2	20.53	4263.90	214.67	525.47	59.39	235.55	44.80	6.47	35.96	4.95	24.71	4.97	12.29	1.72	11.58	1.94	22.79	85.16	53.79	18.53
OLA9052.P9.S3	20.42	4190.61	164.58	372.30	39.71	151.54	26.37	4.42	20.30	2.59	12.62	2.52	6.53	0.84	6.78	0.71	19.85	84.34	45.44	16.97
OLA9052.P9.S4	73.82	13595.06	422.86	946.45	95.09	345.52	59.50	9.85	51.20	6.07	32.73	6.24	18.63	2.53	15.32	2.37	71.69	273.15	156.21	60.81
OLA9052.P12.S1	0.96	694.46	17.41	30.50	2.93	9.97	1.42	1.58	1.01	0.11	0.65	0.11	0.23	0.04	0.24	0.03	0.80	11.30	2.05	0.77
OLA9052.P12.S2	22.59	5289.63	173.90	387.20	37.97	135.62	24.04	5.05	20.27	2.48	14.73	2.54	7.92	1.04	7.14	1.05	33.12	102.77	61.72	19.65
OLA9052.P12.S3	13.86	3493.01	108.49	218.48	23.62	84.54	14.44	3.54	11.43	1.47	7.54	1.39	3.83	0.58	3.45	0.59	16.70	61.57	34.97	11.56
OLA9052.P12.S4	3.20	1996.96	61.31	120.95	11.76	44.82	7.26	3.76	6.04	0.71	4.10	0.46	1.69	0.20	1.22	0.09	4.19	61.40	13.70	2.90
OLA9052.P14.S1	0.04	423.28	19.29	26.73	2.22	5.97	0.50	1.79	0.26	0.02	0.09	0.02	0.03	0.01	0.03	0.00	0.06	11.54	0.04	0.02
OLA9052.P14.S2	9.83	2030.13	64.75	135.81	13.85	50.15	8.12	2.23	6.63	0.78	4.70	0.79	2.32	0.30	2.26	0.34	9.24	43.66	21.25	7.76
OLA9052.P14.S3	55.57	9472.11	322.22	688.54	72.98	257.96	44.45	6.71	33.89	4.70	25.50	4.98	12.70	2.16	12.58	1.76	54.62	211.89	118.71	43.97
OLA9052.P14.S4	57.08	11545.96	364.64	785.43	83.06	295.06	56.18	8.99	42.70	5.76	31.30	5.93	14.34	1.83	13.86	2.19	62.77	220.45	134.46	50.89
OLA9052.P14.S5	9.47	2322.04	68.87	143.61	14.64	51.52	9.17	2.85	6.52	0.91	4.77	0.89	2.64	0.40	2.33	0.34	10.23	44.52	21.84	7.98
OLA9052.P14.S6	3.80	1302.49	32.84	63.00	6.44	22.57	3.66	1.74	2.57	0.34	1.87	0.40	0.93	0.12	1.04	0.15	4.46	18.88	8.85	3.32
OLA9052.P14.S7	42.76	7526.45	275.47	598.49	63.96	230.69	41.86	6.80	34.00	4.39	24.25	4.34	12.18	1.72	12.99	1.69	45.05	166.01	99.94	35.41
OLA9052.P15.S1	0.06	991.56	16.42	22.97	2.01	6.23	0.71	2.45	0.38	0.03	0.15	0.01	0.05	0.01	0.03	0.01	0.11	13.79	0.08	0.06
OLA9052.P15.S2	0.07	1212.08	25.74	34.75	3.13	9.14	1.08	3.17	0.56	0.06	0.19	0.02	0.09	0.01	0.03	0.00	0.00	19.05	0.00	0.00
OLA9052.P15.S3	0.04	1004.11	22.89	32.13	2.79	8.67	0.98	2.36	0.57	0.05	0.08	0.02	0.06	0.01	0.03	0.00	0.08	13.93	0.07	0.03
OLA9052.P15.S4	1.63	960.54	25.43	43.56	4.42	13.55	1.95	1.91	1.48	0.17	1.07	0.16	0.50	0.06	0.34	0.05	1.86	13.75	3.70	1.39
OLA9052.P16.S1	0.03	991.97	22.03	31.05	2.68	7.44	0.68	2.37	0.43	0.04	0.12	0.02	0.05	0.00	0.00	0.00	0.01	14.80	0.07	0.03
OLA9052.P16.S2	0.05	870.13	22.67	32.70	2.81	8.71	1.00	2.14	0.54	0.06	0.25	0.05	0.11	0.01	0.03	0.00	0.06	14.20	0.02	0.02
OLA9052.P16.S3	0.13	1010.93	25.82	37.14	3.17	10.20	1.08	2.89	0.59	0.07	0.18	0.03	0.03	0.02	0.03	0.01	0.14	17.87	0.14	0.10
OLA9052.P16.S4	0.01	828.33	19.53	26.80	2.24	7.17	0.74	2.12	0.43	0.04	0.11	0.02	0.01	0.00	0.03	0.00	0.00	13.36	0.00	0.00
OLA9052.P16.S5	0.03	754.05	23.08	36.71	3.65	10.85	1.26	2.79	0.80	0.07	0.27	0.03	0.09	0.02	0.12	0.00	0.07	16.41	0.09	0.04
OLA9052.P16.S6	0.00	1061.66	22.31	29.92	2.39	6.63	0.55	2.31	0.37	0.03	0.12	0.01	0.03	0.01	0.00	0.00	0.00	14.98	0.00	0.01
OLA9052.P16.S7	1.21	1101.23	27.46	44.34	4.89	15.31	2.41	2.07	1.72	0.25	1.06	0.18	0.49	0.04	0.46	0.07	1.02	16.87	1.68	0.51
OLA9052.P16.S8	0.02	297.56	6.57	10.12	0.91	3.27	0.34	0.83	0.20	0.02	0.09	0.01	0.01	0.00	0.02	0.00	0.06	3.71	0.08	0.02
OLA9052.P17.S1	0.06	665.32	20.11	25.77	1.95	5.37	0.48	1.81	0.19	0.02	0.05	0.00	0.01	0.00	0.00	0.00	0.03	17.59	0.01	0.04
OLA9052.P17.S2	0.01	633.28	17.47	21.13	1.57	4.06	0.34	1.88	0.23	0.01	0.06	0.01	0.01	0.00	0.00	0.00	0.00	13.53	0.00	0.00
OLA9052.P17.S3	0.01	657.86	14.44	21.13	1.94	5.66	0.68	1.61	0.44	0.03	0.14	0.02	0.02	0.00	0.00	0.00	0.00	10.02	0.00	0.00
OLA9052.P17.S4	33.50	7489.24	254.07	518.43	56.42	210.55	36.02	6.93	30.13	4.09	20.10	3.89	9.57	1.46	8.92	1.29	36.61	127.07	81.24	28.02
OLA9052.P18.S1	0.04	711.66	18.02	25.30	2.21	6.04	0.63	2.10	0.31	0.03	0.07	0.01	0.02	0.00	0.00	0.00	0.05	13.01	0.03	0.02
OLA9052.P18.S2	0.01	502.32	22.11	29.10	2.41	6.13	0.52	2.23	0.25	0.03	0.07	0.01	0.03	0.00	0.01	0.00	0.00	20.25	0.00	0.00
OLA9052.P18.S3	0.00	326.74	17.93	24.74	2.05	5.76	0.66	1.63	0.43	0.03	0.12	0.03	0.07	0.00	0.04	0.01	0.00	14.93	0.05	0.02
OLA9052.P18.S4	0.00	446.84	21.09	28.63	2.19	6.09	0.46	2.10	0.27	0.02	0.07	0.00	0.02	0.00	0.00	0.00	0.00	19.03	0.01	0.00